Numerical Simulation of High Pressure Hydrogen Releases into Air through Varying Orifice Geometries

Nasim Shishehgaran

A Thesis

In

the Department

of

Mechanical and Industrial Engineering

Presented in Partial Fulfillment of the Requirements
for the Degree of Master of Applied Science (Mechanical Engineering) at
Concordia University
Montreal, Quebec, Canada

August 2013

CONCORDIA UNIVERSITY

School of Graduate Studies

This is to certify that the thesis prepared

By: Nasim Shishehgaran

Entitled: Numerical Simulation of High Pressure Hydrogen Releases into Air through Varying Orifice Geometries

and submitted in partial fulfillment of the requirements for the degree of

Master of Applied Science (Mechanical Engineering)

Complies with the regulations of the University and meets the accepted standards with respect to originality and quality.

Signed by the final examining committee:

Dr. Hoi Dick Ng _____ Chair

Dr. Ali Dolatabadi _____ Examiner

Dr. Sheldon S. Williamson _____ Examiner

Prof. Marius Paraschivoiu _____ Supervisor

Approved by _____

Chair of Department or Graduate Program Director

08/30/2013 _____

Dean of Faculty

ABSTRACT

Numerical Simulation of High Pressure Hydrogen Releases into Air through Varying Orifice Geometries

Nasim Shishehgaran

Computational Fluid Dynamics (CFD) is employed to investigate the near exit jet behavior of a high-pressure hydrogen release into the quiescent ambient air through different types of orifices. The effect of orifice geometry on the structure, development and dispersion of highly under-expanded hydrogen jet is numerically investigated. Various shapes of orifices are evaluated including holes with constant areas such as elliptical and circular openings, and deforming apertures under different configurations and conditions considering the interactions of enlarging of circular openings and the release time, as well as the deformation of a circular hole to an elliptical hole. A three-dimensional in-house parallel code is exploited to simulate the flow using an unstructured tetrahedral finite volume Euler solver. The transport (advection) equation is applied to track the shape and the location of the hydrogen - air interface. The Abel-Nobel real gas law is used since high-pressure hydrogen flow deviates from the ideal gas assumption. Comparative studies between the dispersion of hydrogen jet issuing from different types of orifices in terms of jet development and pressure expansion are carried out. The numerical simulations indicate that in addition to the hydrogen storage pressure, the shape and the size of the orifice influence the hydrogen jet development which can affect the ignition risks associated with the accidental release of hydrogen.

ACKNOWLEDGMENTS

I would like to express my sincere gratitude to my supervisor, Professor Marius Paraschivoiu, for his guidance, continuous support, patience and all I have learned from him.

I thank Dr. Reza Khaksarfard and Matin Komeili for all their helpful suggestions, especially in the early stages of this research.

I would also like to thank Hui Zhong Lu at the Centre for Scientific Computing at the Université de Sherbrooke for his technical support.

And finally, a special feeling of gratitude to my lovely parents for always believing in me, for their unconditional love, unwavering support and encouragement. To them I dedicated this thesis.

TABLE OF CONTENTS

LIST OF FIGURES

Figure **Page**

LIST OF TABLES

Table **Page**

NOMENCLATURE

a	Speed of sound
A	Orifice area
b	Constant of Abel-Nobel EOS
c	Concentration of air
C_v	Specific heat of the real gas at constant volume
$\tilde{C}_v$	Specific heat of the ideal gas at constant volume
C_p	Specific heat of real gas at constant pressure
u	X-component of velocity
v	Y-component of velocity
w	Z-component of velocity
ρ	Density
P	Pressure
E	Total internal energy
H	Total enthalpy
e_i	Internal energy
T	Temperature
w_x	X-component of grid speed
w_y	Y-component of grid speed
w_z	Z-component of grid speed
ΔS	Surface area of the control volume's boundary
V_i	Cell volume
R_{mix}	Average value of the gas constant
K_{ij}	Stiffness of the edge connecting nodes i and j
t	Time
a	Minor axis
b	Major axis
Δt	Time step
J	Jacobian
Z	Distance from the exit in the z direction
ζ	Compressibility factor
γ	Isentropic exponent

Vectors and Matrices

$\vec{U}$	Vector of conserved variables
$\vec{\vec{F}}$	Convective fluxes in all directions
$\overrightarrow{W}$	Vector of primitive variables

$\vec{n}$	Unit normal vector to boundary surfaces of control volumes

Abbreviations

AR	Aspect Ratio of the orifice
GHG	GreenHouse Gas
CFD	Computational Fluid Dynamics
DNS	Direct Numerical Simulation
CFL	Courant-Friedrichs and Lewy number
EOS	Equation of State
LES	Large Eddy Simulation
MPI	Message Passing Interface
MUSCL	Monotone Upstream Centered Schemes for Conservation Laws
GMRES	Generalized Minimal RESidual method

Chapter 1

INTRODUCTION

1.1 The global demand for alternative fuels

In today's world, concerns about global warming and climate change along with growing universal needs for energy, urge the demand for sustainable sources of energy to reduce Greenhouse Gas (GHG) and CO_2 emissions.

Carbone dioxide (CO_2) is the primary greenhouse gas which accounts for global warming impact. The atmospheric CO_2 levels over the past 55 years are shown in Fig. 1.1[1].

It is obviously seen that the concentrations of CO_2 in the atmosphere have been steadily rising year by year. The current level of atmospheric CO_2 is roughly 390 Parts per Million (ppm), although the safe upper limit is 350 ppm. The largest source of CO_2 emissions comes from fossil fuel combustion. By transforming fossil fuel dependent economy into an alternative energy economy, CO_2 emissions can be reduced back to the safe level of 350 ppm.

The transportation sector is one of the significant sources of CO_2 emissions and currently responsible for approximately 20 percent of carbon dioxide emissions [2]. It is expected that the road vehicle population will triple by 2050 which can cause an increase in CO_2 levels [2]; however, the perspective of the International Energy Agency (IEA) is the 50% reduction in carbon dioxide emissions by that time. Hence, the only way to curb this

increase and to reduce transportation carbon dioxide emissions is by replacing fossil fuels with emission-free alternative fuels such as hydrogen.

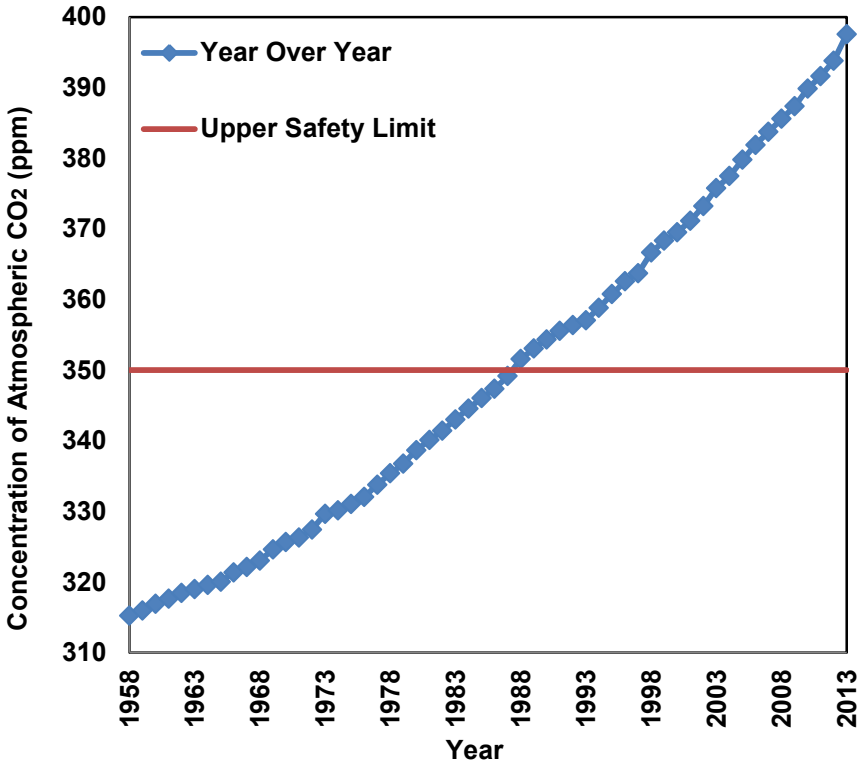

Fig. 1.1: *Annual mean atmospheric CO_2 concentration since 1958 (NOAA-ESRL data)*

1.2 Hydrogen as an alternative fuel

Despite an abundance of hydrogen, it is bound in molecular compound and does not exist naturally as a pure gas and it must be extracted from primary sources of energy. So, hydrogen can be considered as an energy carrier and not an energy source. Hydrogen can be produced from different energy sources using various methods including non-renewable methods such as reforming fossil fuels, natural gas and gasifying coal, or low polluting methods such as biomass decomposition and electrolysis of water using

renewable electricity or nuclear power. Therefore, the total CO_2 emissions of hydrogen depend directly on the method of manufacture.

Hydrogen and electricity are the two competing future energy carriers for the transportation industry with no carbon dioxide emissions at the point of utilization. Hydrogen can be used as a fuel in modified Internal Combustion Engines (ICE) or fuel cells. Fuel cell vehicles (FCVs) similar to Battery Electric Vehicles (BEVs) are fully electric and have higher energy efficiency compared to ICEVs. FCVs are powered by fuel cells, which create electricity using hydrogen and oxygen in a process inverse to the electrolysis of water, while the only emissions are water and heat.

The main advantages of FCVs over BEVs are faster refueling (less than five minutes not the hours needed for BEVs) and longer range which make them to be suited for a larger car segment including buses; however, BEVs are appropriate for short range application and the small size segment. Hence, it is reasonable to consider hydrogen and electricity as complementary energy carriers.

1.3 Hydrogen Safety

One of the major challenges with hydrogen technology is the storage. There are three feasible solutions for storing hydrogen in a transportation application. It can be stored and used in gaseous (GH_2), liquid (LH_2) or metal hydrides form. Although, hydrogen has the highest energy to weight ratio of all fuels, it has a low volumetric energy density as a liquid or gas. 1 kg of hydrogen contains the same amount of energy as 2.1 kg of natural gas or 2.8 kg of gasoline; however, the volumetric energy density for the LH_2 is about 1/4 of crude oil, and for GH_2 is about 1/3 of natural gas. So, in comparison with other fuels, it

contains less energy per volume. As a result, larger storage tanks required to store hydrogen for a specific mile range.

To overcome the aforementioned issues, in gaseous form hydrogen must be compressed to several hundred times the atmospheric pressure in order to decrease the size of the storage tank. In liquid form, since it has a low boiling point compared to other substances, it requires a cryogenic storage system and it must be cooled down to less than 20 K. Although LH_2 has a higher density at low pressure compared to GH_2, liquefaction process and required materials for insulating the tanks are very expensive. In hydrid form, as a chemical storage system, some of metal characteristics make them to release hydrogen gas at relatively high temperature (390K-470K) and low pressure. Despite its higher safety, it has a low energy to weight ratio which cause metal hydrogen system to be heavier and larger than a compressed gas. Hence, storing hydrogen as a compressed gas can be considered as the most probable solution in the short term with lower cost compared to the other methods.

In order to commercialize the hydrogen technology in the transportation industry, safety and standard codes related to production, storage, transportation and utilization must be precisely developed. However, some of the special characteristics of hydrogen provide safety benefits; it is a flammable fuel like gasoline and natural gas but can be dangerous under specific conditions. In comparison with common fossil fuels and natural gas, hydrogen has a wide flammability range in air mixtures (4-74%) and low energy ignition (0.02 mJ). In addition, it has low viscosity and small molecular weight that make it release easily. Its high buoyancy and diffusivity (compared to other fuel gas) make it rise rapidly and dilute into a non-flammable concentration (presence of wind can make

hydrogen disperse even more quickly). Although these properties prevent hydrogen from accumulating near a release exit and can lessen a fire risk especially in the open air, leaks from high pressure storage tanks lead to large release rates which can make a significant flammable gas cloud. Consequently, to ensure that the widespread use of hydrogen can happen with the low associated risk, its cloud dispersion behavior and ignition possibility in case of an incident release must be better quantified. This evaluation will help the development of hydrogen safety codes and standards.

1.4 Aim of this study

Computational Fluid Dynamics (CFD) is an effective tool which is increasingly used to investigate the safety issues related to utilization of hydrogen as a fuel. CFD based analysis can provide accurate and reliable information related to dispersion and auto-ignition of hydrogen caused by an accidental release of pressurized hydrogen into the ambient air. Therefore, in this study, the initial phase of the sudden release of hydrogen from a high-pressure reservoir into the quiescent ambient air and the behavior of a corresponding near exit jet are investigated using a parallel in-house code.

Owing to the lack of study of hydrogen dispersion and its auto-ignition possibility under different conditions in terms of geometrical layout, the work in this thesis aims to numerically investigate the effect of orifice geometry on the behavior and development of hydrogen jet issuing from different types of release exits. This analysis and obtained results then will be used as an input data for investigation of auto-ignition possibility in future work. Hence, the scope of this work is limited to the near field flow at which the influence of orifice shape and occurrence of auto-ignition are dominant.

1.5 Objectives of this study

To achieve the aim of this research, four main objectives have been considered:

- Investigate the hydrogen release through the fixed elliptical orifices with varying aspect ratios of AR=4 and AR=6 under two different storage pressures of 70MPa and 10MPa. Various orifice areas based on 1mm, 2mm and 5mm diameter of circular orifices are considered. The obtained results are compared with the results of their equivalent standard circular orifices. The areas of the comparable orifices in this evaluation are equal and constant.
- Study the gas release through the enlarging orifice with the uniform radial growth rate of v= 200 m/s or 0.2 mm/μs. In this scenario, a small circular aperture is enlarged into a larger circular hole before the escaping of hydrogen into air at which the hydrogen-air interface is in the nozzle (t=0). Then the results are compared with their fixed circular counterparts.
- Simulate the hydrogen release by applying the combination of two above-mentioned approaches. In this case, before the hydrogen discharge, the dimensions of the orifice are fixed and do not change with time, but as the interface reaches the exit of the pressurized vessel, the orifice starts moving with the same expansion rate as a second scenario.
- Study the effect of the time-dependent deformation of a circular orifice to an elliptic orifice on the accidental release of hydrogen. In this case, a small circular hole is stretched into an elliptical orifice, while the minor axis of the elliptic preserves its initial length.

1.6 Methodology of work

To fulfill the aforementioned objectives, a three-dimensional in-house code is exploited using the Message Passing Interface (MPI) library for parallel computing to simulate the flow based on an inviscid approximation. This code has been extensively validated. It demonstrated good agreement with experimental results for a wide variety of CFD problems [3]. Convection dominates viscous effects in strongly under-expanded supersonic jets in the vicinity of the release exit, justifying the use of the finite volume Euler equations. The transport (advection) equation is applied to track the shape and position of the hydrogen-air interface. The Abel Nobel equation of state is used because high pressure hydrogen flow deviates from the ideal gas assumption. The system of non-linear equations is solved by means of a fully implicit scheme which has an accuracy of the first and second orders in time and space, respectively. Convective fluxes are evaluated using Roe-MUSCL scheme. To avoid the numerical instabilities which are generated near the shock or discontinuity regions, the Van Leer-Van Albada limiter is applied.

To simulate the expanding release hole, the dynamic mesh based on the spring analogy method is used to update the volume mesh. Therefore, the relative velocities in each coordinate direction are added in all governing equations. Then the system of equations is solved using an iterative GMRES solver and MPI parallel processing to reduce the solution time.

1.7 Axisymmetric and Non-axisymmetric Jet Structures

The flow fields and jet structures from axisymmetric and non-axisymmetric nozzles have been extensively studied and described in a number of references in the literature [4-10]; however, due to the specific characteristics of hydrogen and a difference in the propensity of ignition between hydrogen and non-hydrogen gases, complete study of the hydrogen jet formation and dispersion is essential. In contrast of a large amount of work exists in the literature related to the hydrogen jet, there is a lack of experimental and numerical studies of highly under-expanded hydrogen jets issuing from irregular orifices as a result of sudden releases from high-pressure tanks into the ambient air.

When a supersonic free jet discharges from a nozzle into the atmosphere, different configurations can occur based on the ratio of the stagnation pressure in the tank to the ambient pressure, the geometry of the orifice and the nature of the gas. If the stagnation pressure in the tank is larger than ambient pressure, a supersonic under-expanded free jet forms. A schematic of an under-expanded axisymmetric supersonic jet structure is shown in Fig. 1.2.

When the flow leaves the nozzle owing to the difference between the jet pressure at the nozzle exit and the ambient pressure, the expansion waves, originated at the rim of the opening, tends to lower the gas pressure to the ambient pressure. After propagation of the expansion fans through the air, they are reflected from the outer jet boundary as compression waves. These waves coalesce to form a curved barrel shock. As the flow passes behind the barrel shock where it is still supersonic, the reflected shock forms. The discontinuities including barrel shock, reflected shock and Mach disk are connected at the triple point where the slip line is started.

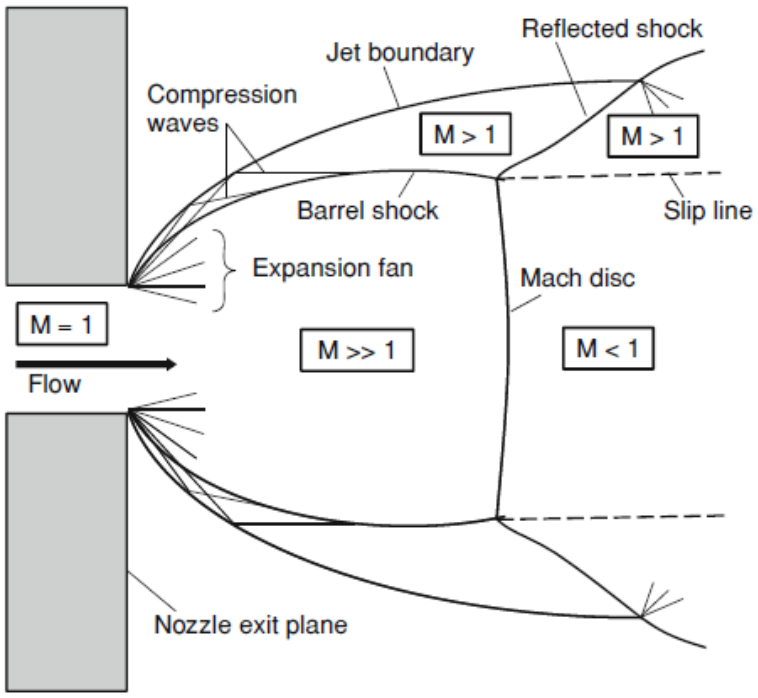

Fig. 1.2: *The schematic of highly underexpanded jet in the near-field region [4]*

The structure of the non-axisymmetric under-expanded jet depends on the pressure ratio of the storage tank to the ambient pressure and the aspect ratio of an elliptic orifice [5]. The incident shock wave formation in non-axisymmetric jet differs between the two symmetry planes of the nozzle. Owing to the less expansion of the jet boundary along the major axis plane compared to the minor axis plane, the tendency for the compression waves to converge and form the barrel shock is greater along the major axis. [5-6] performed an experimental investigation on supersonic jets issuing from elliptical orifices at two different pressure ratios and varying aspect ratios. At a low pressure ratio, the incident shock wave was only observed along the major axis, however, at higher pressure ratio, it was recognized along both minor and major axes. Hence, in the highly underexpanded jet, it can be expected to observe the incident shock wave along both symmetry planes.

A higher spreading rate along the minor axis plane results in the axis switching phenomena which is attributed to the complex factors depends on the jet velocity. The phenomenon produces a rotation of the jet axes, so the major axis becomes the minor axis further downstream. The axis switching in the underexpanded jets can be a result of the interactions between the expansion and compression waves and the jet boundary; however, in the subsonic jets is driven by the vortex self-induction [7].

Among the earliest researches on asymmetric jets is the work by Krothapalli et al. [11]. They investigated incompressible jets through rectangular and elliptical nozzles with aspect ratios greater than 5.5. The results show that a non-circular jet increases the mixing capability. Makarov and Molkov [12] simulated the underexpanded hydrogen jet for both circular and plane nozzle using the ideal gas equation. The hydrogen was released from the reservoir at 35 MPa and the aspect ratio of the plane nozzle was set to 200. It was shown that the plane nozzle jet causes faster mixing in comparison to the round nozzle in the vicinity of the release area. The axis-switching phenomenon was observed during the simulation. It appeared that the hydrogen concentration for both cases with the same mass flow rate drops to the low flammability of 4% at the same location downstream.

1.8 Literature Review

The accidental release of hydrogen from high pressure reservoirs into the low pressure surrounding results in the formation of underexpanded jets and can lead to the auto-ignition or to the dispersion of a hydrogen cloud. Investigation of hydrogen dispersion is reported in various numerical and experimental studies. Some studies have focused on the calculation of the hydrogen concentration and its relation to dimensions of the

circular exit [13] [14]. Han et al. [15] studied the concentration distribution and the mass flux of hydrogen released from a pressurized tank through the different hole sizes (less than 1 mm) and storage pressures (less than 400 bar). They defined the dilution length of a specific hydrogen mole fraction as a distance from the hole. The ideal gas law was applied as the state equation. Results represented a consistent decrease of the centerline hydrogen concentration and the dependency of mass reduction ratio on 1/d for different storage pressures less than 400 bar. Penaeu et al. [16] investigated the release of hydrogen from a 10 MPa pressurized tank through the circular nozzle into both hydrogen and quiescent air. Development of the bow shock and the Mach disk was studied and compared between a binary jet and a single-component jet.

The deviation of the hydrogen behavior from the ideal gas rises with increasing pressure as shown by Mohamed et al. [17]. He used the Beattie–Bridgeman state equation to describe specific heats, internal energy and speed of sound. Cheng et al. [18] simulated the direct release of hydrogen from a 400 bar tank. The differences between the results from the ideal gas law and the real gas law were presented. The Abel Nobel real gas law was used. It was concluded, by applying the ideal gas law at this pressure, the hydrogen mass flow rates were overestimated by 35% in the first 25 seconds of release. Real gas results show a longer horizontal extent and larger volume hydrogen clouds which lead to the incorrect estimation of clearance distance and hazardous zones. The Abel Nobel equation of state was incorporated into the numerical simulation of hydrogen release from higher tank pressure of 70 MPa. By comparing the corresponding results with the results from the ideal gas simulation, it was concluded that applying the real gas law is necessary for studying the discharging of hydrogen from a pressurized tank with storage

pressure greater than 10 MPa and the Abel Nobel law provides an accurate calculation [19]. Hence, in the current study, the Abel Nobel real gas law is applied due to the high pressure storage of 70 MPa.

Other studies have focused on the evaluation of the ignition and the auto-ignition possibility of the hydrogen release. Radulescu et al. [20-21], analyzed the effect of the volumetric expansion on the ignition of high pressure hydrogen release in a diffusion layer by applying the Lagrangian unsteady diffusion-reaction model. It was demonstrated that the strong expansion can lessen the ignition possibility. Furthermore, it was shown that for each storage pressure there exists a size of the hole that separates the non-ignition region from the auto-ignition region. Many researches have been conducted to clarify the effects of tube length and tube diameter on the auto-ignition possibility of the high-pressure hydrogen release [22-25]. Golub V. et al. [22] investigated the hydrogen self-ignition in tubes both numerically and experimentally. The effect of the shape of the release tube on the self-ignition was analyzed. Two different shapes of the tube were considered, circular and rectangular. In addition, the relation between the storage pressure and the possibility of self-ignition was examined. It was shown that the auto-ignition in a rectangular tube occurred at the lower pressure compared to its equivalent circular tube.

Yamada E. et al. [24-25] carried out a direct numerical simulation (DNS) with a detailed chemical model to study the ignition of high pressure hydrogen (40 MPa) discharging into air. By maintaining the same tube diameter of 4.8 mm, the effect of varying tube lengths was evaluated. It was found that there is a relation between the length of the tube and the auto-ignition. Longer tube provides the enough space for hydrogen and air to mix better around the exit, and in turn, the higher possibility of the auto-ignition. Very

detailed direct numerical simulation DNS which is made for smaller release pressures and for longer release tubes, lead to the similar conclusions [27-28]. Furthermore, it was recognized that longer tubes increase the ignition probability and for a higher release pressure, an auto-ignition can occur inside the release tube. This effect is related to the better mixing of hydrogen and air through the molecular diffusion.

In many of these studies Computational Fluid Dynamics (CFD) was used and it was shown to be a powerful tool that provides a good agreement with experimental data [29];

But most of the studies about hydrogen safety issues were focused on the circular nozzles and the development of hydrogen jet exiting from a standard round exit hole. Thus, in this work, Computational Fluid Dynamics is applied to study the near exit jet as this is the critical location for auto-ignition. The novelty of this work is that the influence of the exit geometries including elliptical, expanding and circular on the jet behavior is investigated. Although the study of the ignition of hydrogen jet is not the objective of this work, the obtained results will be applied as an input data to investigate the possibility of an auto-ignition and an ignition in the near exit jet in the future.

1.9 Thesis Outline

The main contents of the following chapters are as follows.

Chapter 2 introduces the equations describing fluid flow and moving mesh, followed by the discussion on methodologies for solving these equations and applied numerical methods including the discretization schemes, techniques to calculate the boundary fluxes and dealing with shock instabilities.

Chapter 3 discusses the physical model, meshing and partitioning the discretized domain for parallel computing. The varying types of orifices and the information related to their geometries and dimensions are provided. The final section of the chapter defines the applied initial and boundary conditions to simulate the pressurized hydrogen release into air.

In chapter 4, the numerical results of the hydrogen release from a high-pressure tank into air through the fixed circular and elliptical orifices with the same area are presented and compared.

In chapter 5, the various configurations of moving orifices are studied and the results are compared with those from the orifices with the constant area.

Chapter 6 draws conclusions and summaries on the study done on this work which is followed by the recommendations for future works.

Chapter 2

GOVERNING EQUATIONS AND NUMERICAL TECHNIQUES

This chapter outlines the equations governing fluid flow and the method of applying moving mesh along with the numerical schemes and techniques used for the discretization of space and time and the numerical flux calculations.

2.1 Unsteady Compressible Euler Equations

Abrupt discharging of hydrogen from a high pressure tank into a low pressure quiescent environment causes a highly underexpanded jet. So in this study, due to the high Reynolds number in the vicinity of the release hole, convection dominates the effect of viscosity and diffusivity. Viscosity effects are restricted to the narrow high-gradient regions such as shock waves and vorticity layers which are not developed at the initial stage of the formation of highly under-expanded jets and the flow can be treated as an inviscid and the compressible Euler Equations can model the flow field evolution [21][30].

In the absence of any source terms, the unsteady Euler equations in conservative form based on fixed grid computations which represent the conservation of mass, momentum and energy can be written as follows [31]:

$$\frac{\partial \vec{U}}{\partial t} + \vec{\nabla}.\vec{\vec{F}}(U) = 0, \tag{2.1}$$

Where the vector of conserved variables, $\vec{U}$, and convective fluxes, $\vec{\vec{F}}$ are defined by

$$\vec{U} = \begin{bmatrix} \rho \\ \rho u \\ \rho v \\ \rho w \\ \rho E \end{bmatrix}, \vec{\vec{F}} = \left(\begin{bmatrix} \rho u \\ \rho u^2 + P \\ \rho uv \\ \rho uw \\ \rho uH \end{bmatrix} \begin{bmatrix} \rho v \\ \rho vu \\ \rho v^2 + P \\ \rho vw \\ \rho vH \end{bmatrix} \begin{bmatrix} \rho w \\ \rho wu \\ \rho wv \\ \rho w^2 + P \\ \rho wH \end{bmatrix} \right) \tag{2.2}$$

Where u, v and w are the fluid velocity along the x, y and z Cartesian coordinates, ρ is the density and P represents the pressure. The total energy in terms of internal energy and kinetic energy, E, and the total enthalpy, H, are given by:

$$E = e_i + \frac{1}{2}(u^2 + v^2 + w^2) \tag{2.3}$$

$$H = E + \frac{P}{\rho} \tag{2.4}$$

The internal energy can be calculated by the following equation.

$$e_i = c_v T \tag{2.5}$$

And the vector of primitive variables is $\vec{W} = \begin{bmatrix} \rho \\ u \\ v \\ w \\ P \end{bmatrix}$.

Since a dynamic mesh algorithm is employed in this study to simulate the enlarging orifices, the Euler equations must be modified in several cases. Considering the dynamic mesh formulation in which the convecting velocity components are the relative velocity

between fluid and coordinates for a time-dependent system, the modified conservative fluxes in the Euler equations will be as follows:

$$\vec{\vec{F}} = \left(\begin{bmatrix} \rho(u-w_x) \\ \rho(u-w_x)u + P \\ \rho(u-w_x)v \\ \rho(u-w_x)w \\ \rho(u-w_x)E + uP \end{bmatrix} \begin{bmatrix} \rho(v-w_y) \\ \rho(v-w_y)u \\ \rho(v-w_y)v + P \\ \rho(v-w_y)w \\ \rho(v-w_y)E + vP \end{bmatrix} \begin{bmatrix} \rho(w-w_z) \\ \rho(w-w_z)u \\ \rho(w-w_z)v \\ \rho(w-w_z)w + P \\ \rho(w-w_z)E + wP \end{bmatrix} \right) \tag{2.6}$$

Where w_x, w_y, w_z are the grid speeds along the coordinate directions, which represent the time rates of change of the position vectors. In the case of fixed mesh, the grid velocities are not considered and the cell volume is not time-dependant. To simulate the hydrogen jet escaping through the expanding orifices, the dynamic mesh model based on the spring analogy is used [32]. This method will be described in the following sections.

A Discrete form of the Euler equations based on the implicit finite volume method can be written as:

$$|V_i| \frac{\vec{U}_i^{n+1} - \vec{U}_i^{n}}{\Delta t} + \sum_{over\ \partial V_i} \vec{\vec{F}}_{\partial V_i}^{n+1} .\ \vec{n}_{\partial V_i} \Delta S_{\partial V_i} = 0 \tag{2.7}$$

Where $\vec{n}_{\partial V_i}$ is the unit normal vector and $\Delta S_{\partial V_i}$ refers to the surface area of the boundary faces. Considering moving mesh, these terms are time dependent and they change with time, but they are constant for the fixed mesh.

By linearizing the convective fluxes using a linear Taylor expansion, the discretized implicit scheme of the Euler equations can be written in the following form:

$$\left(\frac{|V_i|}{\Delta t} \vec{\vec{I}} + \sum_{over\ \partial V_i} \left(\frac{\partial \vec{\vec{F}}}{\partial \vec{U}} \right)_{\partial V_i}^{n} . \vec{n}_{\partial V_i} \Delta S_{\partial V_i} \right) \delta \vec{U}_i^{n+1} = - \sum_{over\ \partial V_i} \vec{\vec{F}}_{\partial V_i}^{n} . \vec{n}_{\partial V_i} \Delta S_{\partial V_i} \tag{2.8}$$

Where V_i is the cell volume and for the fixed mesh it is constant. $\frac{\partial \vec{\vec{F}}}{\partial \vec{U}}$ is the conservative flux-Jacobian. The system of linear equations is solved by means of a fully implicit scheme which has an accuracy of the first and second orders in time and space, respectively.

Convective fluxes, $\vec{\vec{F}}^{n}_{\partial V_i}$, are evaluated using Roe-MUSCL scheme. This method is among the most efficient schemes to calculate the convective fluxes at the boundaries especially for the Euler simulations. The second order Roe-MUSCL scheme is written as follows

$$F_{ij} = \frac{1}{2}\left[{}^{c}F(U_{IJ}) + {}^{c}F(U_{JI})\right] - \frac{1}{2}\partial^{c}F_{IJ} \tag{2.9}$$

Where the interface values related to adjacent cells are evaluated using the linear extrapolation as

$$U_{IJ} = U_I + \frac{1}{2}\,(\nabla U)_I.\vec{n}_{IJ} \tag{2.10}$$

$$U_{JI} = U_J + \frac{1}{2}\,(\nabla U)_J.\vec{n}_{JI} \tag{2.11}$$

In which $(\nabla U)_I$ and $(\nabla U)_J$ are the gradients of variables in cell I and cell J.

And the change in the flux is given by

$$\partial^{c}F_{IJ} = \left|A_{IJ}\right|\partial U_{IJ} \tag{2.12}$$

Where

$$\partial U_{IJ} = U_{JI} - U_{IJ} \tag{2.13}$$

The GMRES iterative solver is used to solve the linearized system of Euler equations (equation (2.8)) at each time step [34].

2.2 VanLeer-Van Albada limiter

To avoid the oscillations generated near the shock or discontinuity regions, the Van Leer-Van Albada limiter is applied to limit the variable values and take the gradient of the interpolation by a function f (x,y) which is called limiter. The limiter controls the accuracy of the spatial approximation at the thin layer near the exit hole (|Z|=0.1orifice diameter) and high pressure gradient regions where the second order approximation is switched to the first order accuracy to prohibit the numerical instabilities in these regions.

The VanLeer-VanAlbada limiter is written as

$$f(x,y) = \begin{pmatrix} 0 & if\ xy < 0 \\ \dfrac{(y^2+\varepsilon)x + (x^2+\varepsilon)y}{x^2+y^2+2\varepsilon} & else \end{pmatrix} \tag{2.14}$$

Where ε is a very small number.

2.3 Real gas Equation of State (EOS)

The system of Euler equations is completed by the equation of state which correlates the density of a gas to pressure and temperature. The ideal gas law is approximately accurate at low pressure and cannot precisely predict the solution of a highly under-expanded jet under the high storage pressure like P_i=70MPa [17] [18] [19] [27] [32] [33] [35] [36] [37] [38] [39]. Hence, in this study owing to the high pressure flow (P_i=70MPa), the Abel Nobel EOS is utilized as a real gas equation which relates pressure, temperature and density with just one constant. The accuracy of this equation is almost the same as the more complicated real gas equations such as Beattie-Bridgeman but it gives the higher

stability in simulation of two species flow and also its simplicity reduces the CPU time and computational cost [35].

The Abel Nobel EOS is defined as

$$p = \frac{R_{mix}T}{(v-b)} = (1-b\rho)^{-1}\rho R_{mix}T = \zeta\rho R_{mix}T, \quad b = 0.00775\ m^3/kg \tag{2.15}$$

Where R_{mix} is the average value of the gas constant for the hydrogen-air mixture and it is calculated from equation (2.20). ζ is the compressibility factor which is a function of density in the real gas model, however it equals to one for the ideal gas EOS [32]. The plot of the compressibility factor as a function of pressure at 300 K temperature is presented in Fig. 2.1. It is shown that by increasing the pressure, compressibility factor deviates from unity which refers to the ideal gas assumption and it shows that the higher volume is required to store hydrogen based on real gas law compared to the ideal gas assumption.

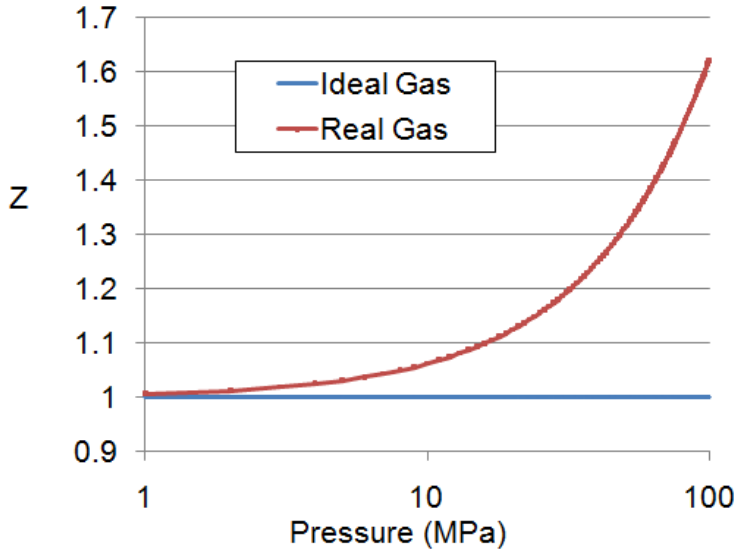

Fig. 2.1: *Compressibility factor of hydrogen at 300 K based on the Abel Nobel EOS [32]*

The speed of sound based on the Abel Nobel real gas law can be written as

$$a = \frac{v}{v-b}\sqrt{\frac{C_p}{C_v}P(v-b)} \tag{2.16}$$

Where specific heat at constant volume based on the Abel Nobel equation of state equals to its equivalent value in the ideal gas law ($\tilde{C}_v$) and specific heat at constant pressure can be found by the equation (2.17)

$$C_v = \tilde{C}_v \tag{2.17}$$

$$C_p = R - C_v \tag{2.18}$$

Hence, the specific heat ratio in the Abel Nobel equation is the same as the ideal gas law and can be assumed constant. Furthermore, the isentropic exponents, γ, of hydrogen and air during the simulation are constant and equal to their initial values (γ =1.4) at the initial temperature of T=300 K.

2.4 Transport (Advection) Equation

To describe the convection of hydrogen into the ambient air and track the shape and location of the contact surface between hydrogen and air, the advection equation is implemented as follows

$$\frac{\partial c}{\partial t} + \frac{\partial (cu)}{\partial x} + \frac{\partial (cv)}{\partial y} + \frac{\partial (cw)}{\partial z} = 0 \tag{2.19}$$

Where c is a step function and it is called fraction function. A unit value of fraction function ($c = 1$) corresponds to a cell occupied only by air and a zero value ($c = 0$) indicates a cell full of hydrogen. The fraction functions between zero and one ($0 < c <$

1) indicate the discontinuity region and shows the cell contains the interface between hydrogen and air. Hence, based on the local value of c, the related properties will be designated to each control volume.

This equation, while being solved, is segregated or decoupled from the Euler equations. It means that at the end of the each time step and after solving the linear system of equations by iterative GMRES solver, the advection equation is solved separately by the same solver. After calculating c, the average value of the gas constant, R, for the hydrogen-air mixture is solved from the following equation

$$R_{mix} = R_{H_2}(1 - c) + R_{air}c \tag{2.20}$$

Given the molecular weights of hydrogen and air which are $\mathrm{M}_{\mathrm{H}_2} = 2.016$ g/mol and $\mathrm{M}_{\mathrm{air}} = 28.96$ g/mol, their specific gas constants will be $R_{H_2} = 4124\ J/kgK$ and $R_{air} = 287\ J/kgK$ respectively. The specific gas constants of both gases maintain their initial values during the simulation.

By applying the dynamic mesh and using the relative velocities between fluid and moving coordinates, the advection equation will be modified and re-written as

$$\frac{\partial c}{\partial t} + \frac{\partial (c(u - w_x))}{\partial x} + \frac{\partial (c(v - w_y))}{\partial y} + \frac{\partial (c(w - w_z))}{\partial z} = 0 \tag{2.21}$$

Where w_x, w_y, w_z are the grid speeds along the coordinate directions.

2.5 Dynamic Mesh: Spring Analogy Method

A moving mesh algorithm is used in which the unstructured grids deform due to the imposed motion of the domain boundary. Based on the spring analogy method, each edge

of each cell is modeled by a linear spring which connects the end vertices [32]. The stiffness of the spring is inversely proportional to the edge length. As the length of the edge decreases, the stiffness of the spring increases, so, the short edges are stiffer than the longer ones. The stiffness in the linear spring method prevents the collision of neighboring nodes; however it cannot prevent the nodes from crossing the edges and may produce the mesh with negative volume elements [34].

The stiffness of the edge connecting nodes I and j in three dimensional mesh can be defined as

$$K_{ij} = \frac{1}{\left(\left(x_i - x_j\right)^2 + \left(y_i - y_j\right)^2 + \left(z_i - z_j\right)^2\right)^{1/2}} = \frac{1}{l_{ij}} \tag{2.22}$$

Where (x_i, y_i, z_i) and (x_j, y_j, z_j) are the coordinates of nodes *i* and *j*. Since in this work, the cross sectional surfaces of the orifices will be deformed, there is no displacement along the z axis.

To satisfy the static equilibrium for the interior displacements by imposing the motion on the boundary nodes, the following equations are solved iteratively

$$\Delta x_i^{m+1} = \frac{\sum_j^n K_{ij} \Delta x_j^m}{\sum_j^n K_{ij}} \tag{2.23}$$

$$\Delta y_i^{m+1} = \frac{\sum_j^n K_{ij} \Delta y_j^m}{\sum_j^n K_{ij}} \tag{2.24}$$

Where n refers to all the nodes connected to the node i, and m denotes the number of iterations.

After convergences of the equations (2.23) and (2.24), the positions of the interior nodes at the next time step will be updated as follows

$$x_i^{n+1} = x_i^n + \Delta x_i \tag{2.25}$$

$$y_i^{n+1} = y_i^n + \Delta y_i \tag{2.26}$$

Since our models consist of both moving and non-moving regions, the spring method is only influenced the moving section by defining the conditions of their respective nodes and cells.

Chapter 3

NUMERICAL SIMULATION

A 3D parallel in-house code is modified to simulate the discharge of hydrogen from a high pressure reservoir into air through varying types of orifices. Since, in recent years, automobile manufacturers have been considering and implementing the 70MPa hydrogen storage to maximize the FCVs range by increasing the storage capacity and providing almost the same storage density as liquid hydrogen, therefore, in this work, 70 MPa storage pressure is considered to evaluate the dispersion of hydrogen in the case of an incident leak through different geometries of exit holes. The obtained results are compared with those under lower filling pressure of 10 MPa.

3.1 Computational Domain, Meshing and Partitioning

The 3D computational domain used in this study is shown in Fig. 3.1. The model consists of a circular cylinder with the diameter of 150 mm and the axial length of 100 mm as a reservoir containing hydrogen gas at the high pressure and a 2mm straight nozzle leading to the exit at the ambient pressure with the dimensions of 100 mm × 100 mm ($20D_{largest\ orifice}$). To examine the influence of orifice geometry on the jet behavior and the ignition possibility, three different shapes of orifices are considered including fixed circular, fixed elliptic and expanding exits.

GAMBIT is used as the pre-processing software to generate the mesh. Since our in-house code uses tetrahedral elements/volumes, the mathematical domain is discretized into an

unstructured tetrahedral mesh. The discretized domain contains almost 2 million nodes and 12 million tetrahedrons. To ensure that the mesh is sufficiently refined to resolve large pressure gradients and all relevant flow features in the proximity to the exit area, a very fine grid resolution is generated in this region. Then the element size increases with a growth rate of 1.02 downstream and in the regions far from the exit (Fig. 3.2). This gradual transition in grid size prevents numerical errors associated with a sudden increase in grid size and also it results in the reduction of the CPU time and in turn, the computational cost.

METIS software package is used to distribute the finite volume mesh to the processors and partition the discretized domain for parallel computing, since it produces high quality partitions. The partnmesh algorithm is utilized which converts the mesh into a nodal graph, i.e. each node of the mesh is assigned as a vertex of the graph.

Parallel computations are carried out on Cirrus (Concordia University parallel-computing cluster) and Mammouth-parallel II (located at the Université de Sherbrooke) supercomputers. The computational domains are decomposed into 64 partitions using the Cirrus cluster and into 120 subdomains using the Mammouth-parallel II cluster.

To study the model sensitivity to grid resolution, three different grid levels including the fine mesh with almost 3 million nodes and 17.5 million elements, the medium mesh with nearly 2 million nodes and 12 million elements and the coarse mesh with virtually 1 million nodes and 6 million elements are considered. The results of the grid sensitivity study will be shown in chapter 4.

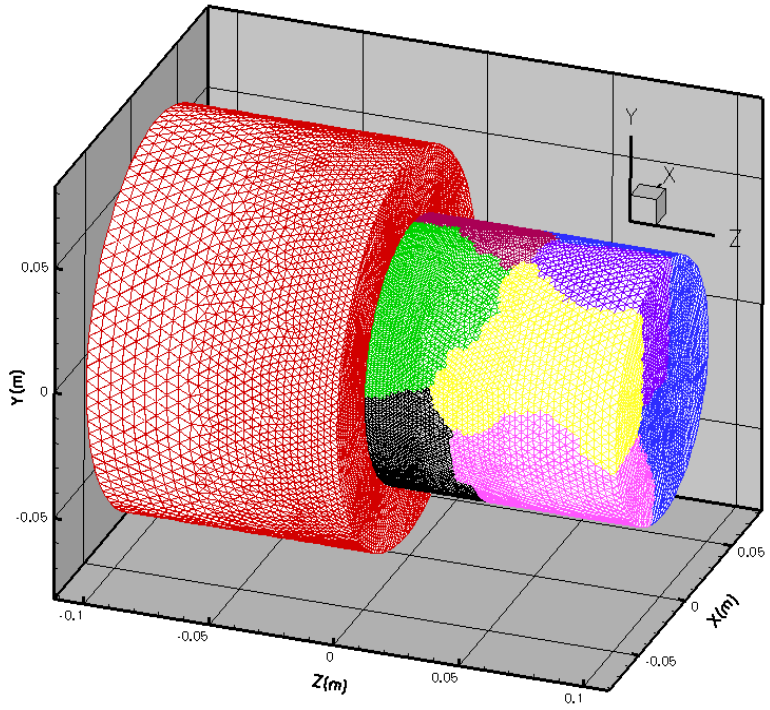

Fig. 3.1: *The unstructured tetrahedral mesh with decomposed zones (partially shown)*

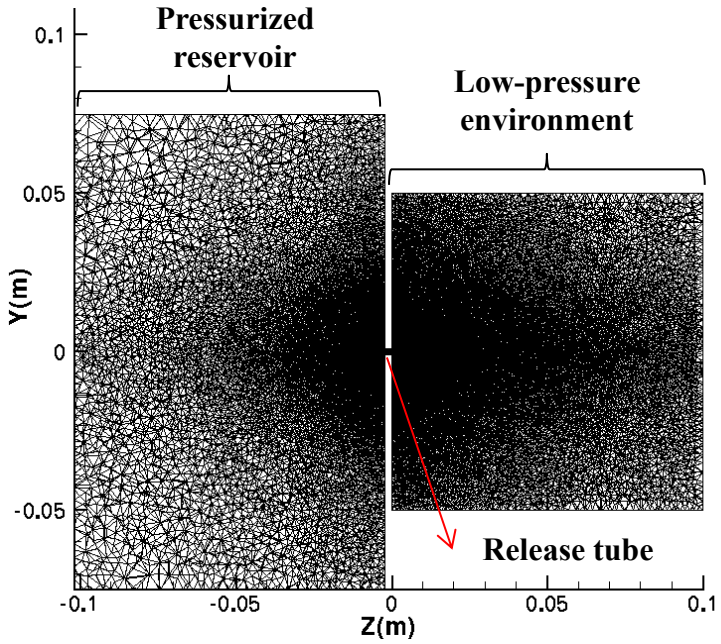

Fig. 3.2: *The 2D slice of the discretized domain*

3.1.1 Orifices with the constant areas: Fixed Elliptical and Circular Orifices

The parameter under consideration for comparable circular and elliptical orifices is the same exit area. Therefore, three different areas based on 1 mm, 2 mm and 5 mm diameters of circular exits are investigated. For each case, two varying elliptical shapes with the aspect ratios (major axis/minor axis) of AR=4 and AR=6 are considered and compared with their comparable circular counterparts (AR=1). In these cases, the elliptical orifice can be regarded as a model of a crack. The major axes in all elliptical cases are perpendicular to the axial axes of the pressurized tanks. The dimensions of all the test cases are listed in Table 3.1 and the cross sectional surfaces of the circular and elliptical exit geometries with the aspect ratios of AR=1, AR=4 and AR=6 and the identical area of A=19.63 mm^2 are depicted in Fig. 3.3.

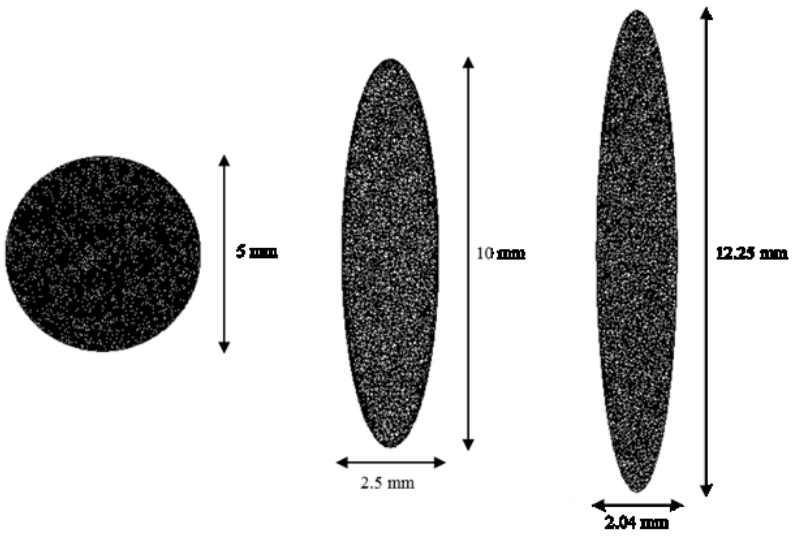

Fig. 3.3: *Cross sectional surfaces of the varying shapes of orifices (A=19.63 mm^2)*

Table 3.1: *The dimensions of different types of orifices*

Area (A) =0. 8 (mm^2)			
Orifice Type	Major Axis, a (mm)	Minor Axis, b (mm)	Aspect Ratio, a/b
Circular	1	1	1
Elliptical 1	2	0.5	4
Elliptical 2	2.45	0.41	6
Area (A) =3. 14 (mm^2)			
Orifice Type	Major Axis, a (mm)	Minor Axis, b (mm)	Aspect Ratio, a/b
Circular	2	2	1
Elliptical 1	4	1	4
Elliptical 2	5	0.82	6
Area (A) =19. 63 (mm^2)			
Orifice Type	Major Axis, a (mm)	Minor Axis, b (mm)	Aspect Ratio, a/b
Circular	5	5	1
Elliptical 1	10	2.5	4
Elliptical 2	12.25	2.04	6

3.1.2 Expanding Orifices

Two cases of the round orifice with initial diameters of D_i=1 mm and D_i=2 mm are considered to evaluate the expanding exit and compare the results to the fixed circular opening with the same initial diameters. The growth rate of the circular hole along the radial direction is 0.2 mm/μs, nevertheless, this rate in a case that a circular hole is stretched into an elliptical orifice only limited to the y-direction velocities of the boundary nodes. The boundary nodes move along the normal surface direction (radial axis) with the proposed speed based on the spring analogy. As mentioned in the previous chapter, the moving region of the computational domain is restricted to the pressurized vessel and the exit hole, so, only the boundary nodes related to this region move and have displacements. Excluding the cross sectional area of the release tube, the dimensions of the domain containing pressurized tank and low-pressure domain along with the length of the release tube are preserved in all cases.

3.2 Boundary and Initial Conditions

As stated before, the viscosity effect and the heat transfer between the gas inside the reservoir and its surrounding are neglected, therefore all the solid walls of the high pressure tank and the release tube are assumed to be slip free and adiabatic. The non-reflecting far field boundary condition was applied around the circumference of the low pressure cylinder (external environment) and at the end of the cylinder. As it was indicated in the Euler equations, it is supposed that there are no external forces. Hence, the effect of the gravity on the fluid is neglected.

The flow is initially at rest with zero velocity. The reservoir and the half of the tube filled with hydrogen at two different pressures of 10 MPa or 70 MPa and the rest with air at the

atmospheric pressure (0.101325 MPa). The initial temperature is 300 K everywhere inside the domain. The initial contact surface is assumed to be located in the middle of the release tube. The air mixture fraction is defined as c=1 and the hydrogen mixture fraction is c=0. The initial conditions are presented in Table 3.2.

Table 3.2: *Initial Conditions*

Initial Reservoir Pressure	70MPa & 10MPa
Initial Temperature	300 K
Air mixture fraction	1
Hydrogen mixture fraction	0
Hydrogen & air isentropic exponent (γ)	1.4
Molecular mass of hydrogen (M_{H_2})	2.016 g/mol
Molecular mass of air (M_{air})	28.96 g/mol

3.3 Time Step Calculation

Owing to the rapid changes of flow characteristics in regions with discontinuities like shock waves and applying the first order implicit scheme for time discretization along with high level grid resolution, a very small time step (10^{-6}-10^{-10}) is required to achieve the stable and accurate solutions.

The time step at each iteration is the minimum value of the local time steps. The local time step for each element based on the given initial and maximum CFL numbers is calculated from the following relation

$$\Delta t_j = \frac{CFL}{a_j + |V_j|} \Delta l_j \tag{3.1}$$

Where a_j is the speed of sound which is calculated from equation (2-16), $|V_j|$ is the flow velocity at element j and Δl_j refers to the length scale of the element. Since hydrogen have the lowest density and in turn the highest sonic speed, the calculated time step is very small and the numerical simulation of the hydrogen jet is very time-consuming.

The initial and maximum CFL numbers are different between the cases with fixed mesh and moving mesh. For fixed mesh, the initial CFL number is set to 0.15. This value is constant for the first 1000 iterations, and then it is augmented with a rate of 0.001 at each time iteration to reach the maximum CFL which in this case is defined as 0.8.

The initial and maximum CFL numbers of moving cases are defined as 0.3 and 5 respectively but the increment step is lower than the fixed cases and is set to 0.0002 at each iteration.

Hence, based on the predefined CFL numbers and the high velocity of hydrogen flow, the initial time step is about 10^{-10}.

Chapter 4

HYDROGEN RELEASE FROM FIXED ORIFICES: ELLIPTICAL AND CIRCULAR HOLES

In this chapter, after presenting the results of the grid convergence study, the comparative studies between the hydrogen release from elliptic orifices and circular orifices under different conditions in terms of the orifice geometry and the storage pressure are carried out. The release of hydrogen from 70 MPa and 10 MPa pressurized tanks through fixed elliptical orifices with two different aspect ratios are investigated and dispersion characteristics and the jet behavior are quantified. The obtained results are compared with those from the comparable fixed standard circular orifices with the same areas.

4.1 Grid Sensitivity Study

In order to guarantee mesh independent results and achieve an accurate and converged solution, the grid sensitivity study for the case with an area of 19.63 mm^2 and aspect ratio of 4 is conducted. As mentioned before, three levels of grid refinement such as fine, medium and coarse with almost 3 million, 2million and 1 million nodes are generated. The contact surface pressure and flow characteristics along the centerline are reported to visualize convergence of the solutions as the grids are refined. The results are shown in Fig. 4.1 and Fig. 4.2. It is recognized that the obtained results are not so sensitive to the grid size and changing the spatial resolution does not significantly affect the numerical

solution, but the coarse mesh with 1 million nodes makes more numerical diffusions especially in the regions with high pressure gradient, i.e. near the discontinuities. Therefore, the 2 million-node mesh is applied in all cases to damp the flow instabilities. However, the flow field along the centerline axis and near the exit is very well captured even with the coarse mesh (Fig. 4.2).

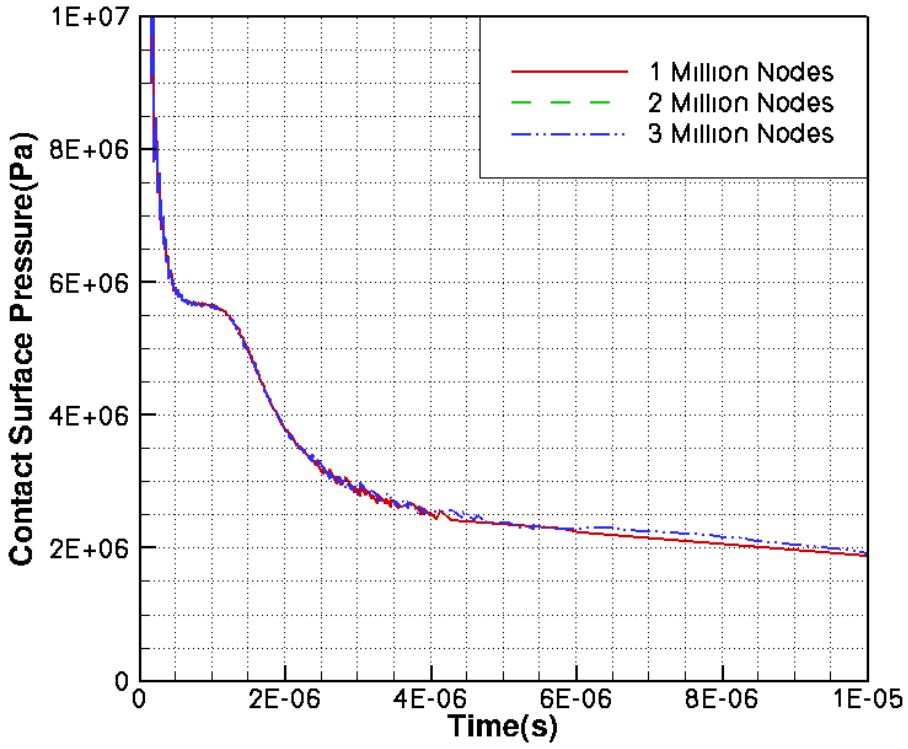

***Fig. 4.1**: Grid convergence study: contact surface pressure along the centerline*

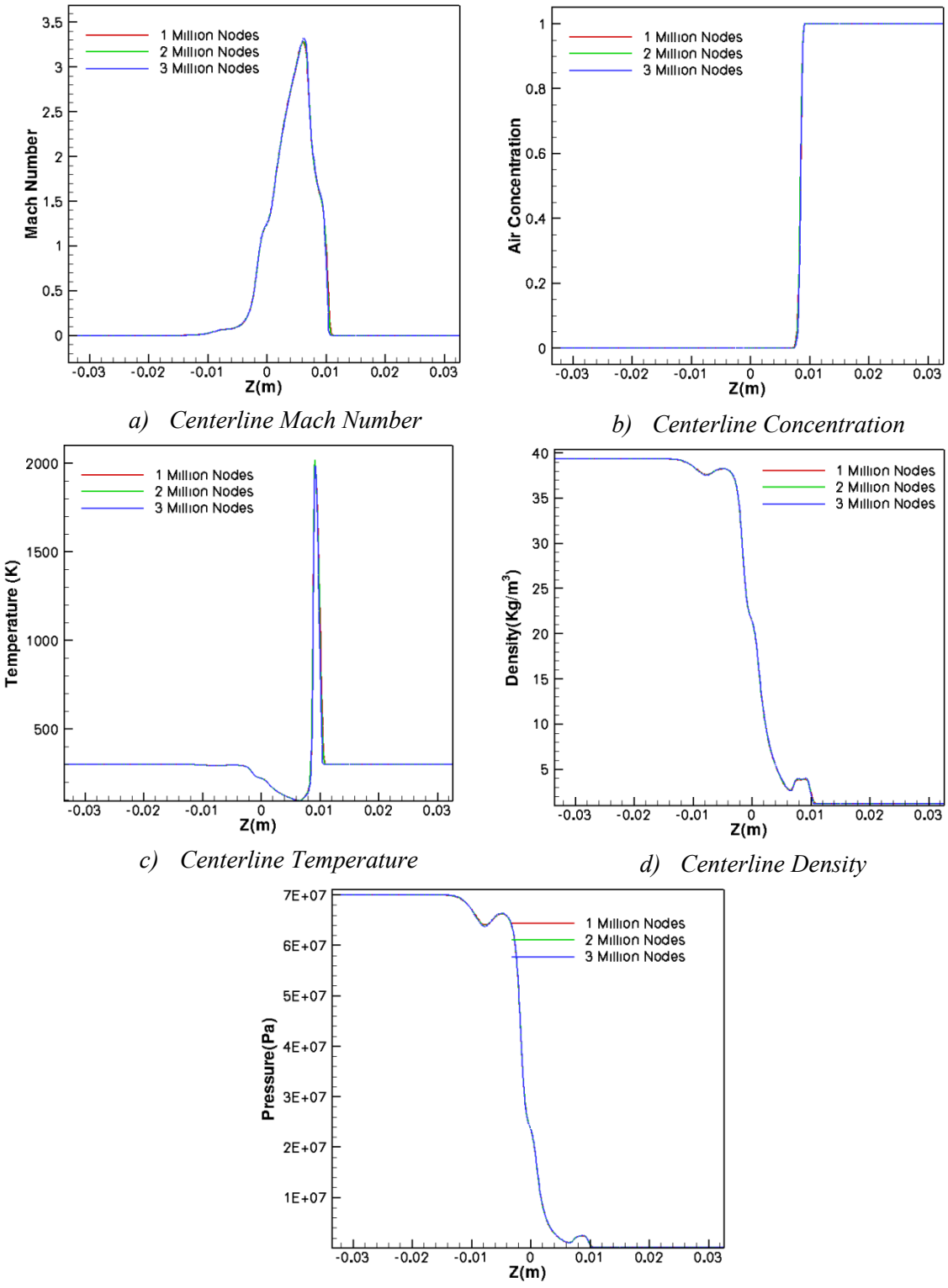

a) Centerline Mach Number

b) Centerline Concentration

c) Centerline Temperature

d) Centerline Density

e) Centerline Pressure

Fig. 4.2: *Grid Convergence Study: flow characteristics along the centerline after 5 μs of hydrogen release into air*

4.2 Evaluation of the contact surface location and the release time

As the effects of the orifice geometry on the gas jet and auto-ignition are dominant in the near field flow and diminish in the far field, this study focuses on the near exit jet behavior. Therefore, mainly the initial 10 μs of hydrogen dispersion are examined.

Owing to the existence of two different species (hydrogen and air) with their specific properties, one of the major issues in this study is to capture the contact surface position accurately compared to the location of the moving shock based on the real gas law and advection equation which is decoupled from the Euler equations. To evaluate the release time and to compare the locations of the hydrogen-air interfaces between the jets starting from varying shapes of orifices with different areas, the time histories of the contact surface location along the jet centerline for all cases under initial storage pressure of 70 MPa and 10 MPa up to 10 μs of hydrogen release are presented in Fig. 4.3 and Fig. 4.4, respectively. It should be pointed out that the release time refers to the specific time at which the hydrogen-air contact surface that is initially located in the middle of the pressurized vessel, reaches the exit hole which is located at z=0. As it is noticed from the time histories of the interface locations (Fig. 4.3), the release time is not affected by the shape of the orifices and even various areas under the same storage pressure of 70 MPa and it equals to t=0.6 μs. The contact surface locations corresponding to varying geometries of orifices including elliptic and circular holes with an equal area are virtually the same up to 2.0μs.

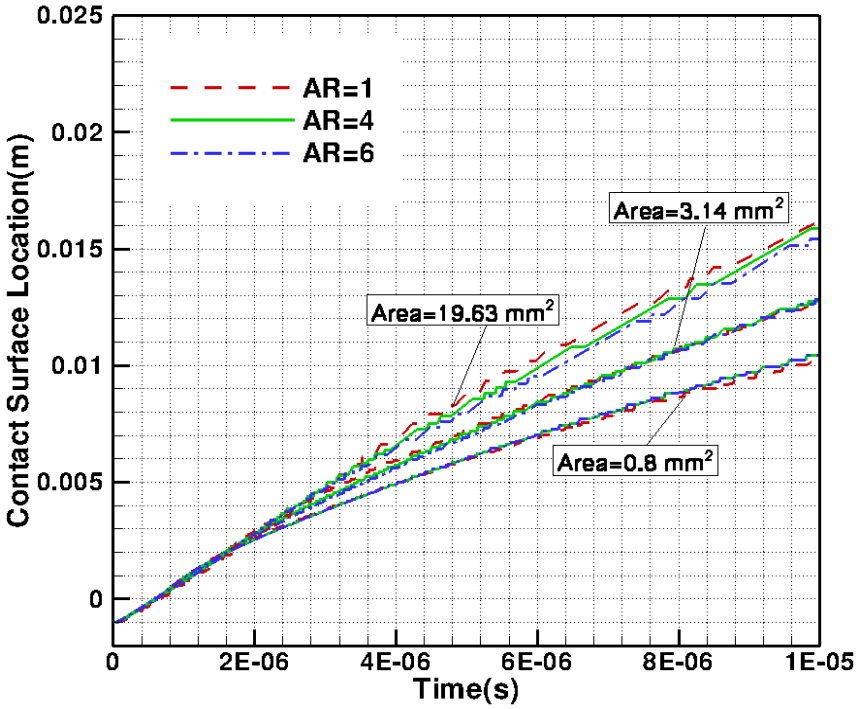

Fig. 4.3: *Contact surface locations as a function of time, fixed orifices, P=70MPa*

After 2.0 μs, the interface location differs by changing the orifice area. It is observed that the slope of the curve related to the largest area is higher than the others which indicates that a jet issuing from the larger area moves faster into air and its contact surface is ahead of the others. For instance, the hydrogen-air interface at t=10 μs in the case with the area of 19.62 mm^2 progresses into air with the velocity of 1100 m/s or 1.1 mm/ μs, but in the cases with the smaller areas of 3.14 mm^2 and 0.8 mm^2, the interfaces advance with lower speeds of 0.9 mm/ μs and 0.75 mm/ μs, respectively. The interface positions of elliptic and circular jets are slightly the same, nevertheless for the largest orifice area (A=19.63 mm^2), the contact surface corresponding to circular case moves slightly faster than its equivalent from the elliptic orifice.

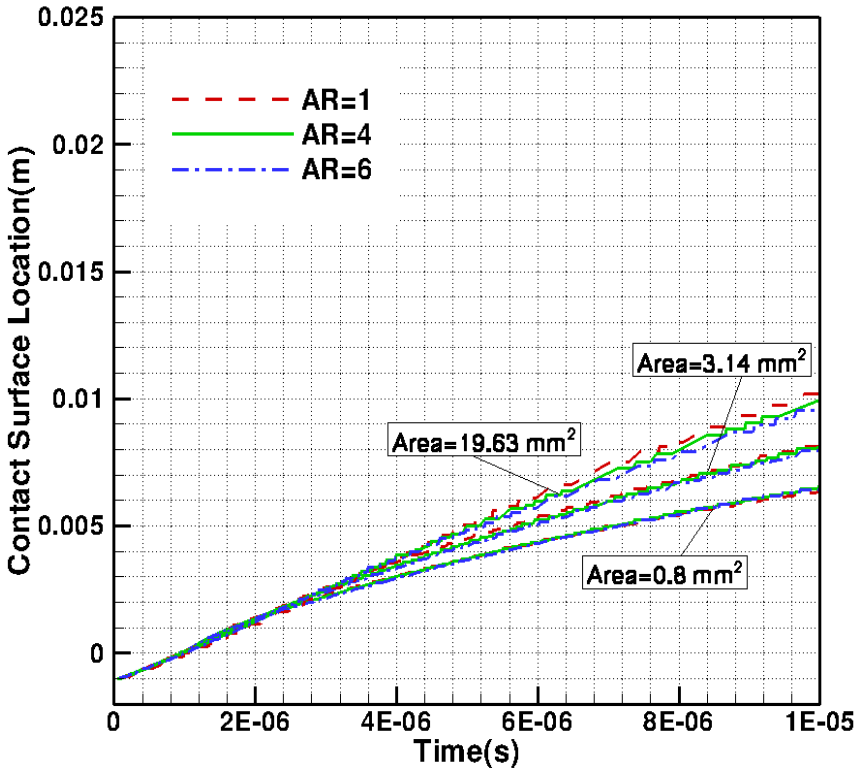

Fig 4.4: *Contact surface locations as a function of time, fixed orifices, p=10MPa*

Reducing the storage pressure to 10 MPa, delays the separation of the locations of hydrogen-air interfaces between varying types of orifices. As it is shown in Fig. 4.4, the moment at which the contact surface locations start to separate is practically 3.0 μs which has a delay compared to 70 MPa jets. As a result, the corresponding release time in all cases with 10 MPa storage pressure is almost 1μs. Similar to the 70 MPa cases, by increasing the orifice area, the related interface location still advances rapidly and there is no significant difference between the locations of interfaces related to elliptic and circular holes. However, the hydrogen/air interface of the jet from 70 MPa moves more rapidly compared to its counterpart in the lower pressure of 10 MPa, since it experiences a higher jet velocity.

4.3 Description of the flow field under the reservoir pressure of 70 MPa

4.3.1 Centerline flow characteristics

The evolution of the centerline Mach number, concentration, temperature, pressure and density for the circular and elliptic hydrogen jet issuing from varying aspect ratios of the orifices (AR=4 & 6) with three different areas under filling pressure of 70 MPa are presented in Fig. 4.5-Fig. 4.13. The flow characteristics are shown at different times, before the interface reaches the exit, at the release time and after the release of hydrogen.

Along the centerline of the jet, as hydrogen starts discharging from the release tube, the pressure continuously decays to a value below the atmospheric pressure. Then, by passing through the Mach disk, the pressure is increased back to the ambient pressure. After a large and continues pressure drop in the release tube, the choked condition is reached at the exit of the pressurized vessel, just before the jet leaves the tube. After the release, the decaying of pressure is completed by a sudden jet expansion into the ambient surroundings. The rate of expansion is a function of the storage pressure, the higher the pressure, the larger the jet expansion into the ambient air. The flow density experiences the same profile as pressure, during the leakage of hydrogen.

As the pressure of the flow decreases by passing through the release tube, the velocity increases until it reaches the sonic velocity at the exit of the nozzle. The incident expansion of the released hydrogen causes the large rise in the velocity of the jet. In all cases after a certain time, the flow reaches the hypersonic velocity. At the end of the expansion of the jet where the flow has the maximum Mach number, the Mach disk is formed. Then, the speed of the jet decreases across the normal shock. The development

of the jet into air causes the generation of the lead shock in front of the contact surface and results the increase in velocity which will be recovered by flow passing through the shock.

The initial temperature inside the reservoir and ambient environment is set to 300 k and the flow is considered to be static. As the jet velocity inside the tube increases, the temperature decreases continuously. After the release of hydrogen and consequently the abrupt jet expansion, the flow temperature is reduced to its lowest peak upstream of the Mach disk. The generation of the Mach disk at the end of the expansion process results in the temperature increase. At the hydrogen-air interface, the temperature profile experiences a discontinuity in which there is a steep rise in the temperature of the air in downstream of the contact surface and it is reduced back to the ambient temperature of 300 K downstream of the lead shock.

By comparing the flow properties distribution before the release of hydrogen from the nozzle and after the release time, the formation of transient hydrogen jet is recognized. As the jet expands into the surrounding air, the high and low peak values of the temperature along the jet centerline experience a monotonic decrease. While the lead shock becomes continuously weaker, the Mack disk becomes stronger as it advances into the expanding gas.

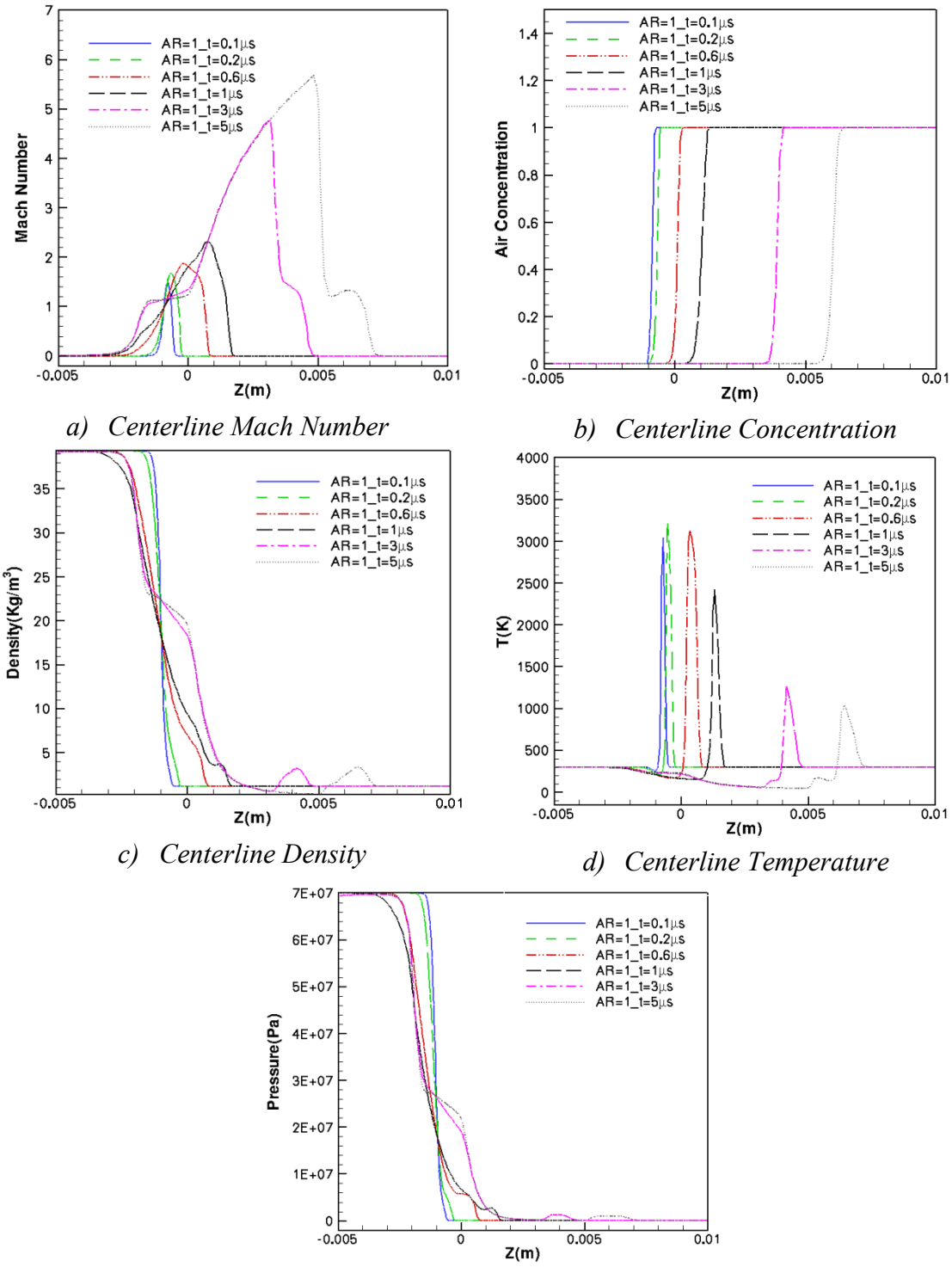

a) Centerline Mach Number

b) Centerline Concentration

c) Centerline Density

d) Centerline Temperature

e) Centerline Pressure

Fig. 4.5: *Flow characteristics along the centerline at different times, circular orifice (AR=1), Area=0. 8 mm^2, P=70 MPa*

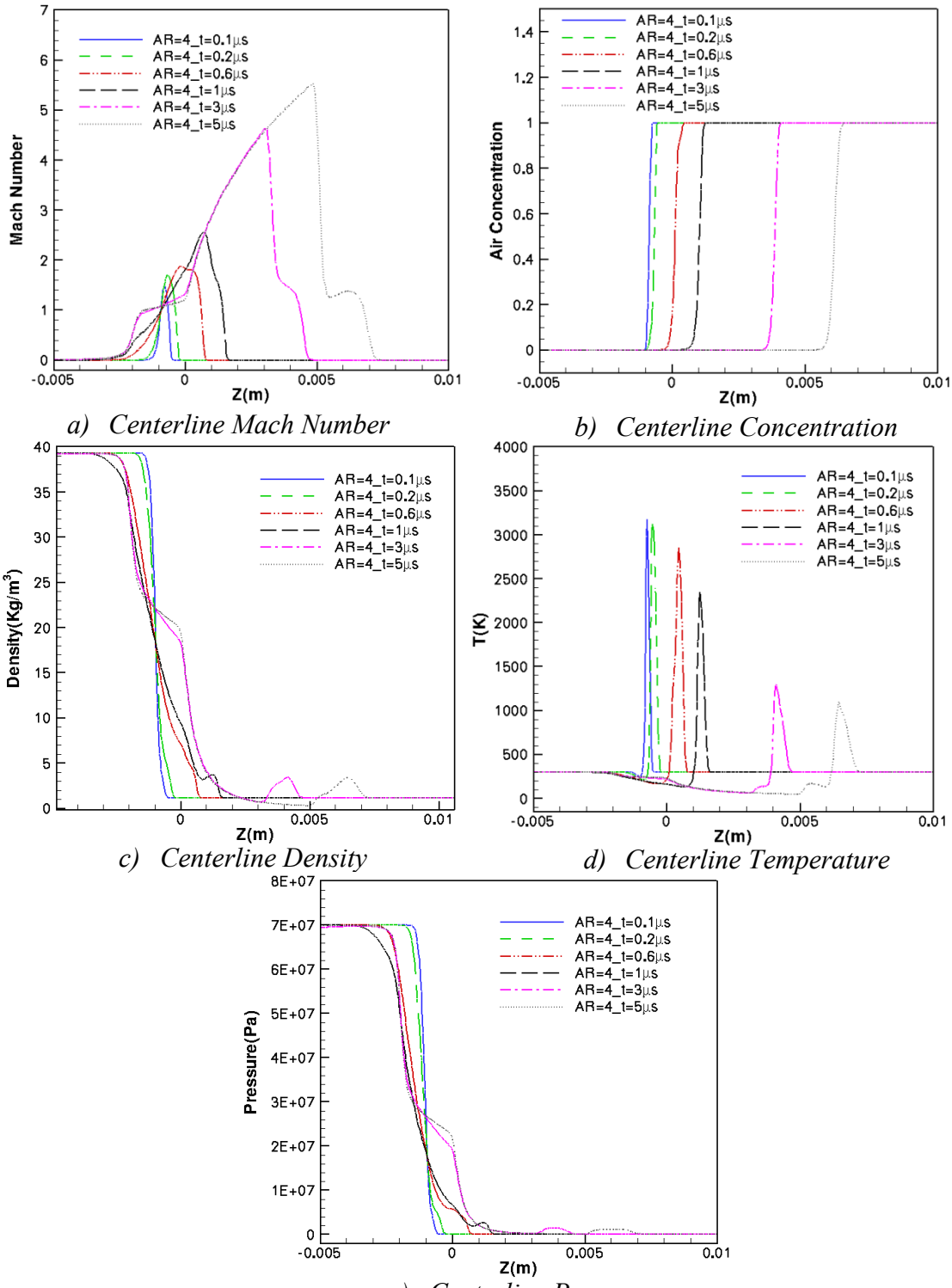

Fig. 4.6: *Flow characteristics along the centerline at different times, elliptical orifice (AR=4), Area=0. 8 mm^2, P=70 MPa*

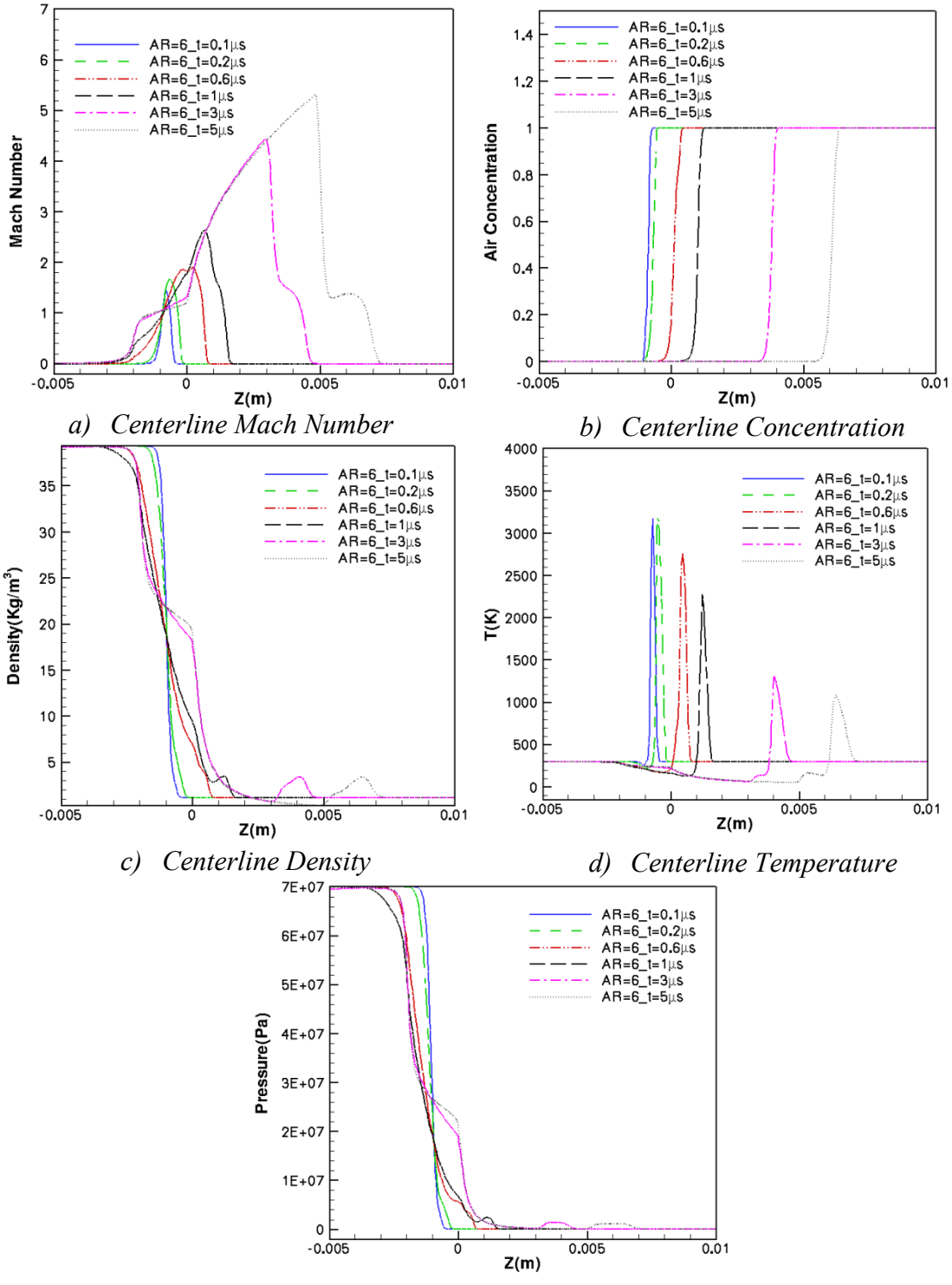

a) Centerline Mach Number

b) Centerline Concentration

c) Centerline Density

d) Centerline Temperature

e) Centerline Pressure

Fig. 4.7: *Flow characteristics along the centerline at different times, elliptical orifice (AR=6), Area=0. 8 mm^2, P=70 MPa*

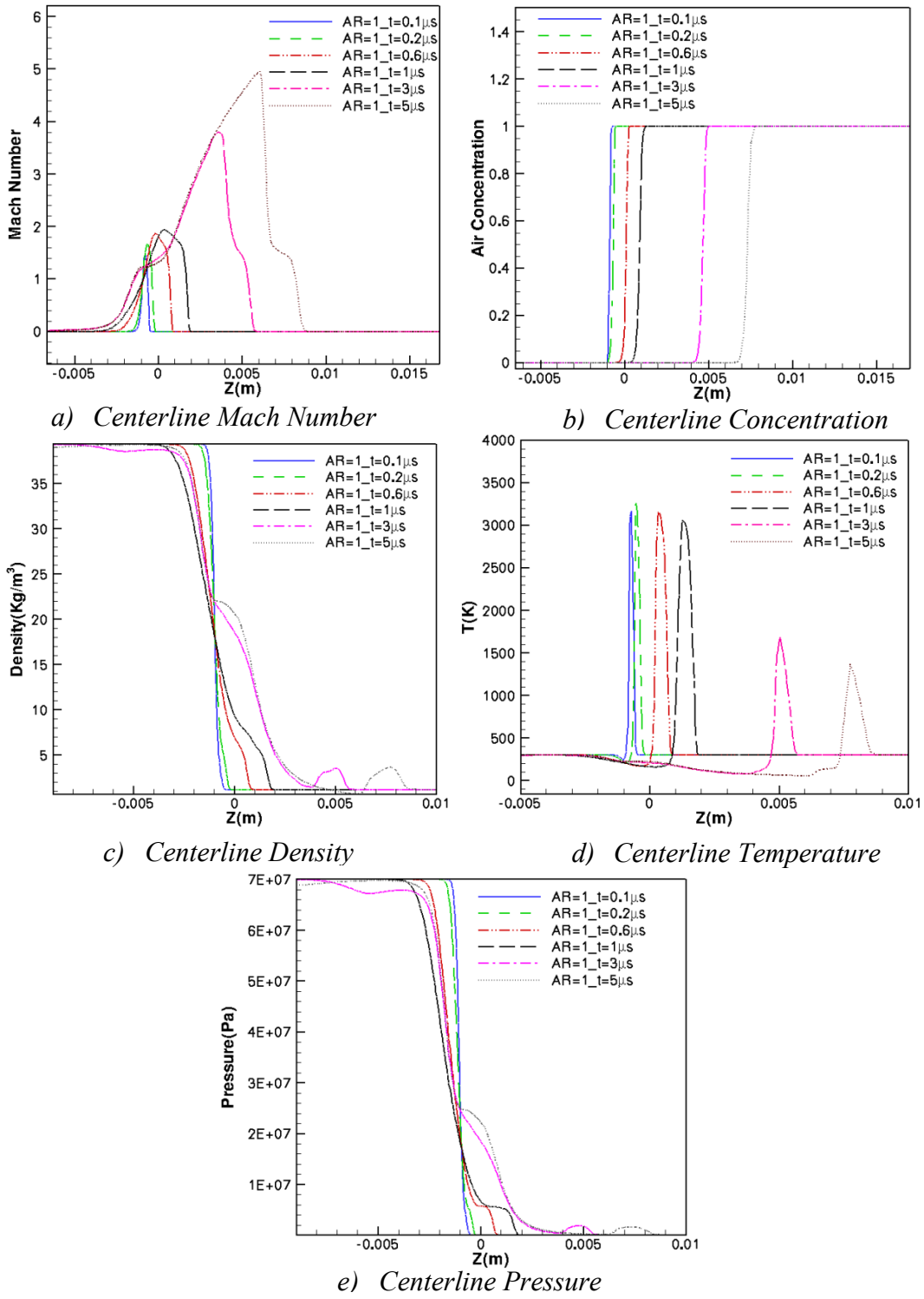

***Fig. 4.8**: Flow characteristics along the centerline at different times, circular orifice (AR=1), Area=3. 14 mm^2, P=70 MPa*

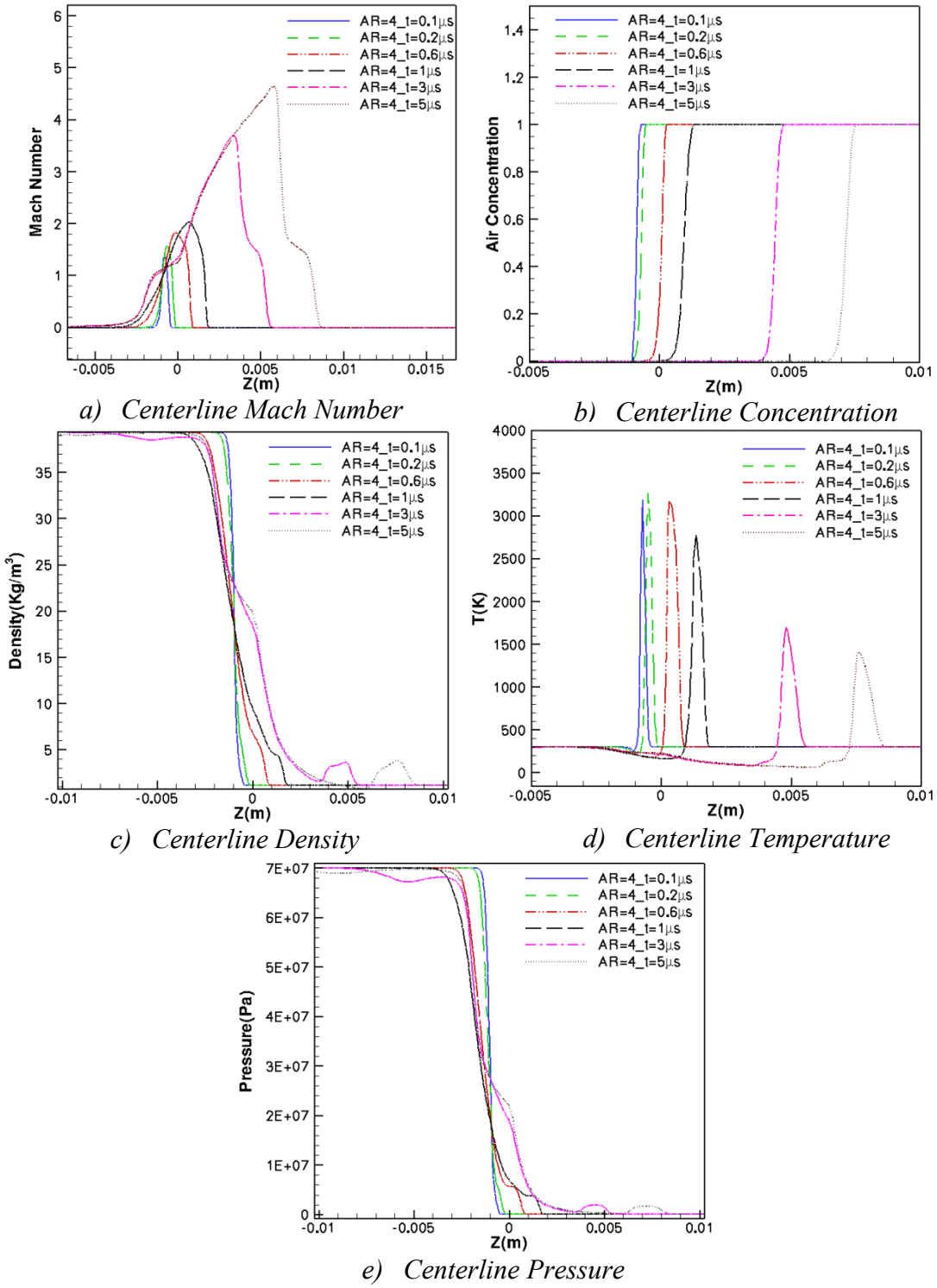

Fig. 4.9: *Flow characteristics along the centerline at different times, elliptical orifice (AR=4), Area=3. 14 mm^2, P=70 MPa*

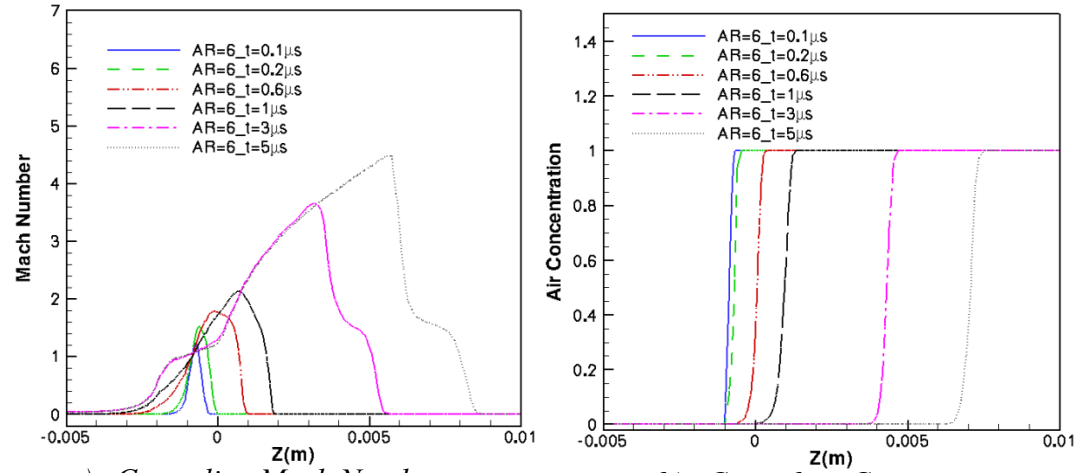

a) Centerline Mach Number

b) Centerline Concentration

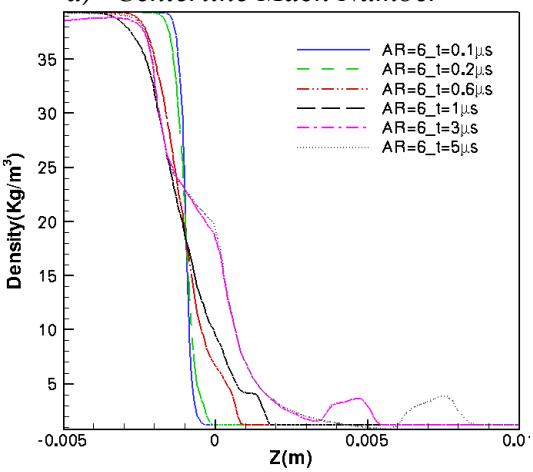

c) Centerline Density

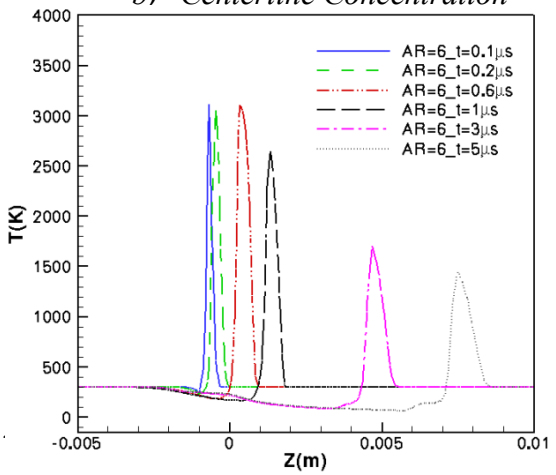

d) Centerline Temperature

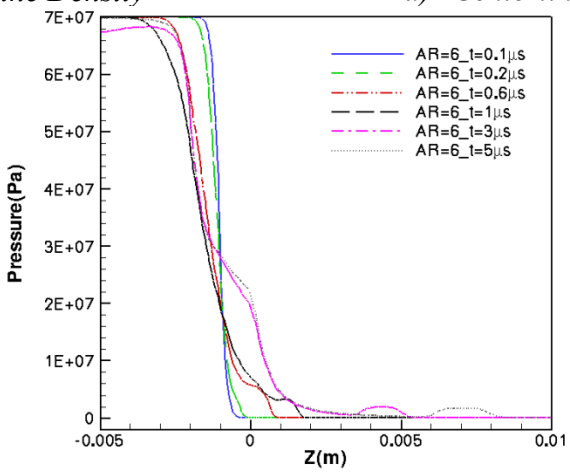

e) Centerline Pressure

Fig. 4.10: *Flow characteristics along the centerline at different times, elliptical orifice (AR=6), Area=3. 14 mm^2, P=70 MPa*

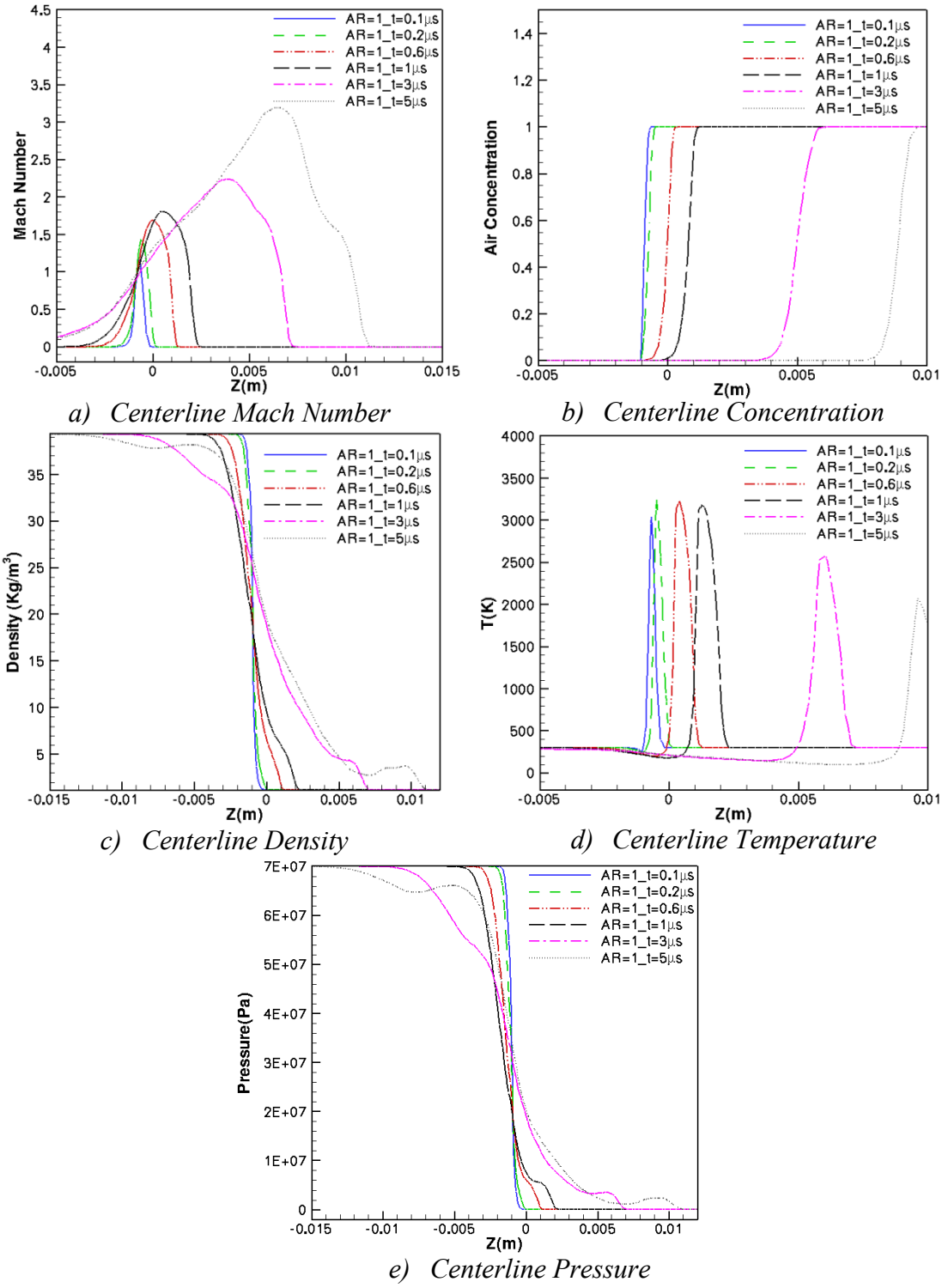

Fig. 4.11: *Flow characteristics along the centerline at different times, circular orifice (AR=1), Area=19. 63 mm^2, P=70 MPa*

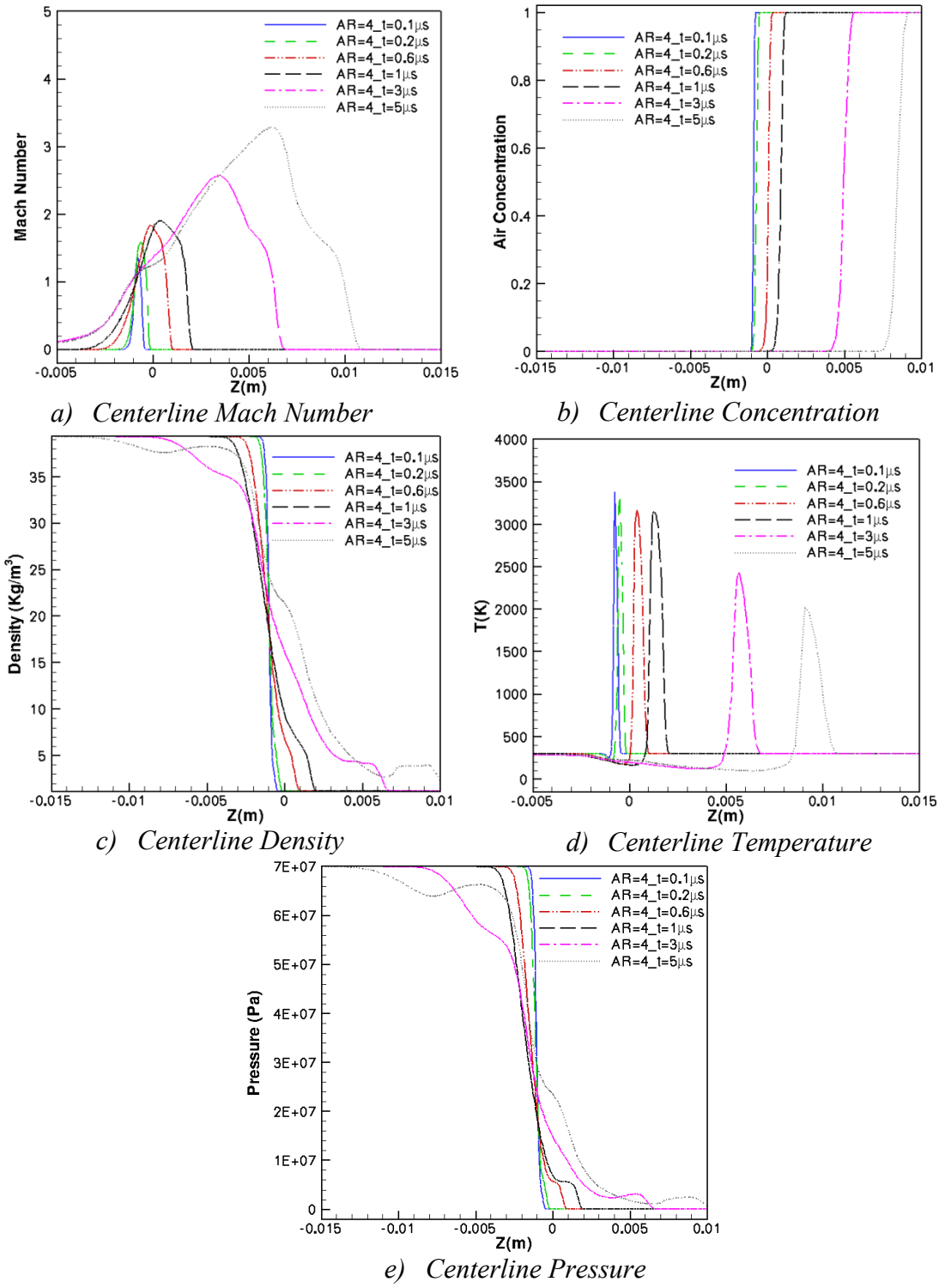

Fig. 4.12: *Flow characteristics along the centerline at different times, elliptical orifice (AR=4), Area=19. 63 mm^2, P=70 MPa*

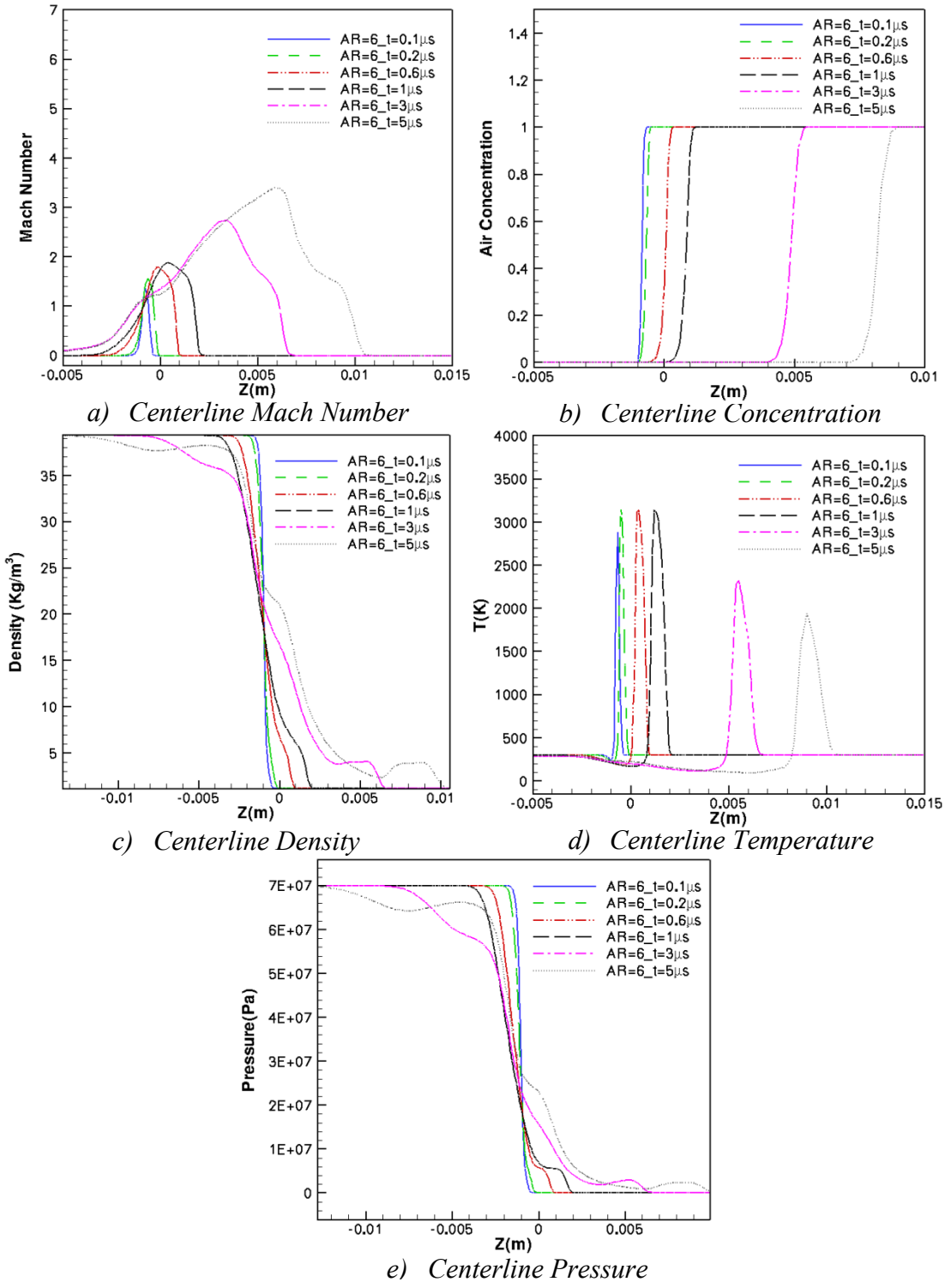

***Fig. 4.13**: Flow characteristics along the centerline at different times, elliptical orifice (AR=6), Area=19. 63 mm^2, P=70 MPa*

By comparing the jet characteristics along the centerline of different shapes of orifices with the same area, it is concluded that centerline pressure and density are slightly affected by using different geometries of holes, however the strength of the Mach disk and the maximum value of the Mach number are evidently changed; the lower the aspect ratio, the stronger the Mach disk. . The locations of the Mach disk and air-hydrogen contact surface do not change with varying shapes of orifices. As it was seen in Fig. 4.3 and also in plots of advection of hydrogen/air interfaces along the centerline, by increasing the opening area, the difference between the contact surface locations regarding different aspect ratios grows but it is insignificant for the orifices with the smaller area.

The hot temperature of air downstream of the hydrogen-air interface is one of the important parameters that affect the auto-ignition process [20] [23]. To evaluate the highest peaks of the temperature during the flow expansion, the temperature profiles along with the locations of contact surfaces are presented at different moments. In all cases (elliptic and circular), the maximum hot temperature occurs in the pressurized vessel, before the release of hydrogen at which the hydrogen-air contact surface reaches the exit ($t<0.6$ μs), however, the exact time that the compressed air experiences the highest temperature differs from case to case. After the leakage of hydrogen into air and during the flow expansion, the maximum peak of the temperature starts decaying to the lower value which proves that the highest possibility of auto-ignition occurs in the early stage of the hydrogen release, however, the other factors such as the storage pressure, jet velocity and the rate of flow expansion can affect the auto-ignition process. At the release time ($t=0.6$ μs) and during the expansion, the highest peaks of temperature profiles for the

cases with elliptic orifices are slightly lower than their equivalent values in cases with circular openings. This effect is more dominant in the cases with smaller cross sectional area (A=0.8 mm^2), since the rate of expansion is greater compared to the pressure drop from the larger exit area. For instance, the highest temperature peak at the release time for the circular case with the area of 0.8 mm^2 is almost T=3200 K, but this value in elliptic cases with AR=4 and 6 are T=2850 K and T= 2750 K, respectively. In addition, as it is shown in Fig. 4.11-Fig. 4.13, the high temperature peaks during the expansion from the orifice with the area of A=19. 63 mm^2 for both elliptic and circular jets decrease at a lower rate and maintain their highest hot temperature for a longer time compared to those from the smaller orifice areas such as A=0. 8 mm^2 and A=3. 14 mm^2 (Fig. 4.5- Fig. 4.10)[36].

4.3.2 Contact surface pressure along the centerline

One of the important parameters to determine the ignition possibility is the pressure expansion at the interface of the hydrogen and air along the jet centerline. The auto-ignition may occur for sufficiently low rates of expansion [21]. Therefore, the centreline pressures as a function of time on the contact surface for both circular and elliptical exits with different diameters are compared together up to a time of 10 μs. To evaluate the interactions between an orifice area, the dimensions of an elliptic exit and the interface pressure, three various areas based on 1 mm, 2 mm and 5 mm diameters of circular orifices are considered. The results are shown in Fig. 4.14-Fig. 4.16.

Considering all cases, the contact surface pressure decays with time until reaching the ambient pressure. For a given area by increasing the aspect ratio of a release hole, contact surface pressure expands more rapidly in the vicinity of the exit hole where a significant

pressure drop is achieved. This behavior can be negligible for the smallest area of the exit hole (Area=0. 8 mm^2), while it is crucial for a larger orifice size (Area=19. 63 mm^2) [37]. In other words, the elliptical jet escaping from a small hole behaves the same as its comparable circular jet. However, as the orifice area increases, the differences between the pressure expansions from varying elliptic and circular holes are more considerable. For the nozzle area of 19.63 mm^2, the contact surface pressure in the case of elliptic jet drops faster than its comparable circular jet. However, there is a slight change between the pressure expansions through two varying elliptic orifices; the more elongated case shows the higher expansion with virtually the same expansion rate. Although the slope of the pressure-time curve is not affected by applying different shapes of orifices with an identical area, it differs by changing the orifice area that a smaller area presents the steeper slope and a higher rate of pressure drop. In addition, by preserving the orifice geometry and decreasing its area, it is concluded that a smaller release hole has a more pronounced expansion and a steeper slope which cause the hydrogen jet reaches the ambient pressure faster and sooner. It can be recognized that the contact surface pressures for different orifice layouts at t=10 μs in the case with the smaller orifice area (A=0.8 mm^2) are virtually the same and the value practically equals to P=0. 6 MPa, however, this value in the case with the area of A=3.14 mm^2 is almost P=1 MPa and in the case with the largest area of A=19.63 mm^2 is about P=2.5 MPa. So there is a rapid depressurization for the jet issuing from the hole with a smaller area but elliptic and circular jets starting from the hole with an identical area are depressurized and reached the ambient pressure at the same time.

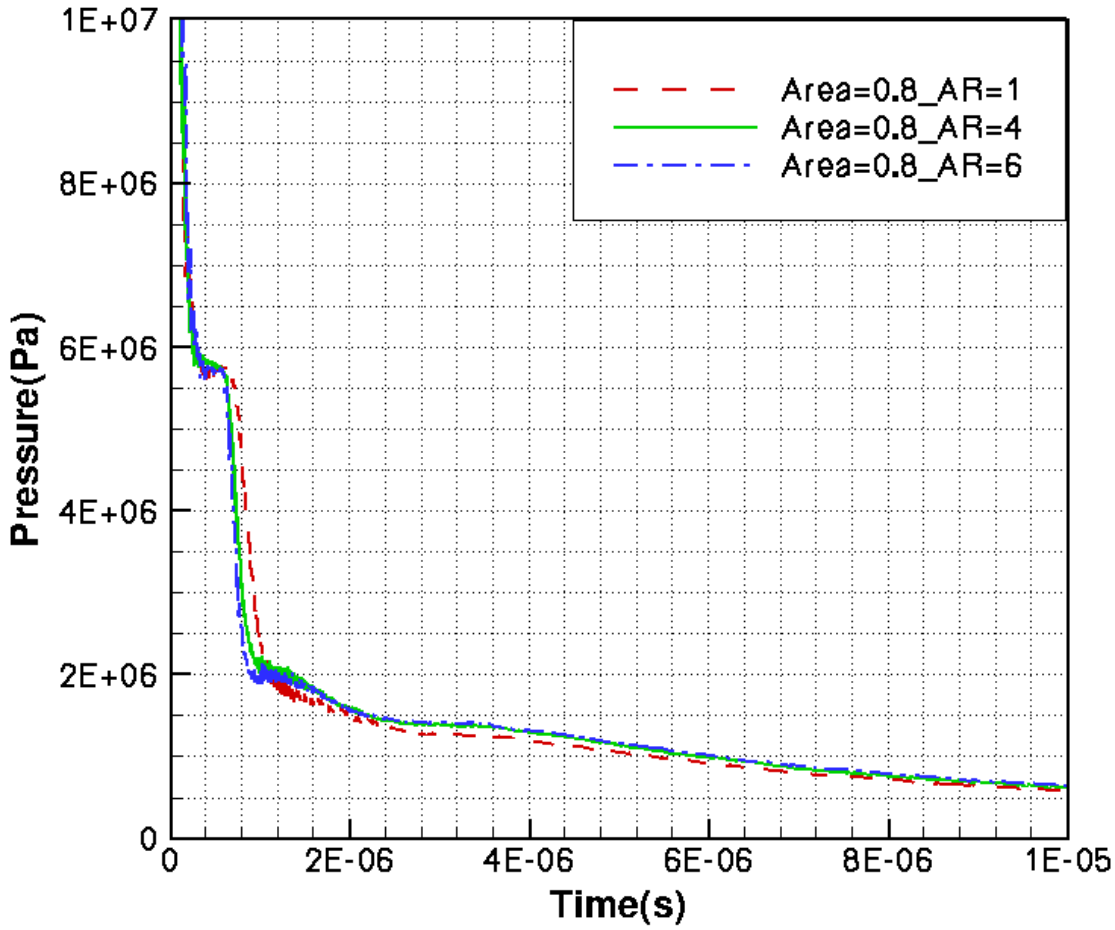

***Fig. 4.14**: Contact Surface pressure versus time along the centerline, fixed orifices (circular & elliptical), Area=0.8 mm^2, $P_{reservoir}$ =70 MPa*

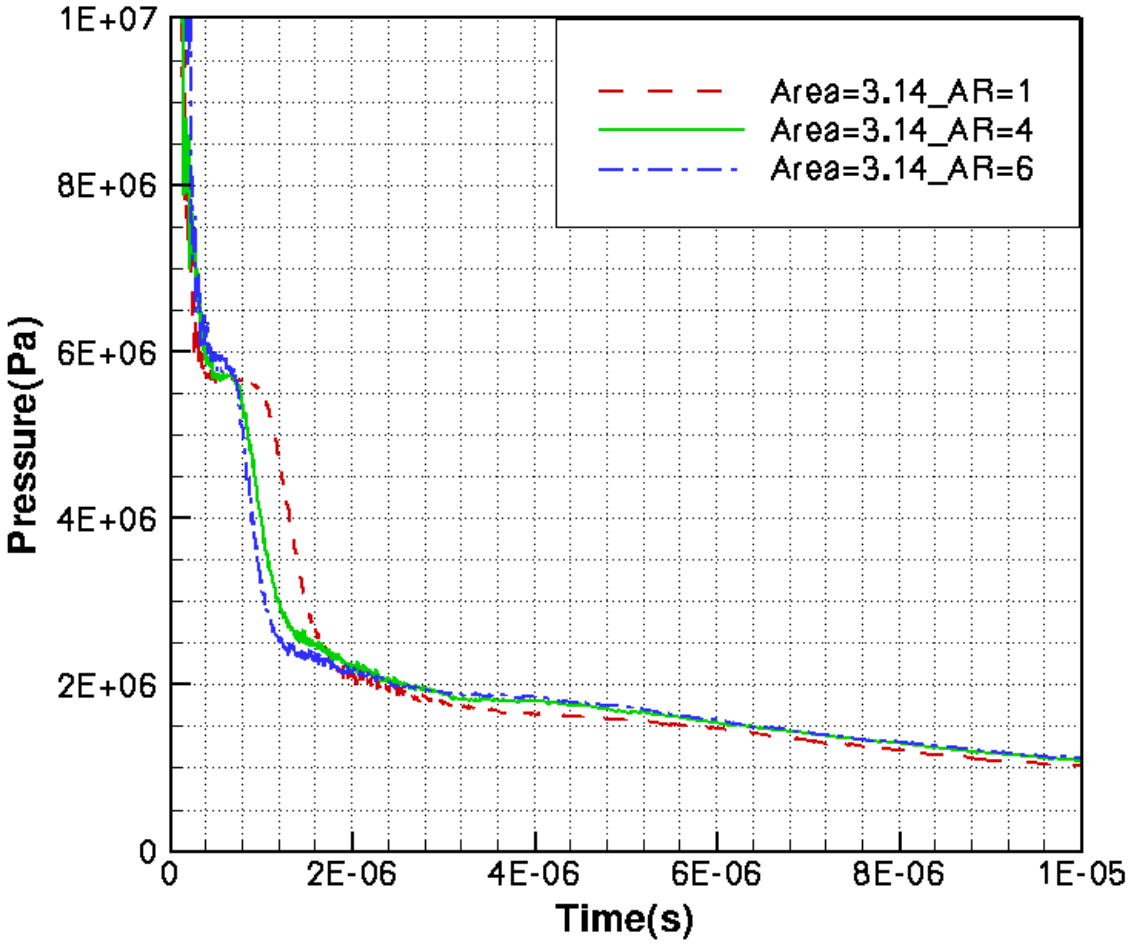

***Fig. 4.15**: Contact Surface pressure versus time along the centerline, fixed orifices (circular & elliptical), Area=3.14 mm^2, $P_{reservoir}$ =70 MPa*

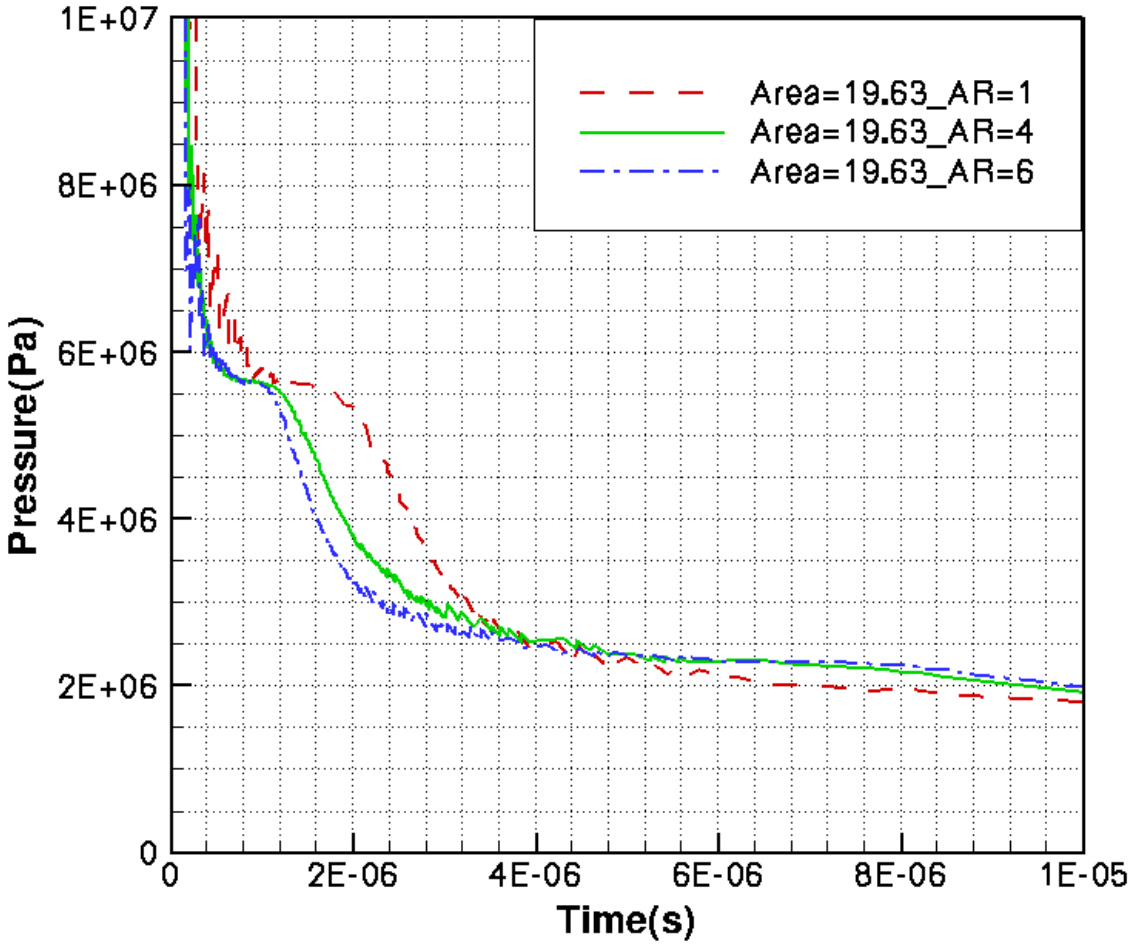

***Fig. 4.16**: Contact Surface pressure versus time along the centerline, fixed orifices, (circular & elliptical), Area=19.63 mm^2, $P_{reservoir}$ =70 MPa*

In order to accurately evaluate the expansion of the contact surface pressure along the centerline, the contours of the pressure and the concentration in the case of the round orifice with the area of A= 19.63 mm^2 at different times during the release of hydrogen into the air are illustrated in Fig. 4.17. As indicted, between t=0.8 μs and t= 2 μs, the contact surface pressure on the centerline does not change significantly and a pressure drop during this initial period of discharging of the interface from an exit is infinitesimal. As a result, the plateau appears in the contact surface pressure curve, which is longer for

a circular jet compared to an elliptic jet. After, t=2 μs, the pressure expands more quickly which can be understood from both Fig. 4.16 and Fig. 4.17 (d).

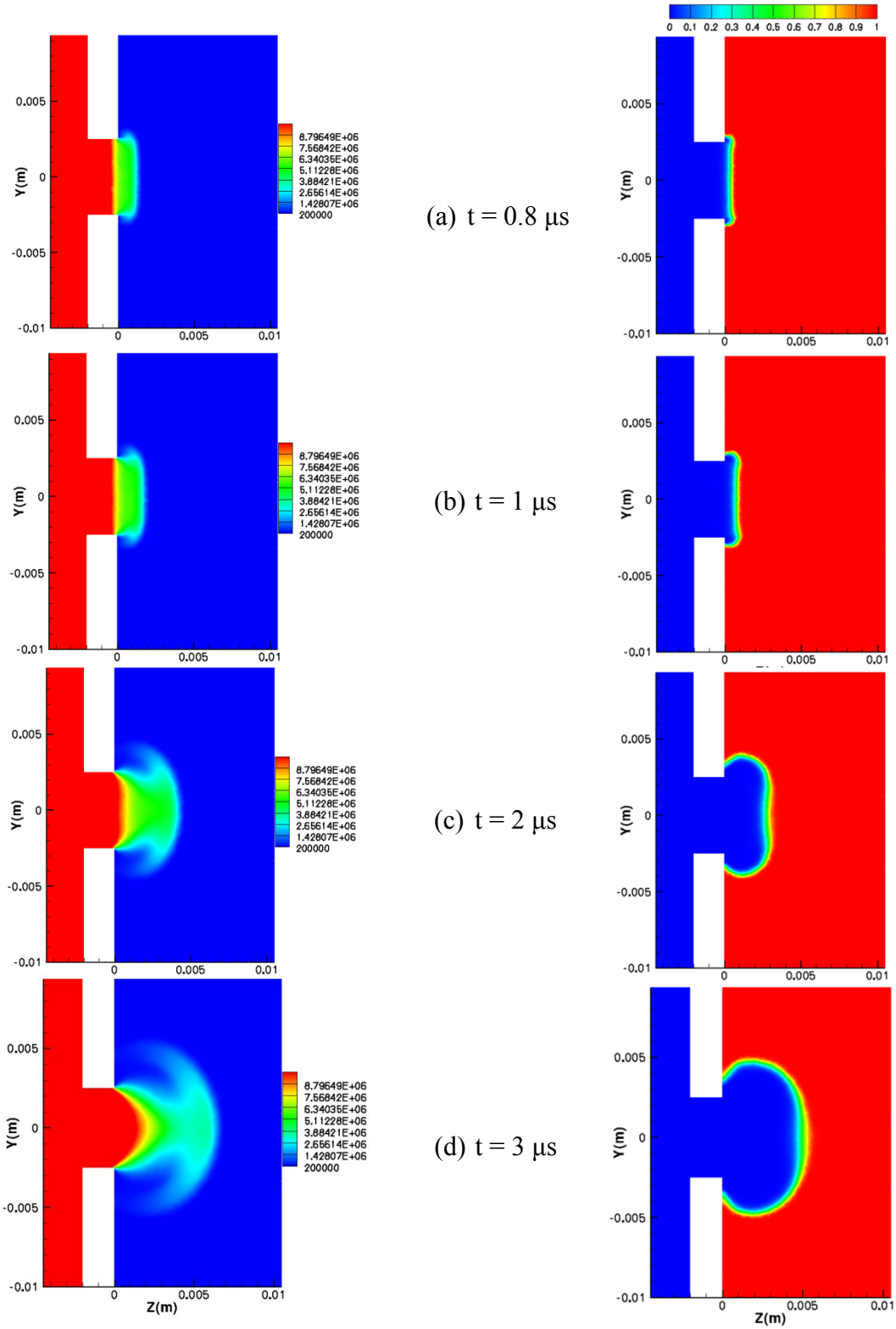

Fig. 4.17: *Contours of left) pressure and right) concentration at different times after the release, orifice Area=19.63 mm^2, P=70 MPa*

The distribution of the concentration, temperature and Mach number after 10 micro seconds for circular and elliptical (AR=4) orifices with the equivalent area of A=3.14 mm^2 are presented in Fig. 4.18-Fig. 4.20.

By comparing Mach numbers and concentrations along the minor and major axes, it is understood that the change in the orifice geometry affects the development of the jet. Spreading and mixing characteristics differ from elliptical and circular jets. The hydrogen jet releasing from the elliptical hole spreads more quickly in the minor axis plane than the major axis plane and, in turn, it mixes with air faster along the minor axis and advances through the ambient air more quickly. While the circular hydrogen jet spreads with the same rate in both directions and the mixing rate does not change along the minor and major axes. The unequal spreading rates are because of the non-uniform curvature variation of the elliptic orifice [38].

The higher spreading rate along the minor axis plane results in the axis switching phenomena which is recognized in the elliptic jets for both aspect ratios of 4 and 6 and under both pressures of 10 MPa and 70 MPa.

In addition, the magnitude of the Mach number along the major and minor axes at different axial positions of z=5 mm and z=10 mm after 10 μs of release for both elliptic and circular jets are shown in Fig. 4.21. These curves clearly depict different velocity magnitudes along the major and minor axes of the elliptic jet which cause the difference in spreading rate of hydrogen into air between the axes; however, as shown in Fig. 4.22, there is no change in the magnitudes of the Mach number for the circular jet along two different axes.

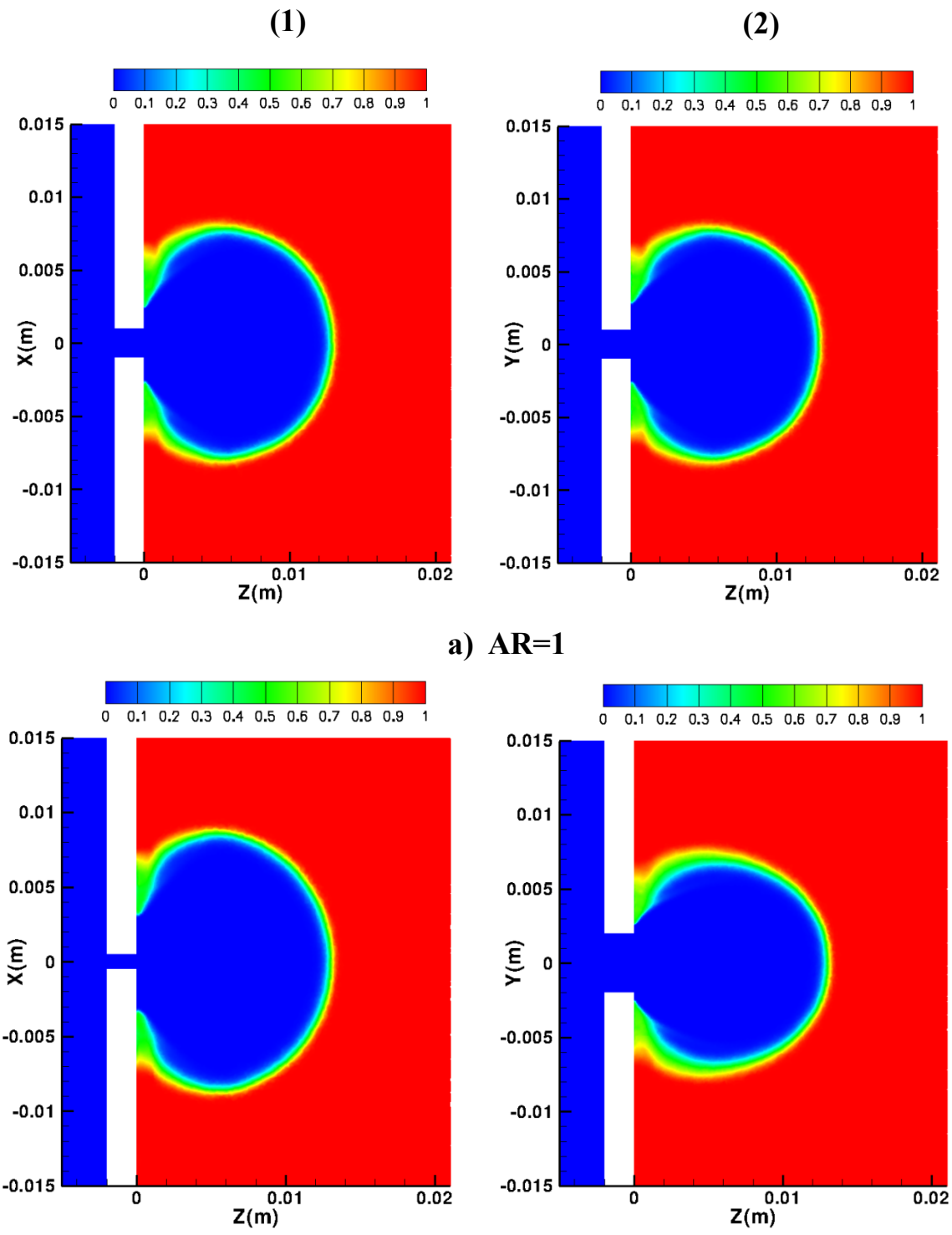

Fig. 4.18: *Concentration after 10 µs of hydrogen release from the circular and elliptical orifices (Area=3.14 mm^2 & P=70Mpa), 1) Minor axis plane, 2) Major axis plane*

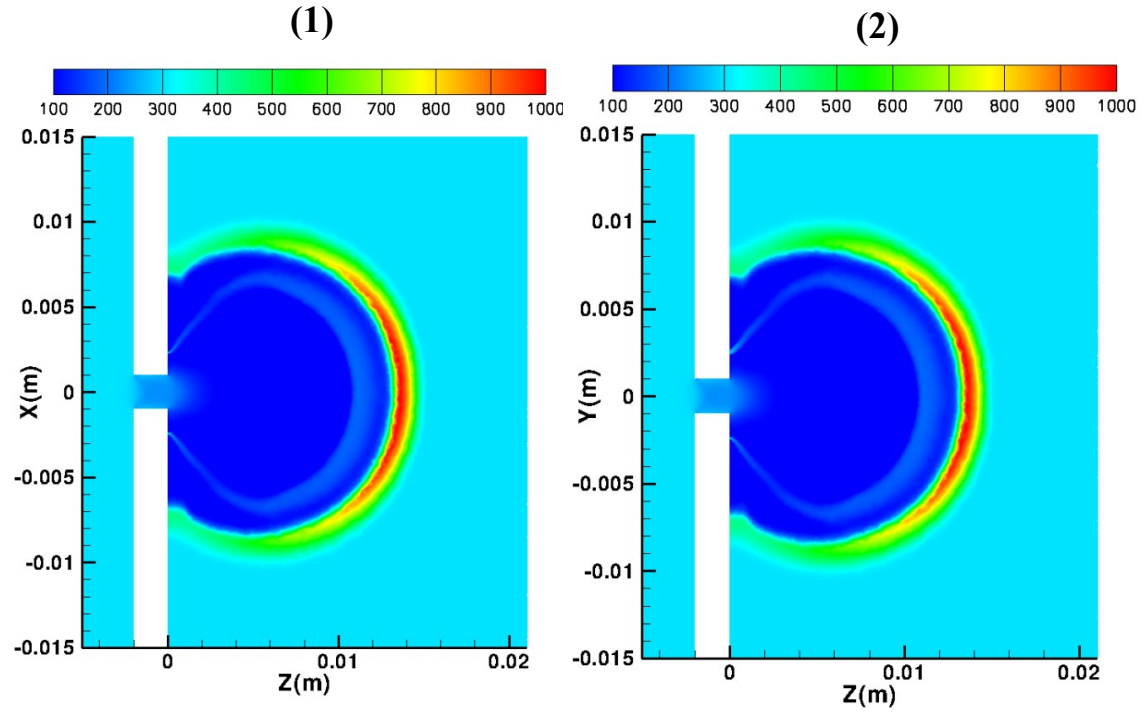

a) AR=1

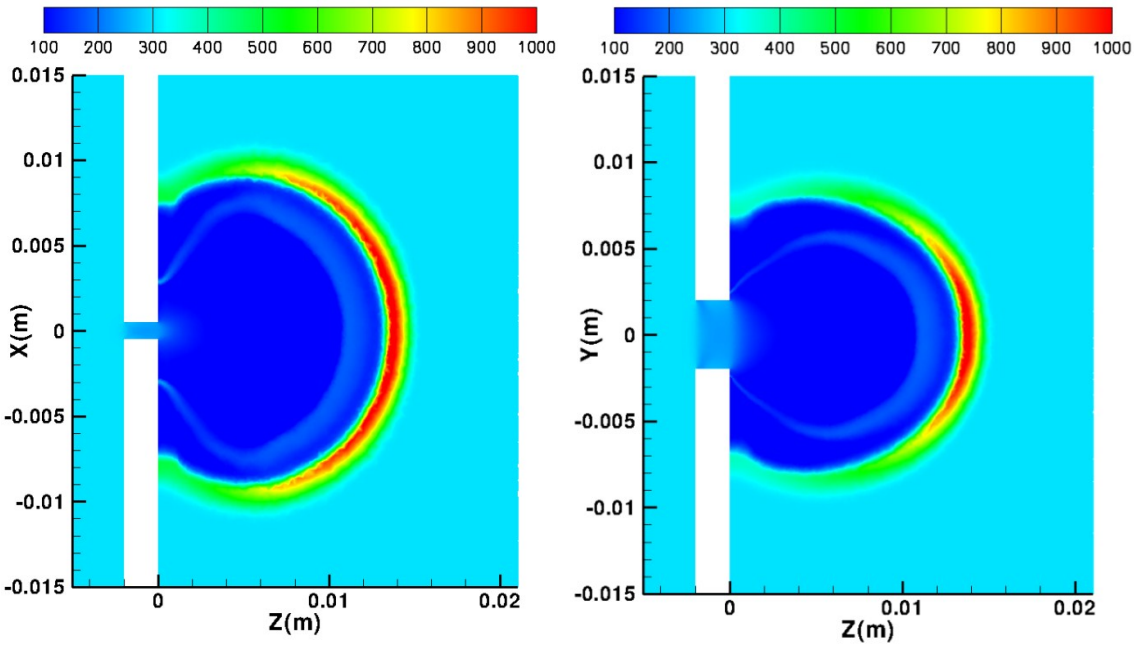

b) AR=4

Fig. 4.19: *Temperature after 10 µs of hydrogen release from the circular and elliptical orifices (Area=3.14 mm^2 & P=70Mpa), 1) Minor axis plane, 2) Major axis plane*

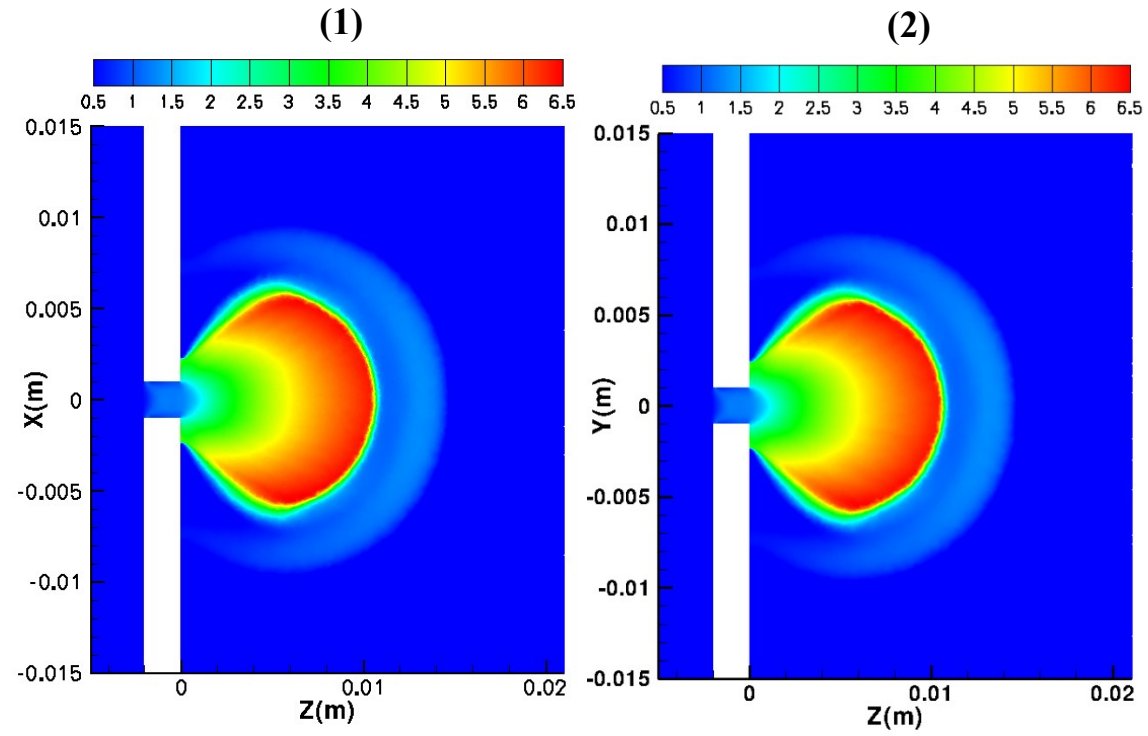

a) AR=1

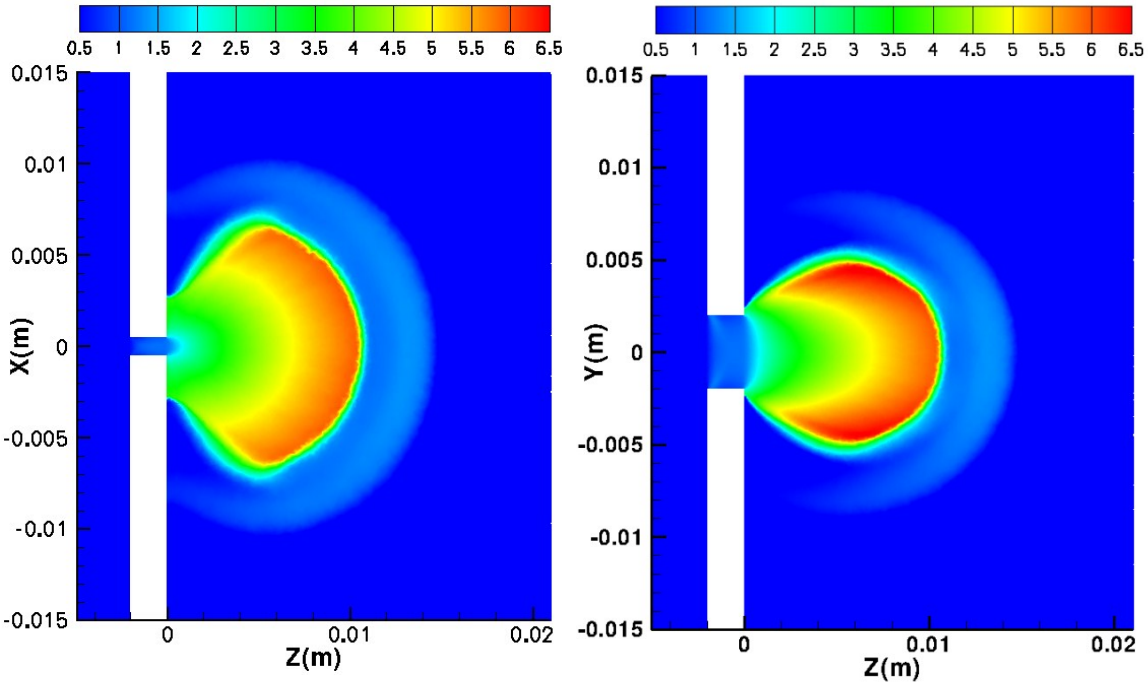

b) AR=4

Fig. 4.20: *Mach number after 10 µs of hydrogen release from the circular and elliptical orifices (Area=3.14 mm^2 & P=70Mpa), 1) Minor axis plane, 2) Major axis plane*

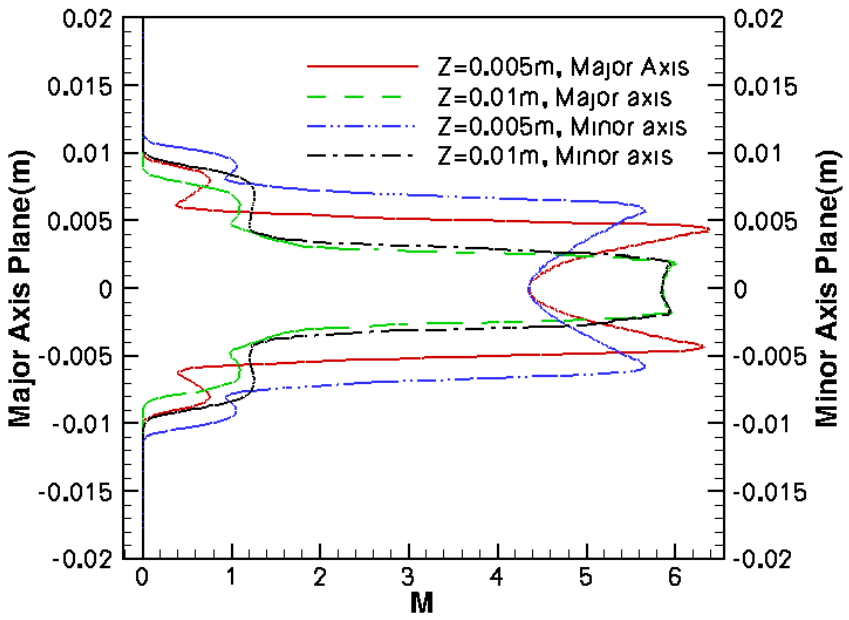

Fig. 4.21: *Mach number magnitude plots of the elliptic jet along the major and minor axes at different axial locations, (t=10 μs)*

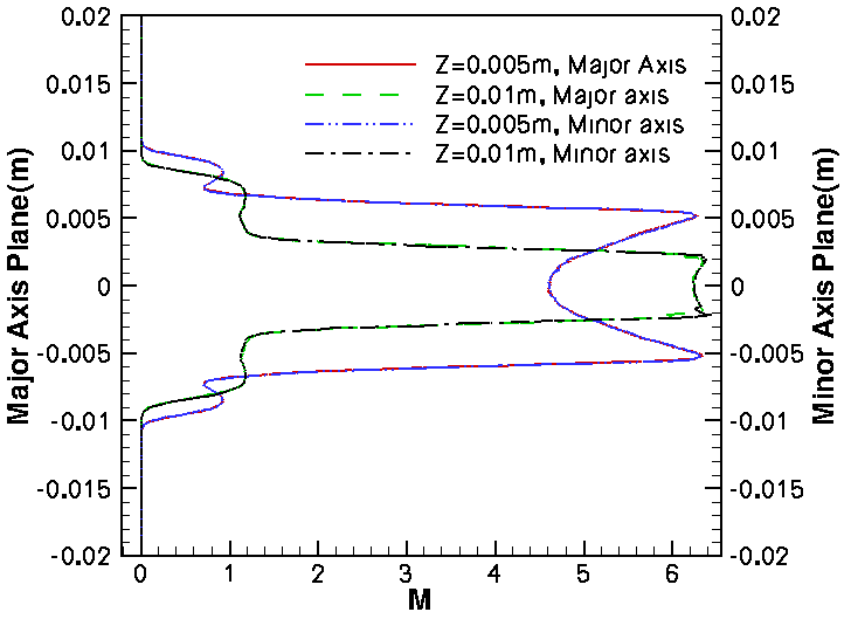

Fig. 4.22: *Mach number magnitude plots of the circular jet along the major and minor axes at different axial locations, (t=10 μs)*

4.4 Description of the flow field under the reservoir pressure of 10 MPa

4.4.1 Centerline flow characteristics

To evaluate the influence of the orifice geometry on the release of hydrogen from a reservoir with a lower pressure (compared to 70 MPa) into the quiescent ambient air, the evolution of the flow under the filling pressure of P=10 MPa is investigated. Same as the presented study in the previous section, the centerline flow properties such as Mach number, concentration, temperature, pressure for both circular and elliptic hydrogen jets issuing from varying dimensions of orifices are provided in Fig. 4.23-Fig. 4.31. Easily perceived that the structure of the jet is similar to the underexpanded jet from the 70 MPa reservoirs, however the flow field from 10 MPa tank developed sooner, since it has a lower jet velocity.

As previously detailed, the release time in the case of 10 MPa storage pressure is t=1 μs. The hydrogen-air interfaces along the centerline for both elliptic and circular cases stand in the same location from the exit during the expansion of the jet. The location of the Mach disk same as the cases with the pressure of 70 MPa does not alter by changing the shape of the orifice. However, as the aspect ratio of the elliptic orifice increases, the Mach disk becomes weaker.

The temperature profiles before the time of release, at the release time and during the expansion are presented. The maximum value of the high peaks of the temperature like cases with 70 MPa occurs in the tube, when the interface has not exited the nozzle (t=1 μs), however the maximum hot air temperature in the case of 10 MPa is much lower than its equivalent value under 70 MPa pressure (about 1000 K).

During the expansion, the hot air cools down and the highest peak temperature gradually decreases along the centerline. The rate of decay of the highest temperature during the expansion under 10 MPa storage pressure is higher compared to 70 MPa pressure. By comparing temperature profiles between the circular and elliptical cases, it can be concluded that under the lower storage pressure (10 MPa) and larger orifice area (A=19. 63 mm^2), the differences between the highest peak of temperature in the elliptic case with larger aspect ratio and its circular counterpart is clearly larger than the cases with the 70 MPa pressure, however, this difference is not significant for the smaller area (A=0. 8 mm^2). In all cases, circular jets experience a higher value of hot temperature compared to their equivalent elliptic jets. The temperature gradient is not affected by using different shapes of orifices.

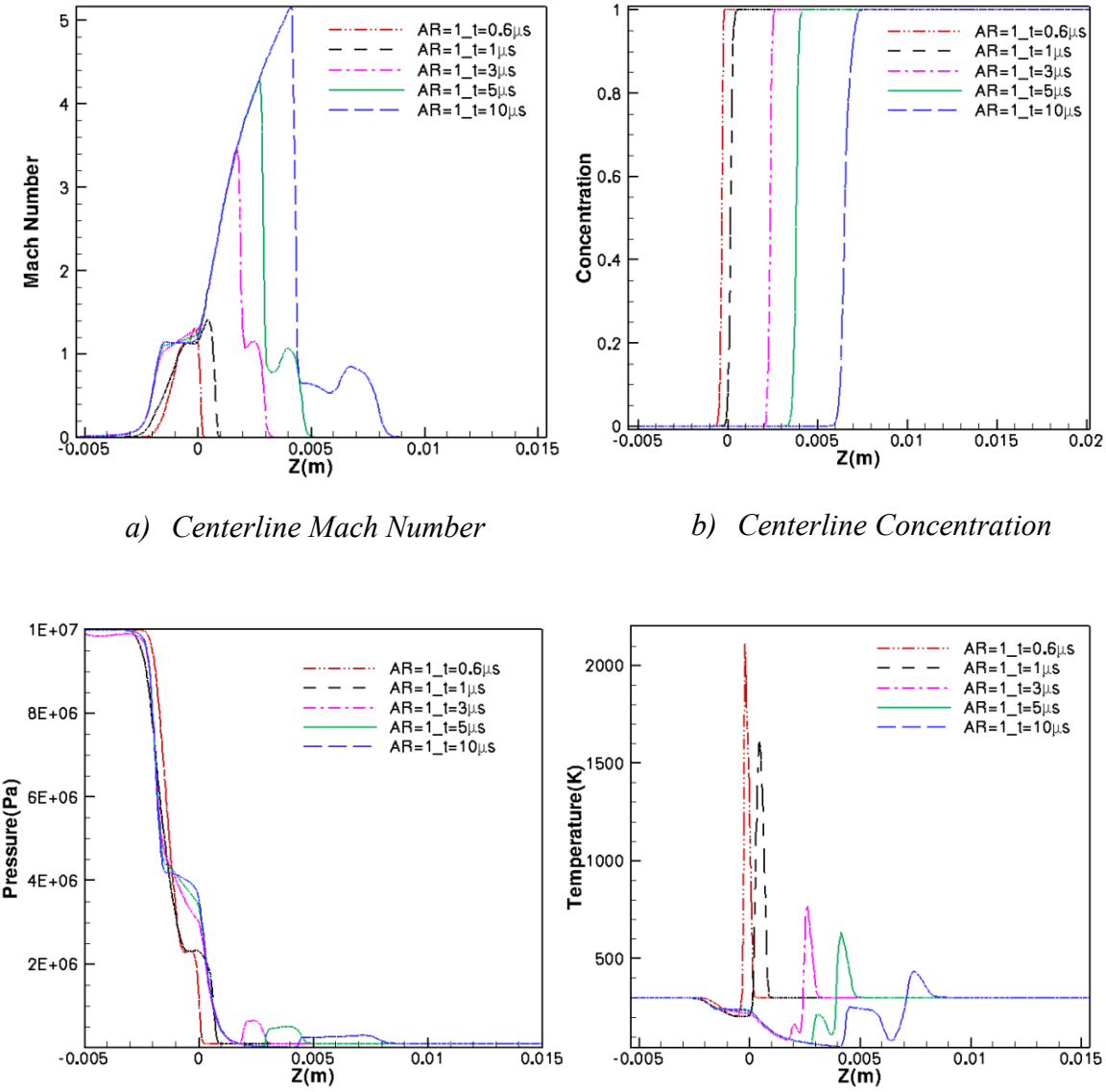

a) Centerline Mach Number

b) Centerline Concentration

c) Centerline Pressure

d) Centerline Temperature

***Fig. 4.23**: Flow characteristics along the centerline at different times, circular orifice (AR=1), Area=0.8 mm^2, P=10 MPa*

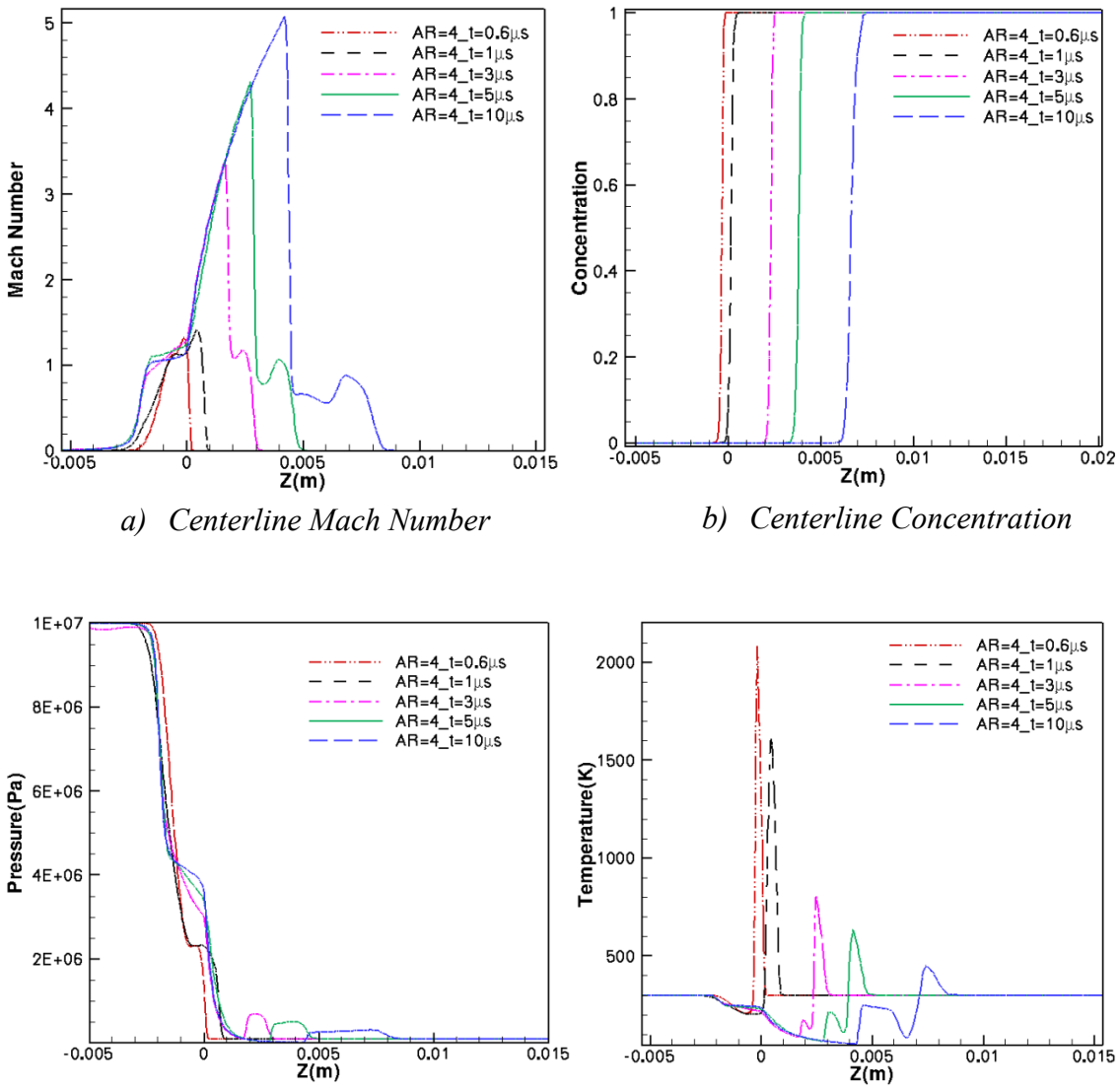

a) Centerline Mach Number

b) Centerline Concentration

c) Centerline Pressure

d) Centerline Temperature

***Fig. 4.24**: Flow characteristics along the centerline at different times, elliptical orifice (AR=4), Area=0.8 mm^2, P=10 MPa*

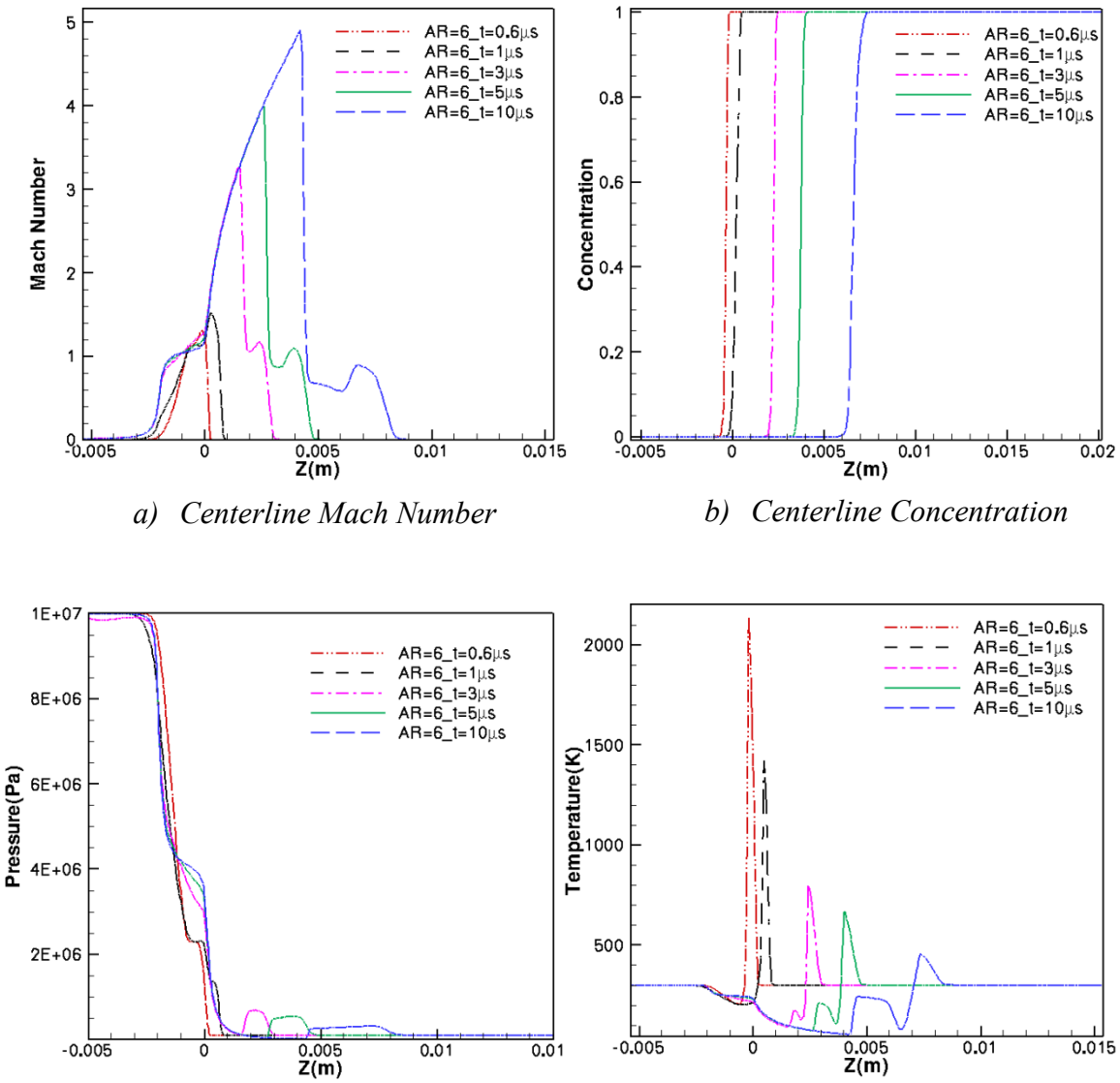

a) Centerline Mach Number

b) Centerline Concentration

c) Centerline Pressure

d) Centerline Temperature

***Fig. 4.25**: Flow characteristics along the centerline at different times, elliptical orifice (AR=6), Area=0.8 mm^2, P=10 MPa*

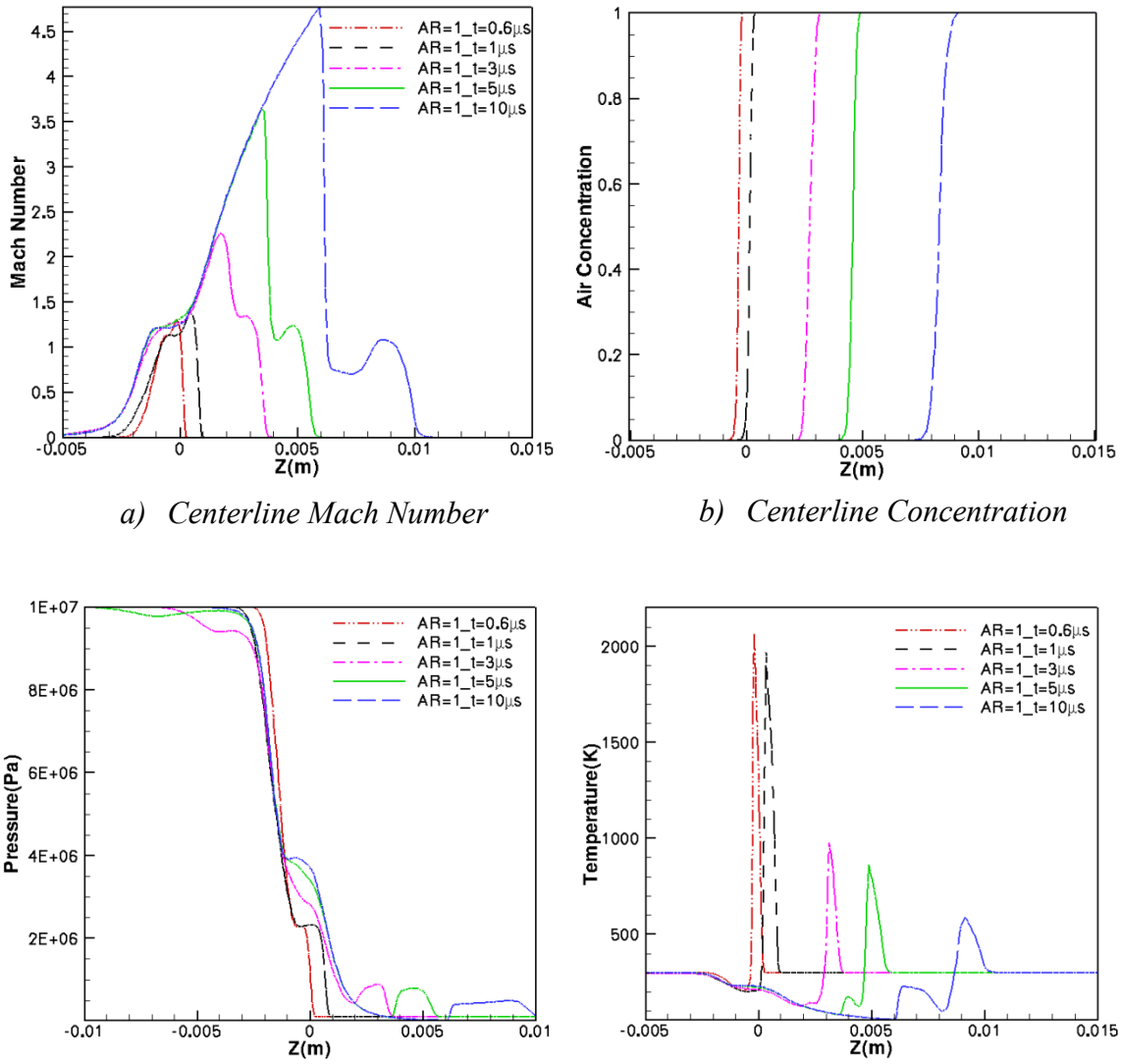

a) Centerline Mach Number

b) Centerline Concentration

c) Centerline Pressure

d) Centerline Temperature

***Fig. 4.26**: Flow characteristics along the centerline at different times, circular orifice (AR=1), Area=3.14 mm^2, P=10 MPa*

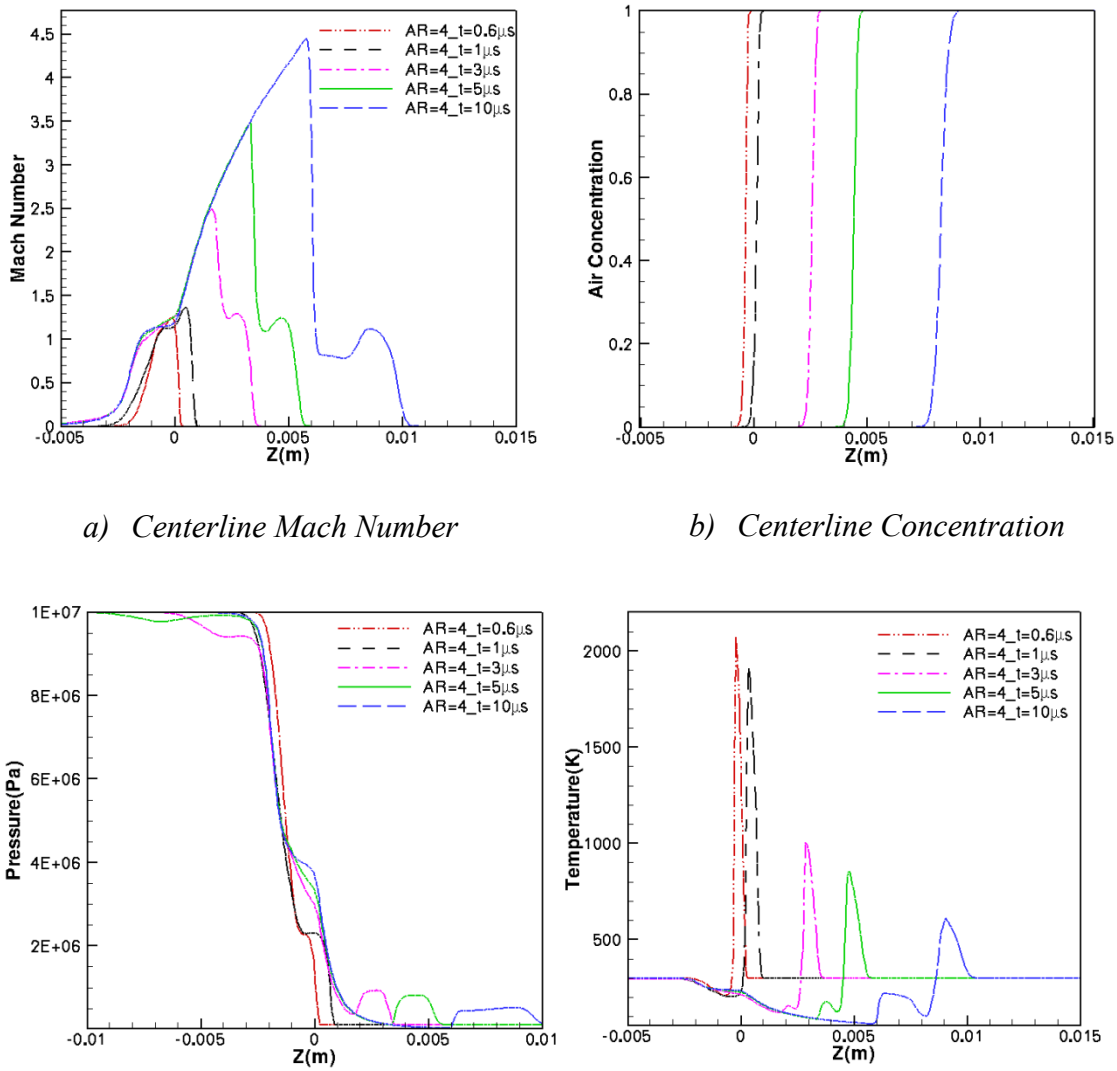

a) Centerline Mach Number *b) Centerline Concentration*

c) Centerline Pressure *d) Centerline Temperature*

***Fig. 4.27**: Flow characteristics along the centerline at different times, elliptical orifice (AR=4), Area=3.14 mm^2, P=10 MPa*

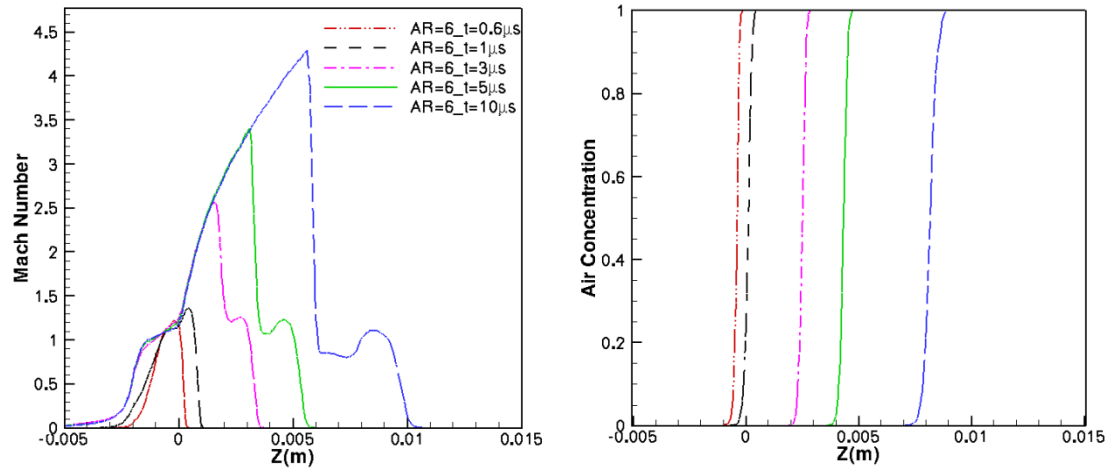

a) Centerline Mach Number *b) Centerline Concentration*

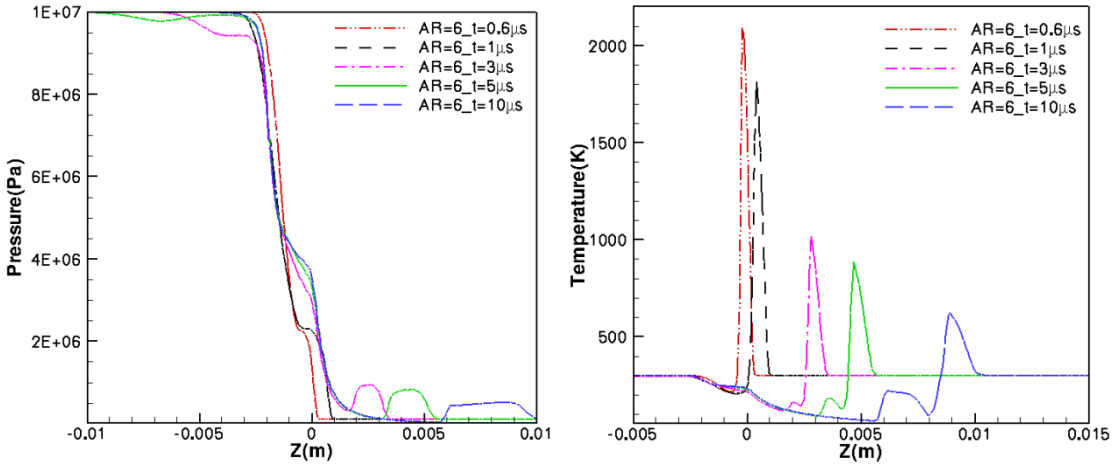

c) Centerline Pressure *d) Centerline Temperature*

Fig. 4.28: *Flow characteristics along the centerline at different times, elliptical orifice (AR=6), Area=3.14 mm^2, P=10 MPa*

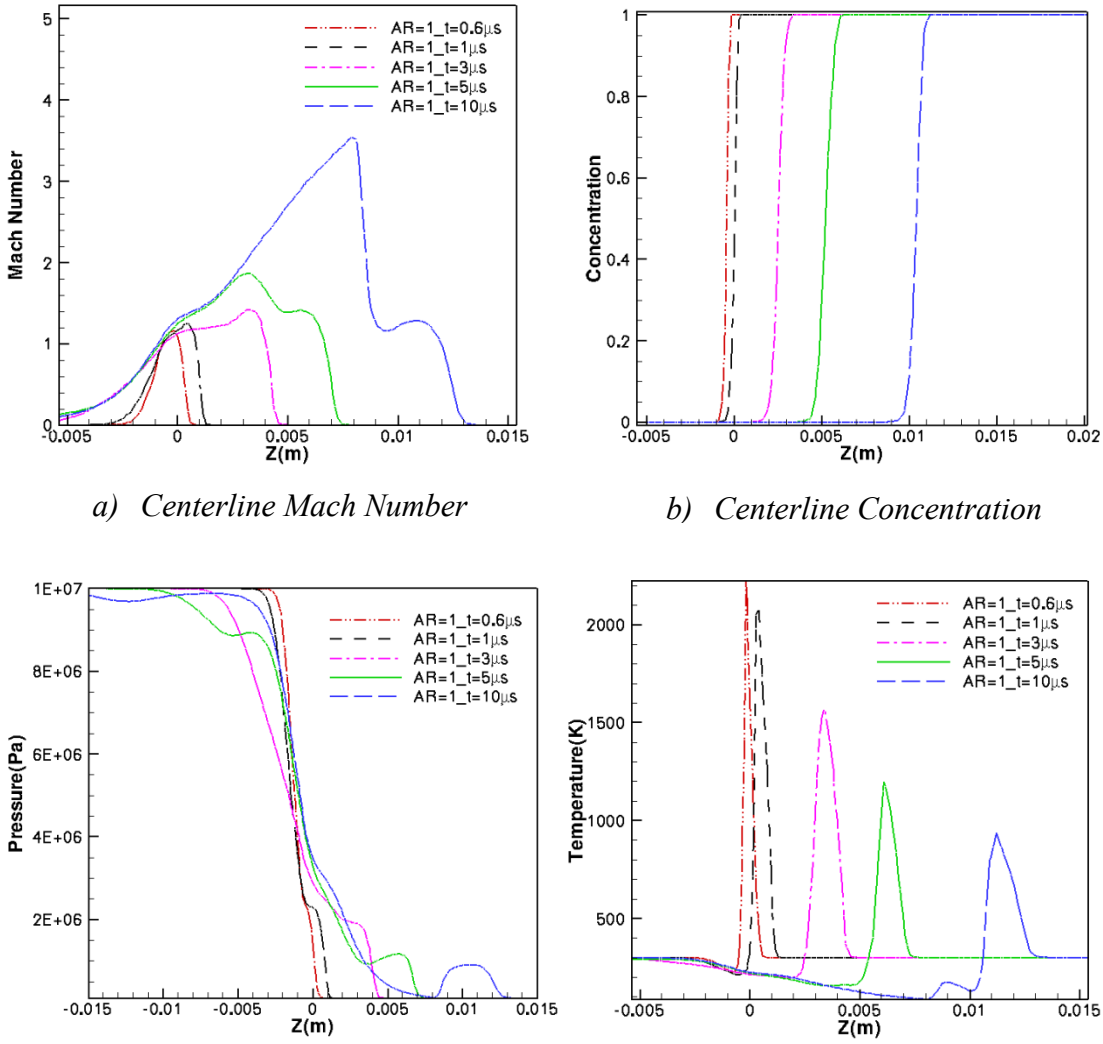

a) Centerline Mach Number

b) Centerline Concentration

c) Centerline Pressure

d) Centerline Temperature

Fig. 4.29: *Flow characteristics along the centerline at different times, circular orifice (AR=1), Area=19.63 mm^2, P=10 MPa*

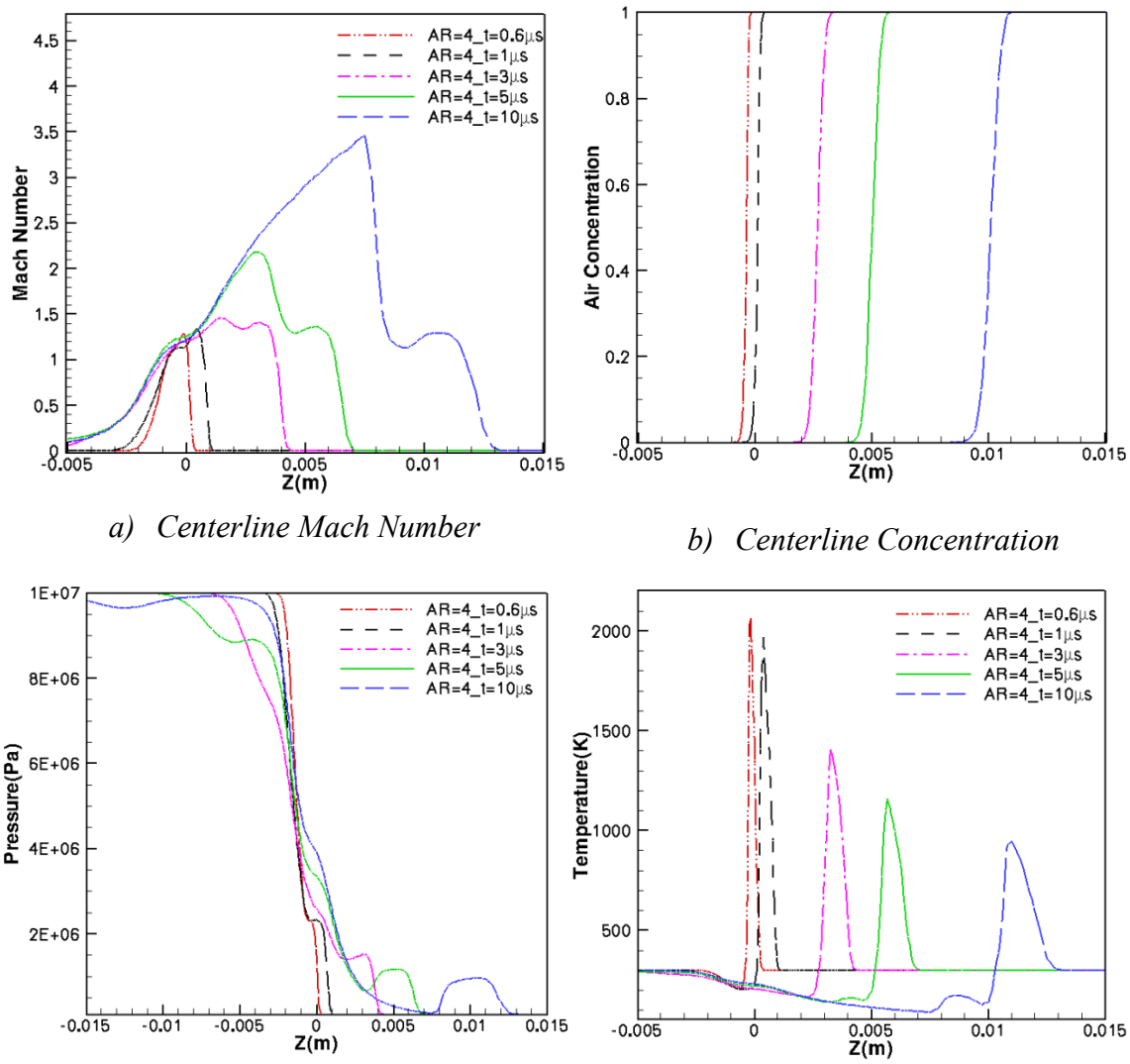

a) Centerline Mach Number

b) Centerline Concentration

c) Centerline Pressure

d) Centerline Temperature

Fig. 4.30: *Flow characteristics along the centerline at different times, elliptical orifice (AR=4), Area=3.14 mm^2, P=10 MPa*

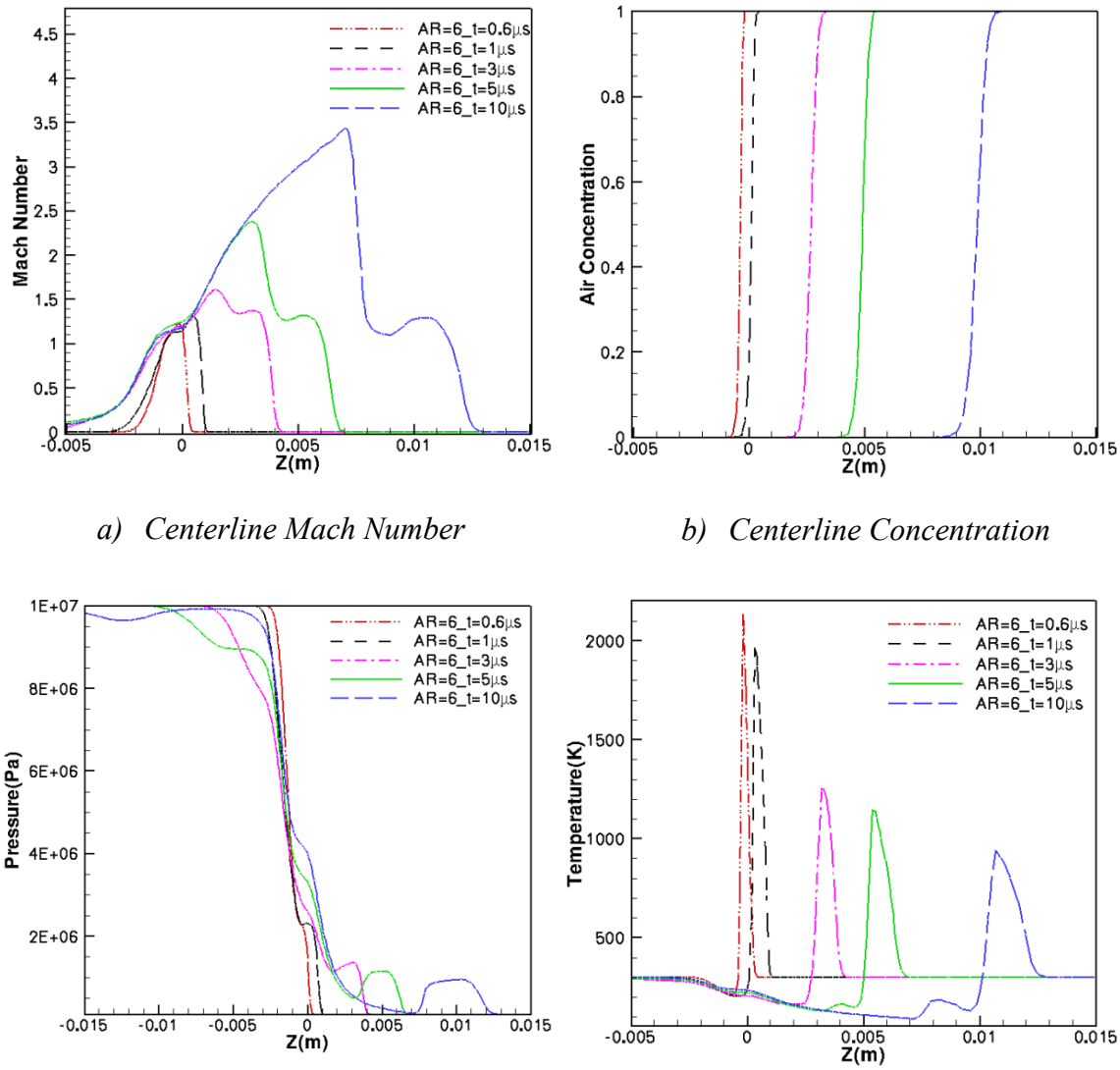

a) Centerline Mach Number *b) Centerline Concentration*

c) Centerline Pressure *d) Centerline Temperature*

Fig. 4.31: *Flow characteristics along the centerline at different times, elliptical orifice (AR=6), Area=19.63 mm^2, P=10 MPa*

4.4.2 The contact surface pressure along the centerline

The pressure ratio of the storage tank to the ambient air affects the expansion of the contact surface pressure and the depressurization of the flow. So in this section, the expansion process of the contact surface pressure along the centerline for both elliptical and circular orifices under the pressure ratio of 10 MPa is investigated.

As it was observed from the 70 MPa cases and also in this section from the 10 MPa storage pressure, the rate at which the pressure at the contact surface decays depends on the dimension and geometry of the orifice. As it is shown in Fig. 4.32-Fig. 4.34, the hydrogen jets issuing from an elliptic orifice with the higher aspect ratio experiences a rapid expansion compared to the jet from an elliptic orifice with the lower aspect ratio and also its circular counterpart. The temporal pressure gradients for different shapes of orifices are almost equal and are not affected. The hydrogen jet issuing from an elliptic orifice expands sooner than the jet from the standard circular orifice, nevertheless it does not expand faster and they have the same expansion rate. Although the expansion process is affected by the shape of the orifice, the depressurization is similar under the same area.

Compared to the jet expansion from a 70 MPa tank, the temporal pressure gradient is not affected by lowering the pressure ratio, but due to the lower pressurized tank, the contact surface pressure decreases to the ambient pressure in a short time. At t=10 μs, the 10 MPa jet from the orifice with the area of 0.8 mm^2 has the contact surface pressure of P=0.3 MPa along the centerline but this value under 70 MPa pressure is P=0.6 MPa.

A steeper slope of the contact surface pressure as a function of time for the small hole compared to the larger orifice confirms that the jet issuing from the big hole experience a

less pronounced expansion and more gradual depressurization which results in a lower temperature diffusion and higher temperature values. These characteristics with the large orifices can intensify the auto-ignition possibility.

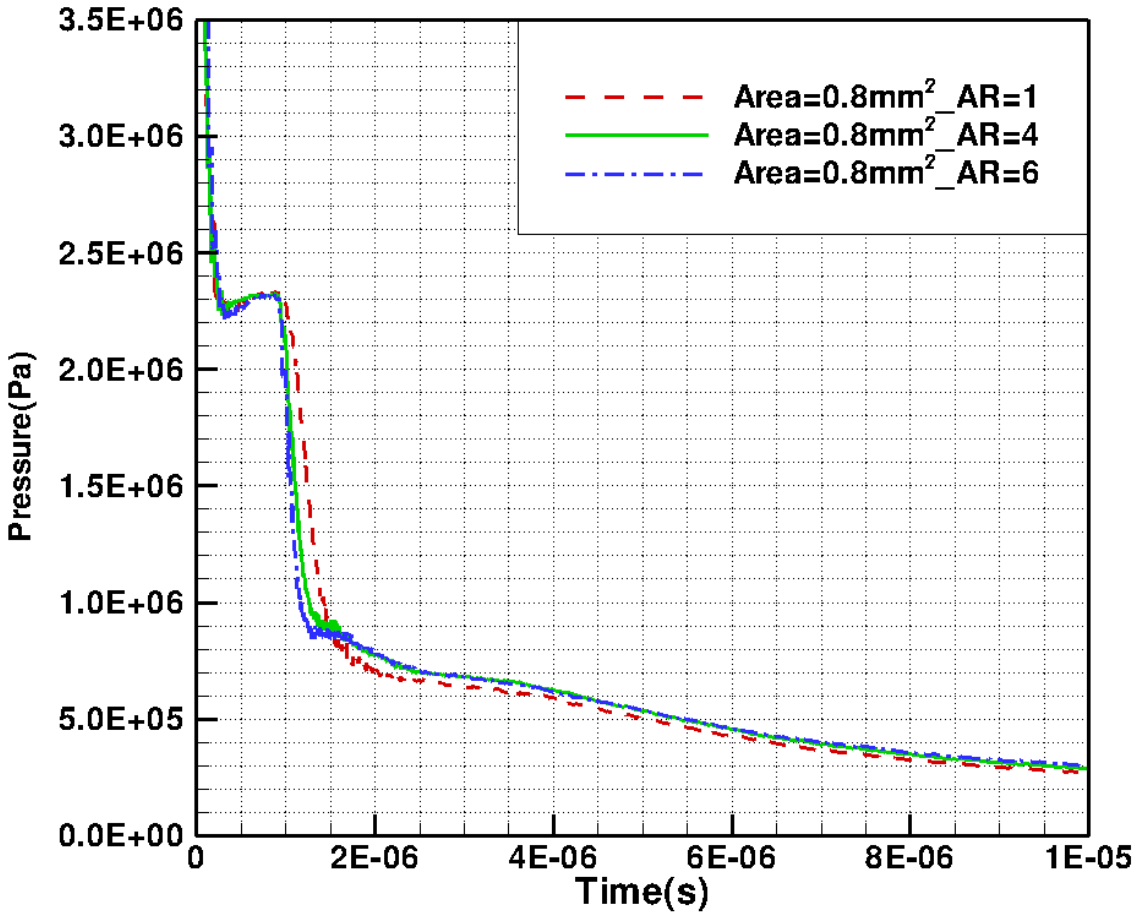

Fig. 4.32: *Contact Surface pressure versus time along the centerline, fixed orifices (circular & elliptical), Area=0.8 mm^2, $P_{reservoir}$ =10 MPa*

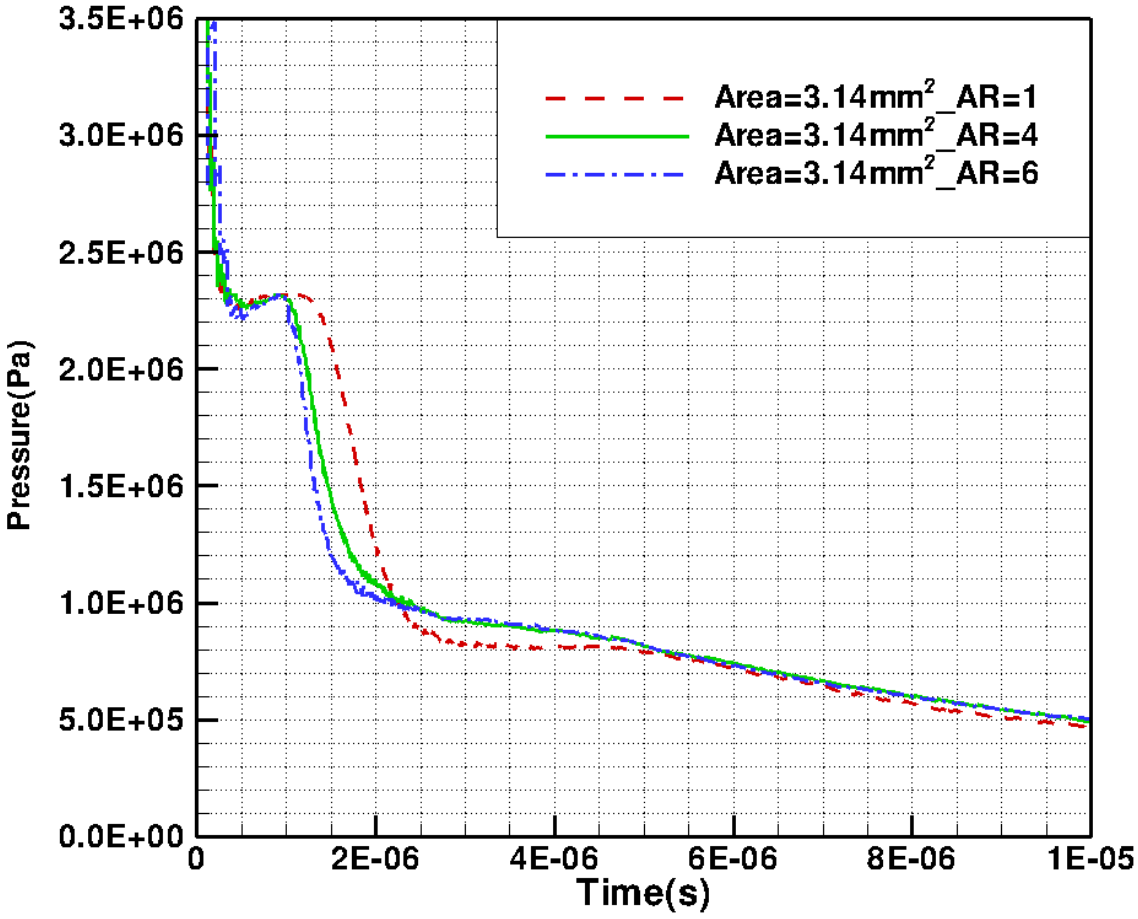

Fig. 4.33: *Contact Surface pressure versus time along the centerline, fixed orifices (circular & elliptical), Area=3.14 mm^2, $P_{reservoir}$ =10 MPa*

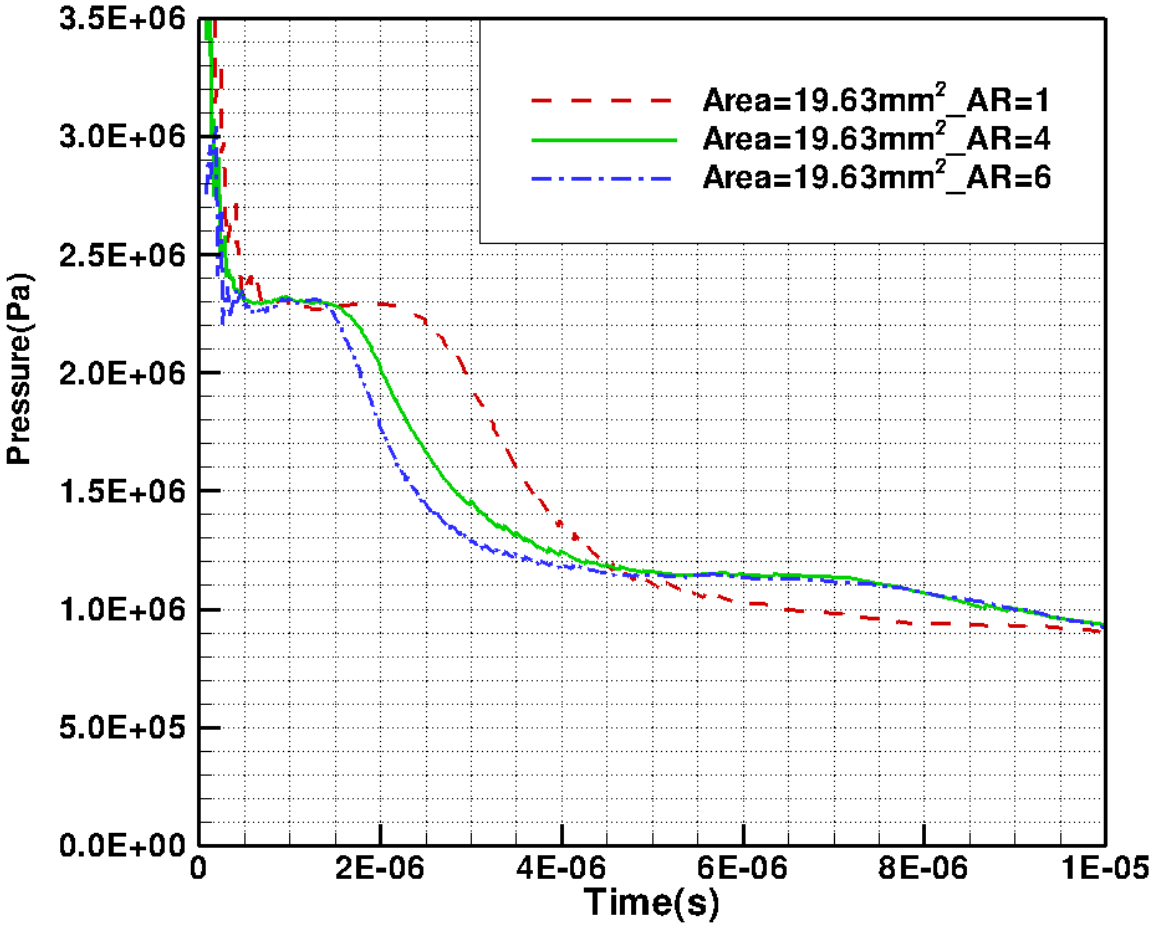

Fig. 4.34: *Contact Surface pressure versus time along the centerline, fixed orifices (circular & elliptical), Area=19.63 mm^2, $P_{reservoir}$ =10 MPa*

Chapter 5

HYDROGEN RELEASE FROM ENLARGING ORIFICES

Owing to the deformation of the exit hole during the hydrogen release in some real situations, the moving mesh is applied to expand the orifices through three feasible scenarios. In this section, firstly, the results related to the expansion of small circular holes with the uniform and equal growth rates which are imposed from the beginning of the simulation (t=0) are presented for two different initial orifice sizes, secondly, the aforementioned cases are evaluated when the orifice starts moving after a release of hydrogen with a uniform and constant speed. Finally, the deformation of a small circular orifice to an elliptical one started from the beginning of the simulation are analyzed. In each section, the comparative study between the hydrogen releases from expanding orifices and their equivalent fixed orifices is carried out.

5.1 Expanding orifices with a uniform radial speed imposed from t=0

In this study, a release hole with a small circular area is expanding into a larger circular hole. It is assumed that the release hole is enlarged from the beginning of the simulation (t=0), i.e. before the hydrogen/air interface reaches the exit of the nozzle. The radial growth rates in all cases in both x and y directions are similar and equal to 200 m/s or 0.2 mm/μs which are imposed based on the predefined velocities on the boundary grids. Two initial orifice diameters of 1mm and 2mm under two filling pressures of 10 MPa and 70

MPa are examined. The two dimensional mesh slices of the expanding release hole with an initial diameter of 2 mm before the mesh deformation at t=0 and at two varying times (t=5 μs & t=10 μs) after discharging the hydrogen into air are illustrated in Fig. 5.1. As stated previously, the computational domain consists of both moving and non-moving sections, so the boundary motion only considered for the release tube and does not influence the rest of the domain.

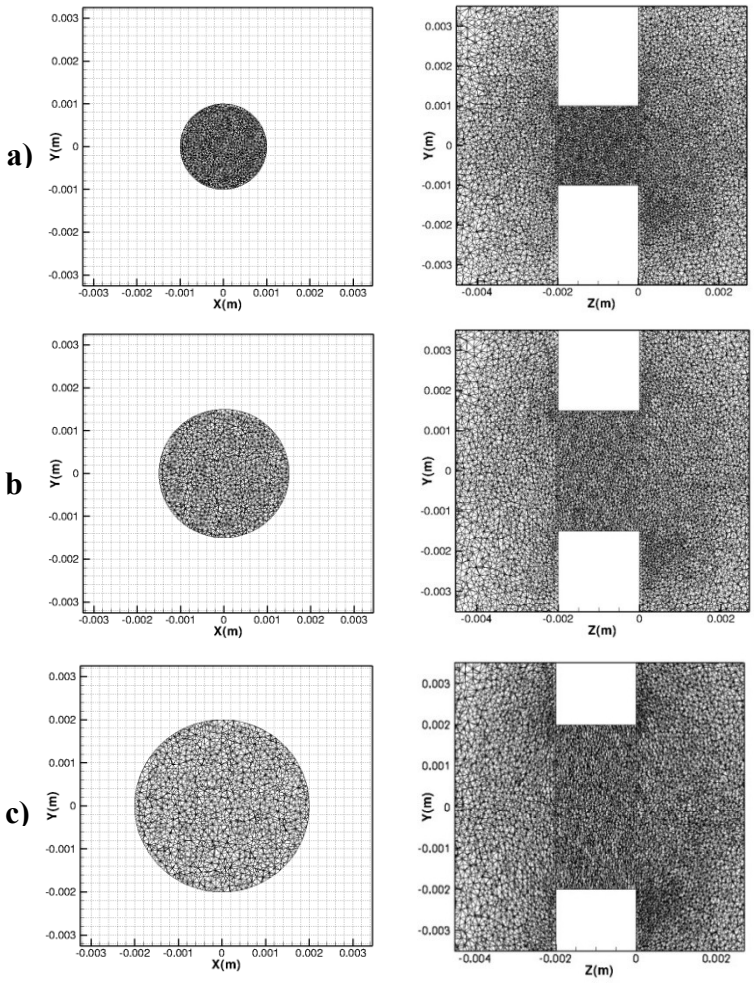

Fig. 5.1: *Two dimensional views of the expanding release hole (D_i=2mm, v=0.2mm/μs), left) cross sectional area, right) side view, a) t=0 (initial diameter), b) t=5 μs, c) t=10 μs*

5.1.1 Hydrogen release from 70 MPa reservoirs

The time histories of the contact surface location in both cases with initial diameters of D_i=1 mm and D_i=2 mm during the first 4 μs of release are compared in Fig. 5.2. It can be recognized that the release time is not affected by applying moving mesh and it is similar to the time of the release from the fixed orifice area. In all cases under the 70 MPa pressure, the hydrogen-air interface reaches the exit at t=0.6 μs. The interfaces in both moving and fixed cases stand in slightly the same location from the exits; however, the interfaces in fixed-mesh cases are a little ahead of their counterparts in the expanding cases. Meanwhile, the contact surface of the jet escaping from a larger area has a steeper slope which means it develops more rapidly into air relative to the interface from a smaller orifice.

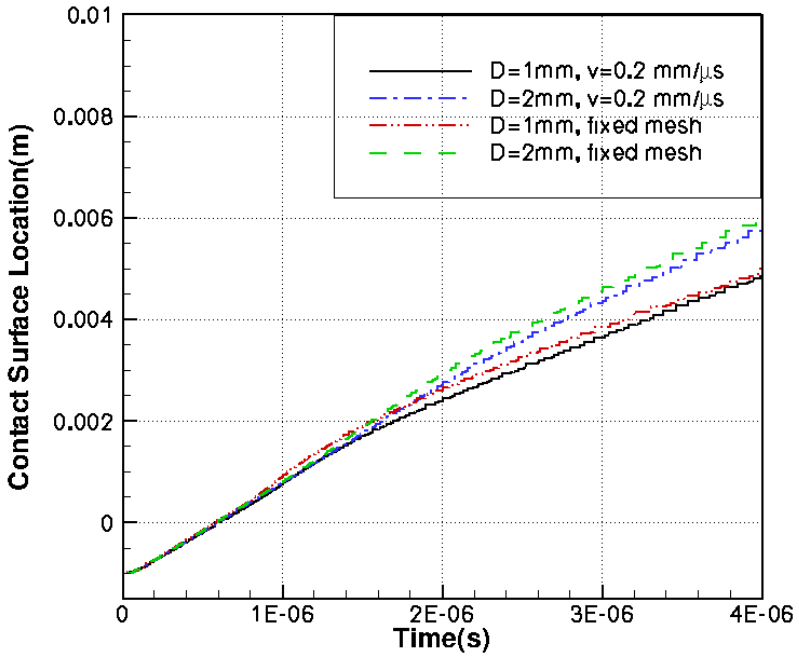

Fig. 5.2: *Contact surface location along the centerline as a function of time, expanding and fixed orifices (D_i=1 mm and D_i=2 mm)*

The time histories of the contact surface pressure along the centerline for enlarging orifices and fixed orifices with two varying initial diameters are illustrated in Fig. 5.3. Along the centerline of the jet, as hydrogen starts releasing from the nozzle, the contact surface pressure related to the expanding exit hole decays sharply and continuously to the atmospheric pressure compared to the expansion of the centerline contact surface pressure in the fixed cases. This behavior starts from t=0, i.e., before the interface of the hydrogen-air leaves the nozzle. The slope of the pressure decay as a function of time is steeper for the moving case in comparison to the fixed case, nevertheless the curves converge at the same time after the expansion and they reach the ambient pressure with the same rate. In addition, the centerline pressure at the interface of hydrogen and air releasing through a smaller area drops more sharply than a larger area and as a result, it reaches the near-ambient pressure with the higher depressurizing rate. This pattern is similar to the cases with the fixed holes (Fig. 4.14).

The evolution of the centerline Mach number, concentration, temperature and pressure of the hydrogen jet issuing from the expanding orifice with the initial diameter of D_i=2 mm and the storage pressure of P= 70 MPa at different moments before and after discharging are shown in Fig. 5.4.

By comparing the evolution of the flow from moving orifices with the fixed orifice, it is concluded that the locations of the contact surface and Mach disk do not change, however, the shocks generated due to the release from the expanding hole is weaker than those from the exit hole with a constant area, since the cross sectional area of the nozzle in moving case is larger than the fixed case at the same moment during the flow expansion. This behavior can describe the bow shock as well.

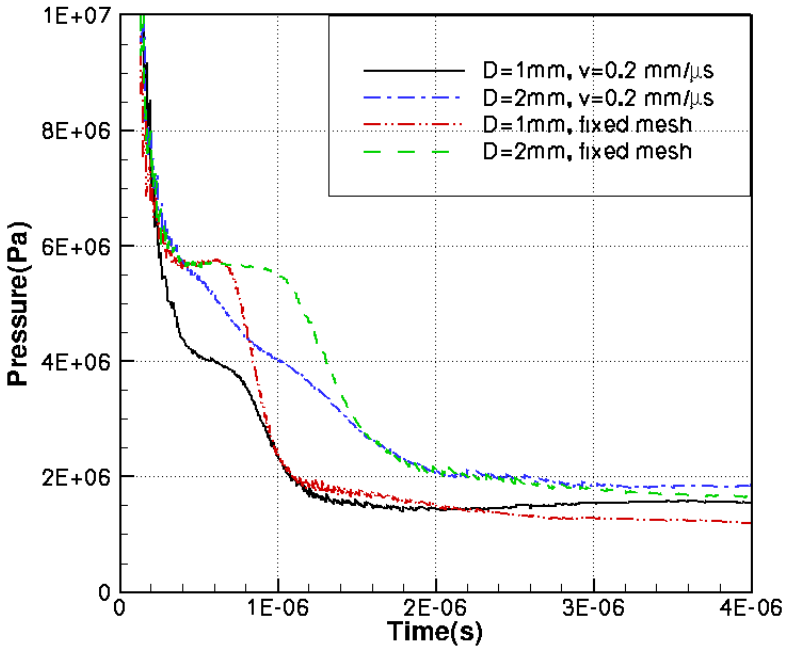

Fig. 5.3: *Contact surface pressure versus time along the centerline, expanding and fixed orifices, (D_i=1 mm and D_i=2 mm), $P_{storage}$=70 MPa*

Similar to the fixed cases, as the jet expands into the surrounding air, the high and low peaks of the temperature along the jet centerline experience a steady decrease, however in moving cases this decay occurred sooner. The maximum hot air temperature along the centerline is located in the release tube. Since the interface pressure of the moving case along the jet centerline decays sharply and more quickly compared to its equivalent fixed case, the temperature of the hot air downstream the interface starts decreasing sooner and with the higher rate of decay [36]. It is noticed, at the release time, both cases have practically the same value of temperature peak, but after discharging of hydrogen jet and during the expansion (at t=1 μs), since the contact surface pressure in the enlarging case decays faster; it has a lower peak of temperature compared to the fixed orifice.

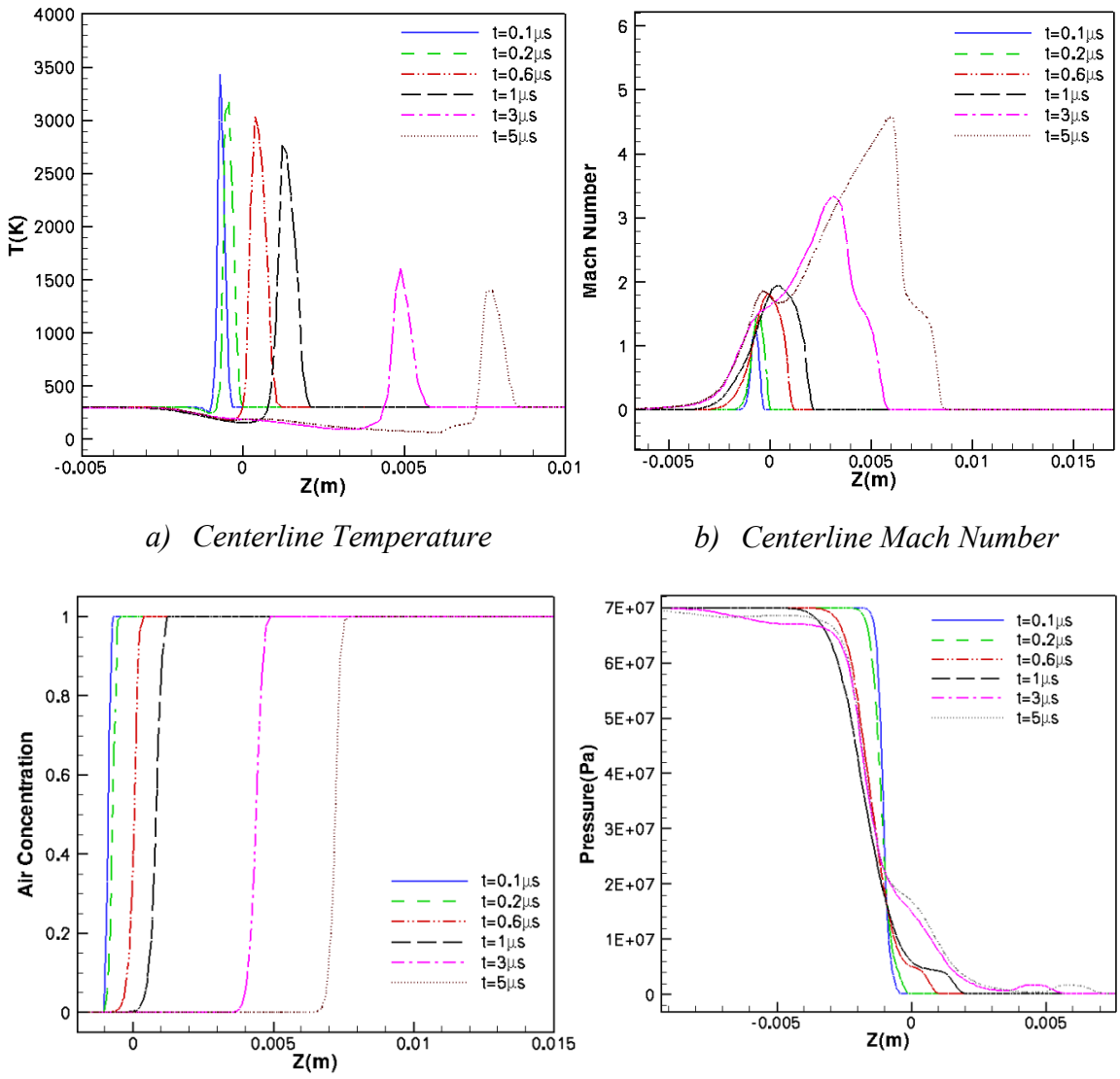

a) Centerline Temperature *b) Centerline Mach Number*

d) Centerline Concentration *c) Centerline Pressure*

Fig. 5.4: *Flow characteristics along the centerline at different times, enlarging orifice, D_i=2mm, P=70 MPa*

5.1.2 Hydrogen release from 10 MPa reservoirs

As it is illustrated in Fig. 5.5, the contact surface at t= 1μs stands on the exit of the nozzle for both fixed and moving orifices with different cross sectional area. From these results and previous ones, it can be concluded that the location of the species interface in the early stage of the release is not affected by changing the orifice geometrical layout and it is only a function of storage pressure, however, it can differ far from the exit, as it is seen for orifices with 2 mm diameter.

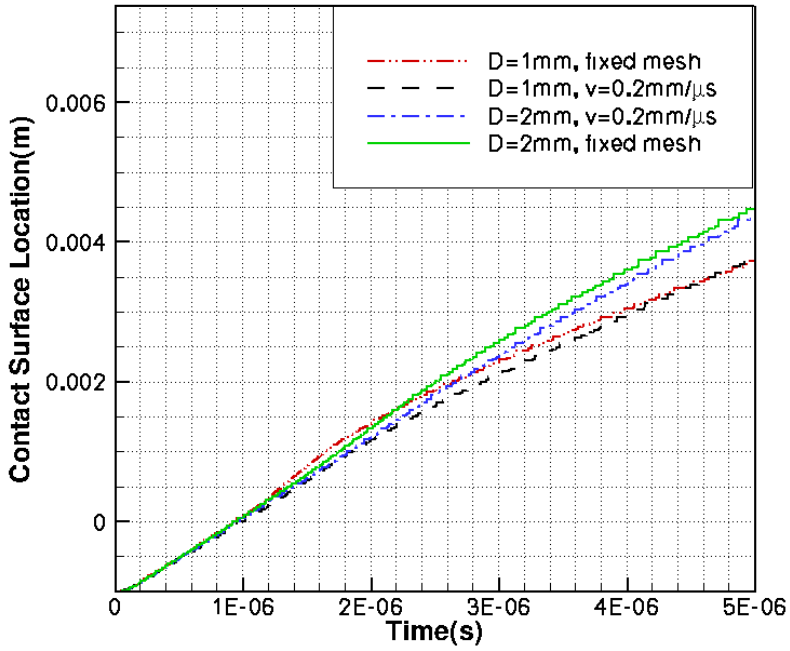

Fig. 5.5: *The comparison of the contact surface locations as a function of time between the cases with expanding and fixed orifices (D_i=1 mm and D_i=2 mm), $P_{storage}$=10 MPa*

Under the lower storage pressure of P=10 MPa, akin to the expanding results from 70 MPa pressure, the expansion of the jet from the enlarging orifices is significantly higher than the pressure drop from the fixed cases. As reported in Fig. 5.6, the contact surface pressure in the expanding cases starts decaying instantly even before the interface reaches

the exit especially in the case with the smaller initial diameter of D_i=1mm. In contrast of the 70 MPa results, the depressurization process is not similar between fixed and moving cases with a lower pressure.

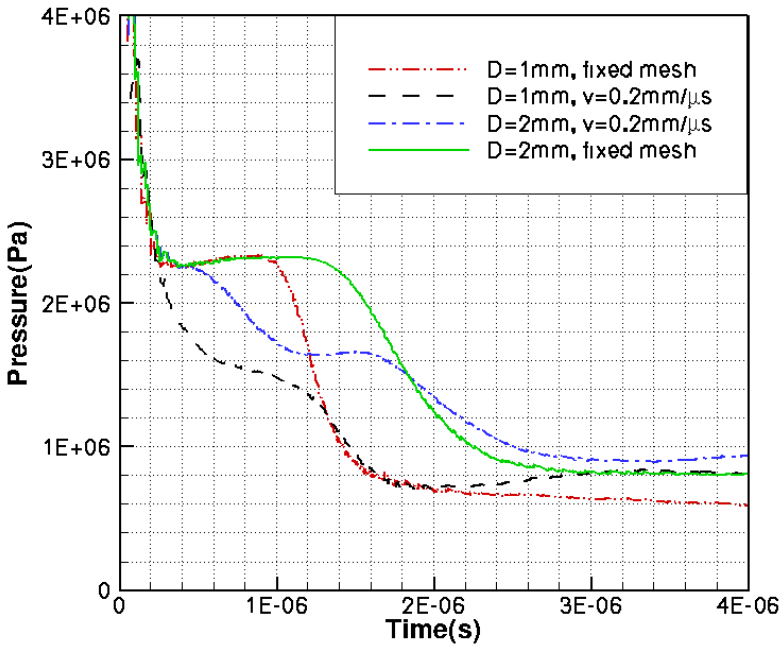

Fig. 5.6: *Contact Surface pressure versus time along the centerline for expanding and fixed orifices, (D_i=1 mm and D_i=2 mm), $P_{storage}$=10 MPa*

5.2 Expanding orifices with a uniform radial speed effective after the release

The aim of this study is to investigate what happens if the orifice starts enlarging once the hydrogen-air interface reaches the exit of the nozzle. So instead of considering the expanding of the release tube from the beginning of the simulation, it is assumed that during the initial period of discharging of hydrogen at which the contact surface is still in the tube, the dimensions of the orifice are fixed and constant, but as soon as the contact surface is at the location of the exit hole that is at the release time, the boundary domain

of the orifice starts enlarging with a uniform radial speed of v=200 m/s or equivalently v=0.2 mm/μs. This evaluation can predict the abrupt release of hydrogen from the release tube more accurately based on the real scenario.

In order to compare the results obtained in this section with the fixed cases, the CFL number is defined akin to the fixed case. As it was studied in previous sections, the hydrogen-air interface in the case with the filling pressure of P=70 MPa leaves the exit hole at t=0.6 μs, while this time for 10 MPa pressure is t=1 μs. Hence, in this study, before the release time, the mesh is fixed and does not change with time but at t=0.6 μs (for the cases with the pressure of 70MPa) and t= 1 μs (for the cases with the pressure of 10 MPa) and greater than those, the boundary of the release tube starts moving in both the x and y directions uniformly with the rate of v=0.2 mm/μs.

The contact surface pressures versus time for orifices with initial diameters of D_i=1 mm and D_i=2 mm under the storage pressure of 70 MPa are compared with their counterparts in the case that the hole is expanding from t=0 and for the fixed orifices. Results are shown in Fig. 5.7 and Fig. 5.8. In addition, the obtained results under the tank pressure of 10 MPa are presented in Fig. 5.9 and Fig. 5.10. It is noticed that if the orifice starts enlarging when the contact surface reaches the exit of the nozzle, the pressure along the centerline decreases slowly compared to the cases at which the orifice deforms when the interface of the hydrogen-air is in the middle of the release tube. By comparing the pressure expansion in this scenario with that from the fixed orifice area, it is concluded that the interface pressure decays with virtually a similar pattern as the fixed case and there is no difference in terms of pressure gradient and expansion during the release of hydrogen into air; however, the depressurization for the expanding case occurs slightly

sooner compared to the fixed case. Hence, the study of discharge of hydrogen from a pressurized tank through the fixed orifice can accurately predict the behavior of the hydrogen dispersion and even the possibility of the auto-ignition in the vicinity of the release exit.

By comparing the jet characteristics from the moving orifice with the initial diameter of D_i=2 mm which is shown in Fig. 5.11, with their equivalents from the fixed orifice (Fig. 4.8), it can be recognized that the jet behavior is not affected by applying the deformation of the orifice at the release time. The temperature profile and the highest peak of the temperature at various times after the release of hydrogen present the same values as the fixed case. This condition also exists for the Mach number and the pressure profiles.

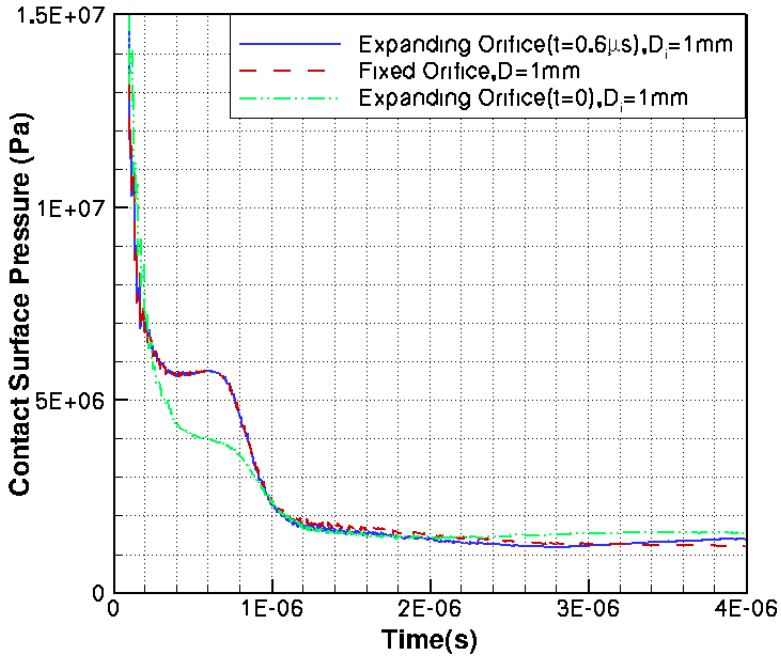

Fig. 5.7: *The comparison of the contact surface pressures along the centerline between expanding orifices (started at t=0. 6 μs & t=0) and fixed orifice, (D_i=1 mm, P=70 MPa)*

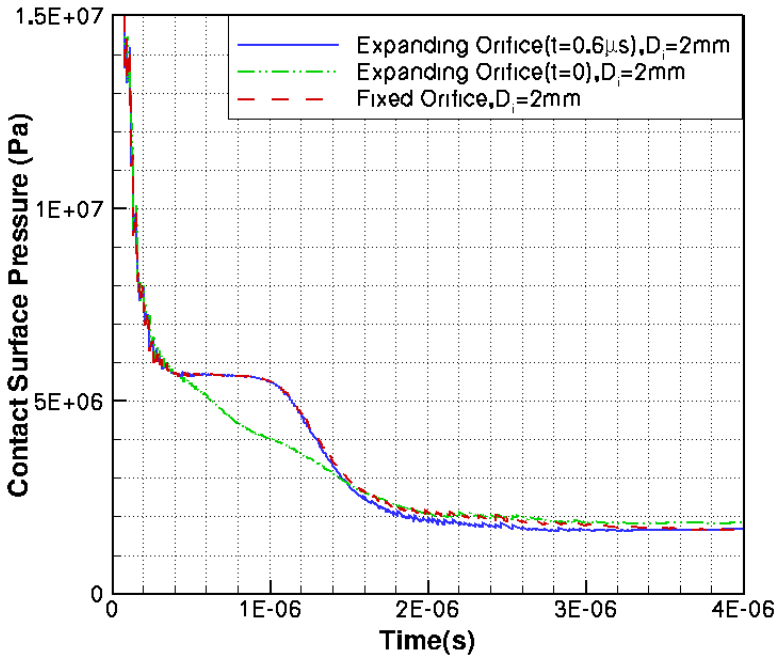

Fig. 5.8: *The comparison of the contact surface pressures along the centerline between expanding orifices (started at t=0.6 μs & t=0) and fixed orifices, (D_i=2 mm, P=70 MPa)*

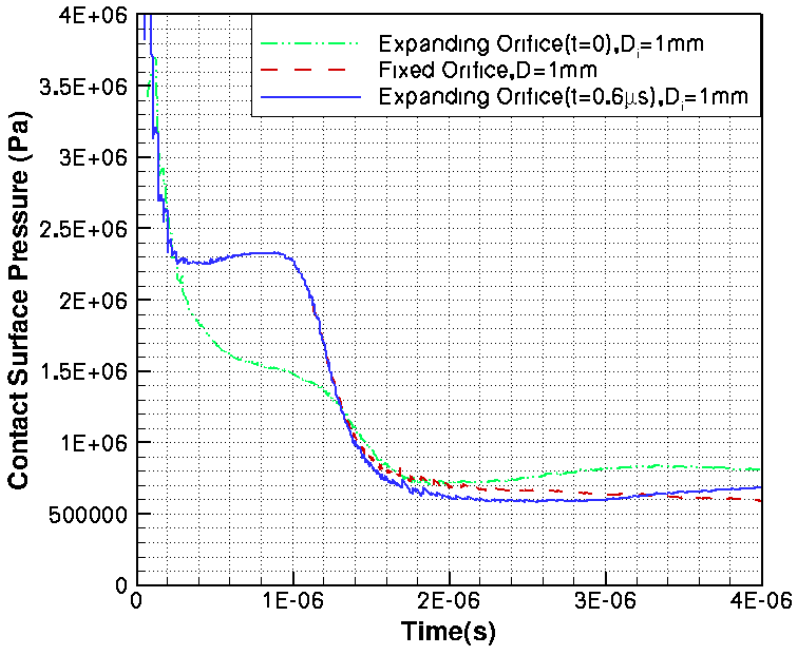

Fig. 5.9: *The comparison of the contact surface pressures along the centerline between expanding orifices (started at t=0.6 μs & t=0) and fixed orifices, (D_i=1 mm, P=10 MPa)*

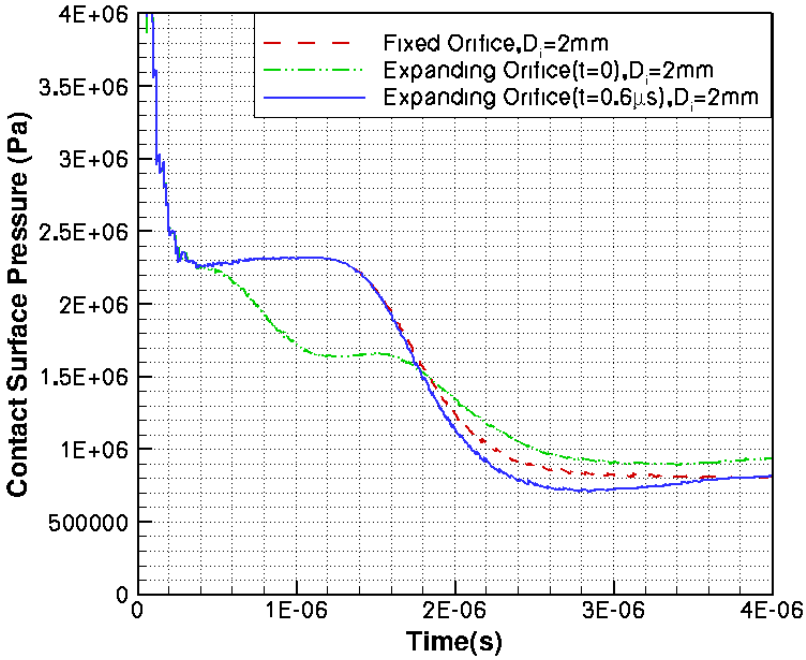

Fig. 5.10: *The comparison of the contact surface pressures along the centerline between expanding orifices (started at t=0.6 μs & t=0) and fixed orifices, (D_i=2 mm, P=10 MPa)*

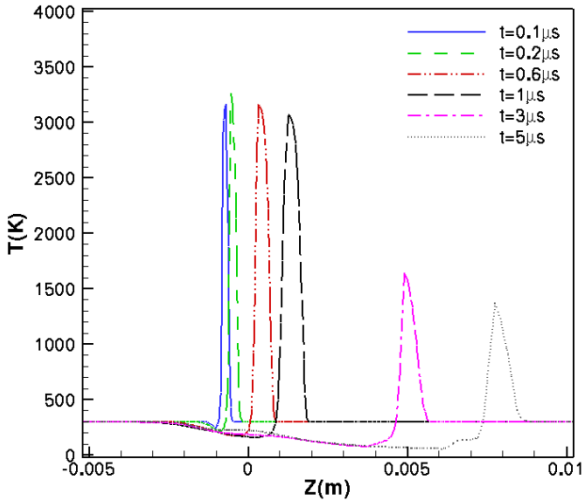

a) Centerline Temperature

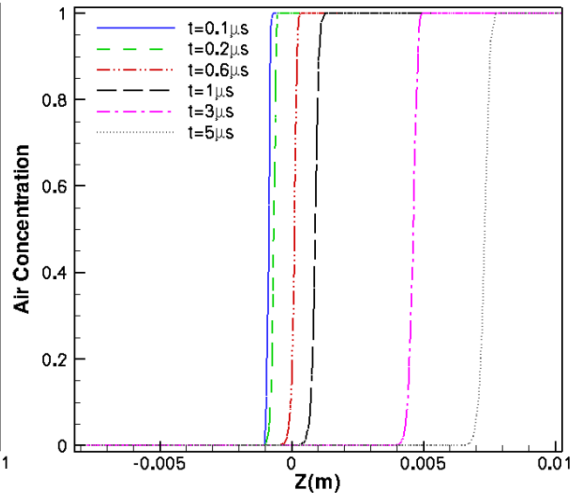

b) Centerline Concentration

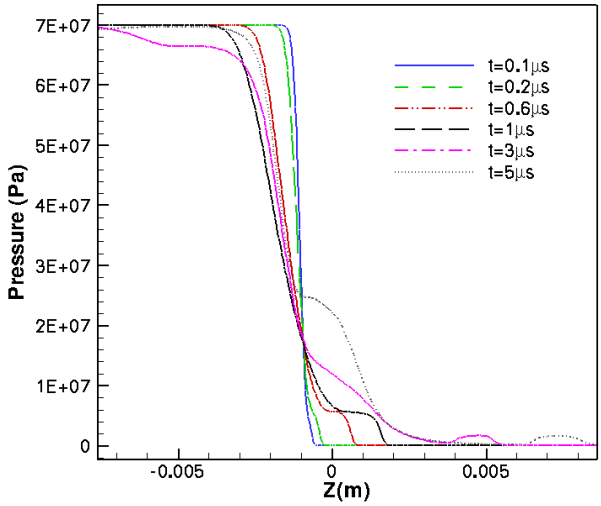

c) Centerline Pressure

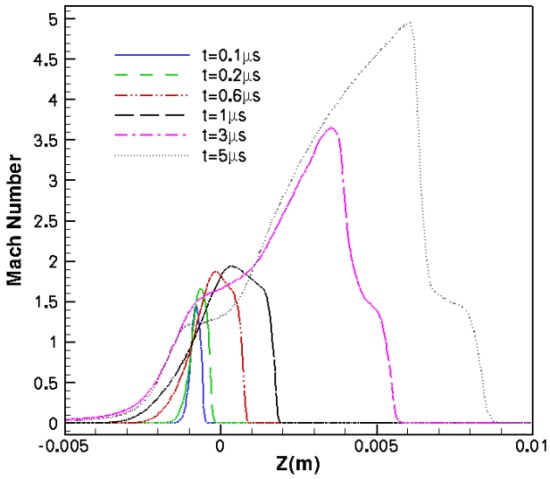

d) Centerline Mach Number

Fig. 5.11: *Flow characteristics along the centerline at different times, moving orifice (D_i =2mm), Area=3.14 mm^2, P=70 MPa*

5.3 The deformation of a small circular hole to an elliptical opening

In this section the effect of the deformation of a small circular opening to an elliptic exit hole on the dispersion of hydrogen is investigated and the results obtained are compared with those from the fixed orifice and the expanding orifice.

In this approach, a small circular opening is stretched into an elliptical hole in the direction perpendicular to the axial axis of the reservoir, while the other axis (minor axis) of the circular orifice preserves its initial length which equals to the diameter of the circular aperture. The stretching rate is akin to the expanding rate of the previous aforementioned scenarios and it is v=200 m/s.

Based on the spring analogy, detailed in chapter 2, to satisfy the static equilibrium for the interior displacements by imposing the grid velocity on the boundary nodes along only the y coordinate direction, the calculation of the grids displacements and updating the positions of the interior vertices are only done in the y direction, since there is no displacement along the x coordinate axis.

To evaluate the deformation of a circular opening to an elliptical exit, small circular holes with the diameters of D=1mm and D=2mm under two different filling pressures of 10 MPa and 70 MPa are considered.

The two dimensional mesh slices of the round release hole with the initial diameter of D=2 mm which deforms to an elliptical opening at different moments including the initial time (t=0) and three different times (t=5 μs, t=10 μs & t=20 μs) during the dispersion of hydrogen into the ambient air are illustrated in Fig. 5.12 and Fig. 5.13.

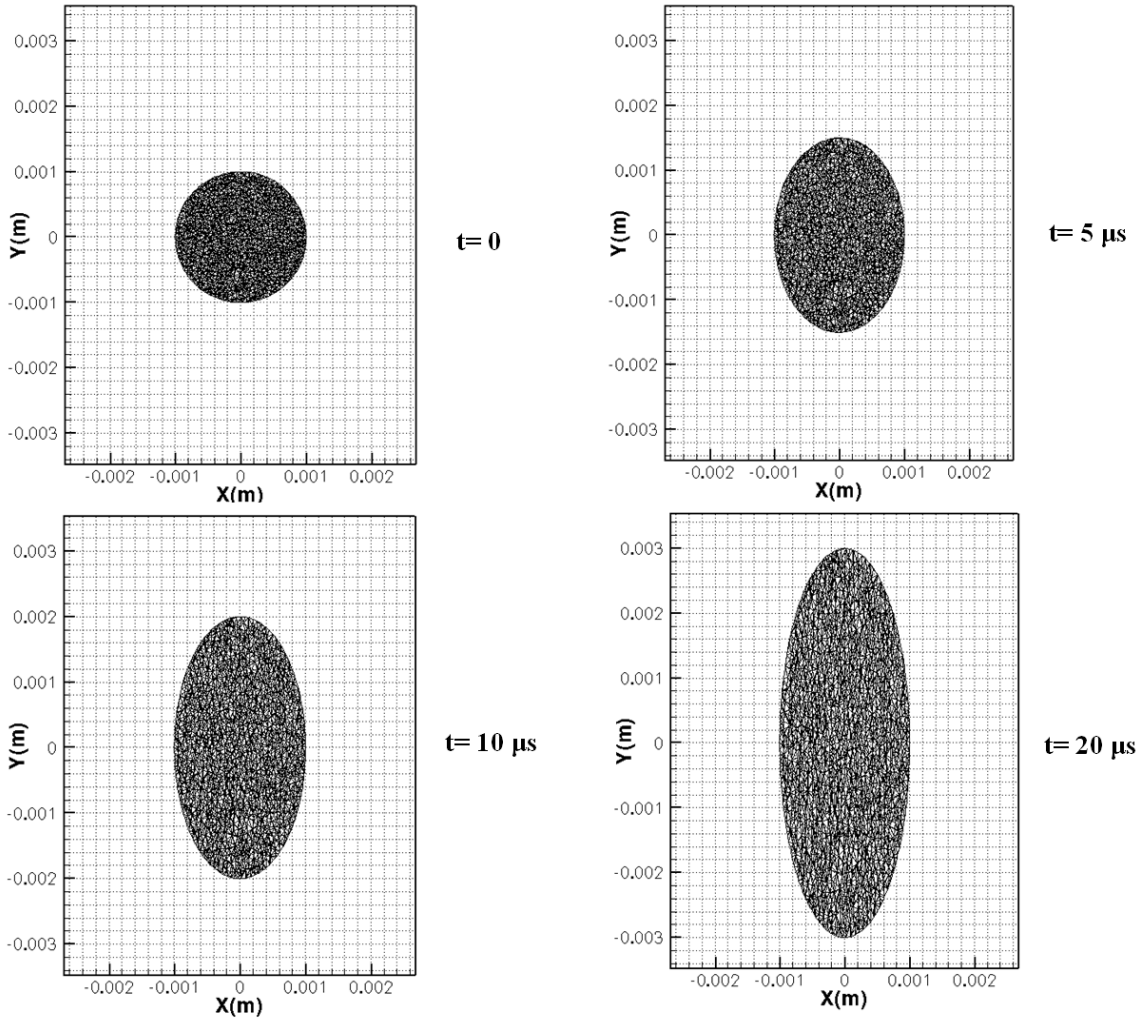

Fig. 5.12: *Cross sectional areas: the deformation of a circular opening to an elliptic hole at different moments (t=0, t=5 µs, t=10 µs & t=20 µs), D_i=2mm, v=0.2mm/µs*

To understand the time of release of hydrogen in this case and evaluate the influence of this deformation on the contact surface location, the position of the interface is tracked in time. The obtained results for the initial diameter of D=1 mm under two different pressures of 70 MPa and 10 MPa are shown in Fig. 5.14 and Fig. 5.15, respectively.

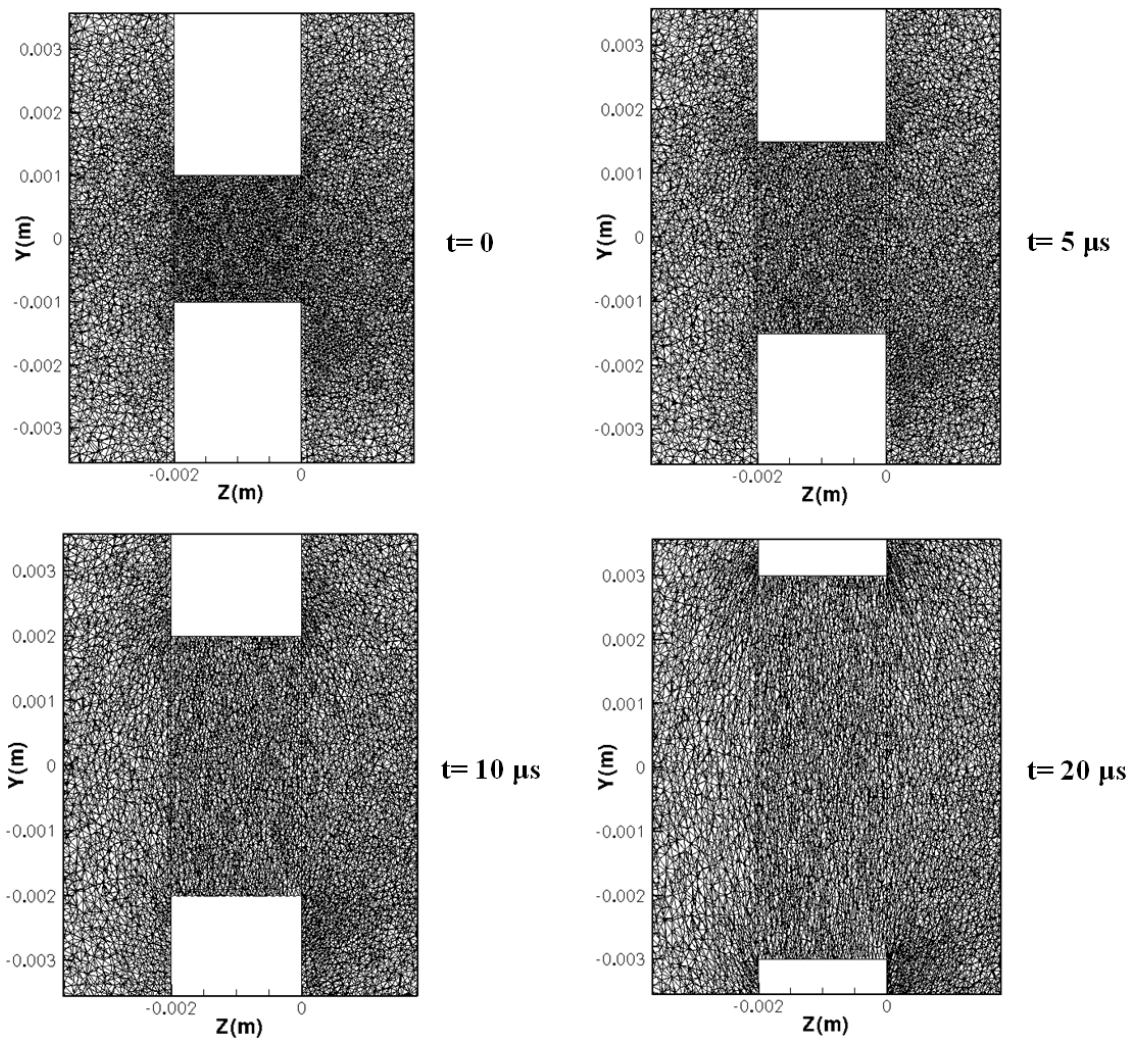

Fig. 5.13: *Side views (y-z plane) of the deformation of a circular opening to an elliptic hole at different moments (t=0, t=5 µs, t=10 µs & t=20 µs), D_i=2mm, v=0.2mm/µs*

The release time in this case same as the other cases under the pressure of 70 MPa is t=0.6 µs and under the pressure of 10 Mpa is t= 1 µs.

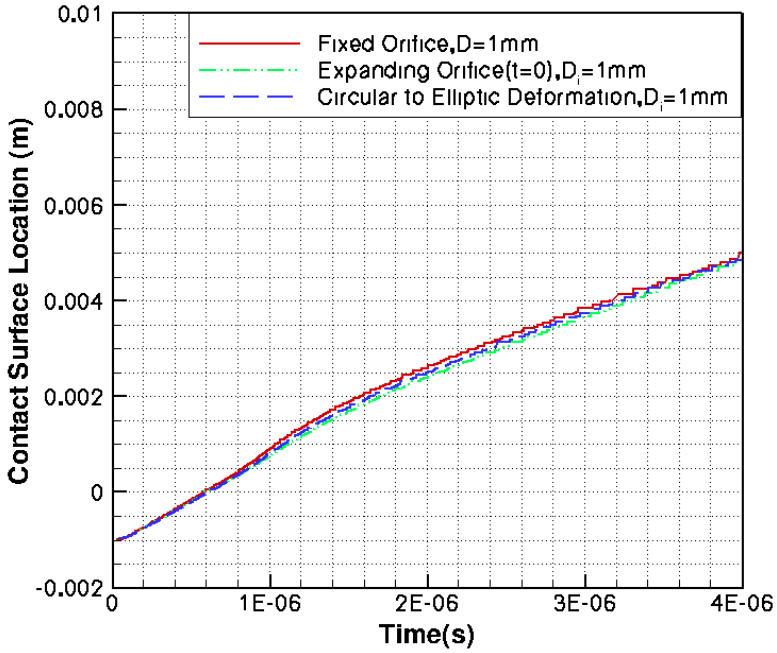

Fig. 5.14: *The comparison of the contact surface locations as a function of time between the cases with the deformed, enlarging and fixed orifices (D_i=1 mm), $P_{storage}$=70 MPa*

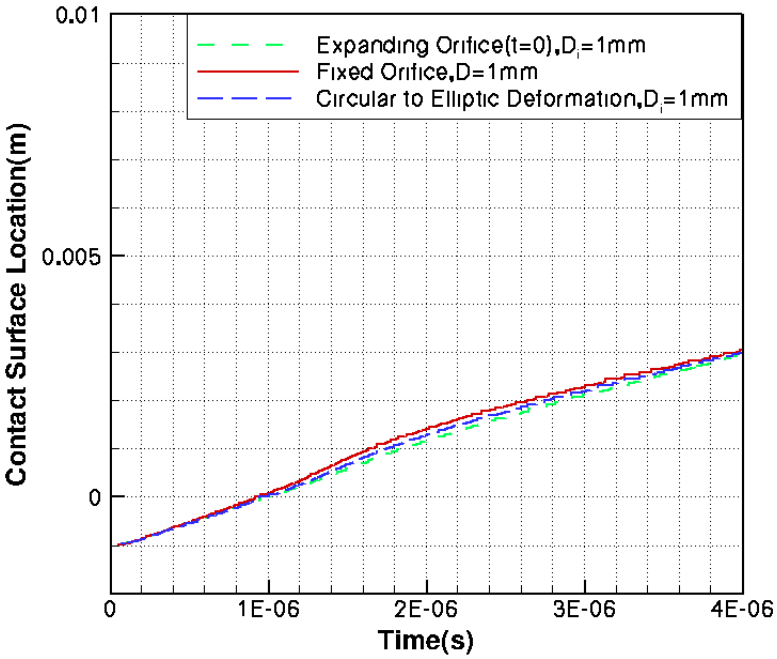

Fig. 5.15: *The comparison of the contact surface locations as a function of time between the cases with the deformed, enlarging and fixed orifices (D_i=1 mm), $P_{storage}$=10 MPa*

The location of the contact surface is not affected by deformation of the exit hole and it stands on the same location as fixed and expanding cases from the exit of the nozzle during the expansion.

The expansion of the contact surface pressure on the centerline in this case is compared with the pressure drops from its equivalent fixed and expanding orifices. The result corresponding to the initial orifice diameter of D=1 mm for two varying pressures of reservoir are shown in Fig. 5.16 and Fig. 5.17. It can be recognized that in both moving cases (deformation of circular to elliptic and expanding orifice) the pressure starts decaying sharply from the beginning of the release process; the expansion from the orifice which is stretching into an elliptic shape occurs slowly compared to the circular enlarging orifice but it is faster than the fixed case. Generally, the temporal pressure gradient is identical in all cases, but the initial slope of the pressure curve versus time during the expansion related to the expanding case is steeper than the stretching case, and the slope of the pressure decay for the stretching hole is higher than the fixed case. All curves after the expansion process converge at the same time to the equal value of the contact surface pressure. Hence, they depressurized into the ambient pressure with a same rate.

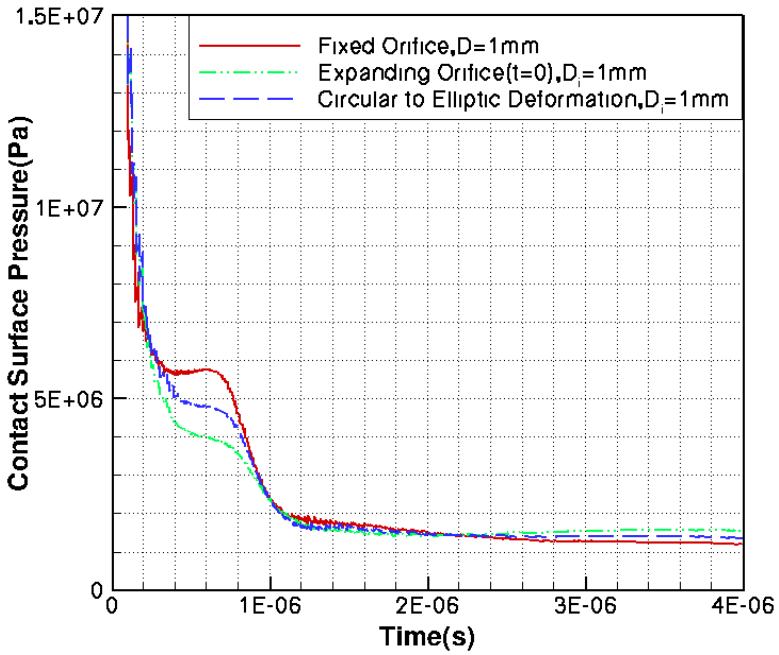

Fig. 5.16: *The comparison of the contact surface pressures along the centerline between the deformed, the expanding (started at the release time) and the fixed holes, (D_i=1 mm), P=70 MPa*

The flow characteristics along the centerline at different moments of discharging of hydrogen from 70 MPa pressurized tank and the orifice with an initial diameter of D=2 mm are illustrated in Fig. 5.18. By comparing the temperature profiles during the expansion with their counterparts from the fixed and circular enlarging orifices (Fig. 4.8 (d) & Fig. 5.4 (a)), it is concluded that before the release of hydrogen into the air, i.e. in the period that the interface has not left the release exit, the deforming case experience a higher value of hot air temperature compared to the circular enlarging orifice but this value is still lower than the fixed case. Upon the release of hydrogen, the diffusion of hydrogen from deforming and enlarging cases are practically the same and they have the

similar temperature profile. The Mach disk and the lead shock in this case is weaker than the fixed case, however they propagate into the air with the same rate.

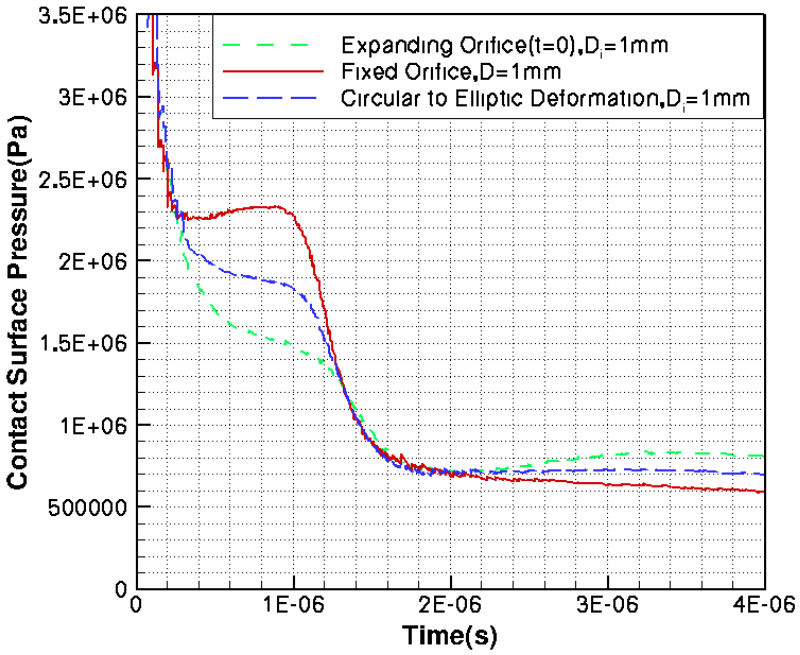

Fig. 5.17: *The comparison of the contact surface pressures along the centerline between the deformed, the expanding (started at the release time) and the fixed holes, (D_i=1 mm), P=10 MPa*

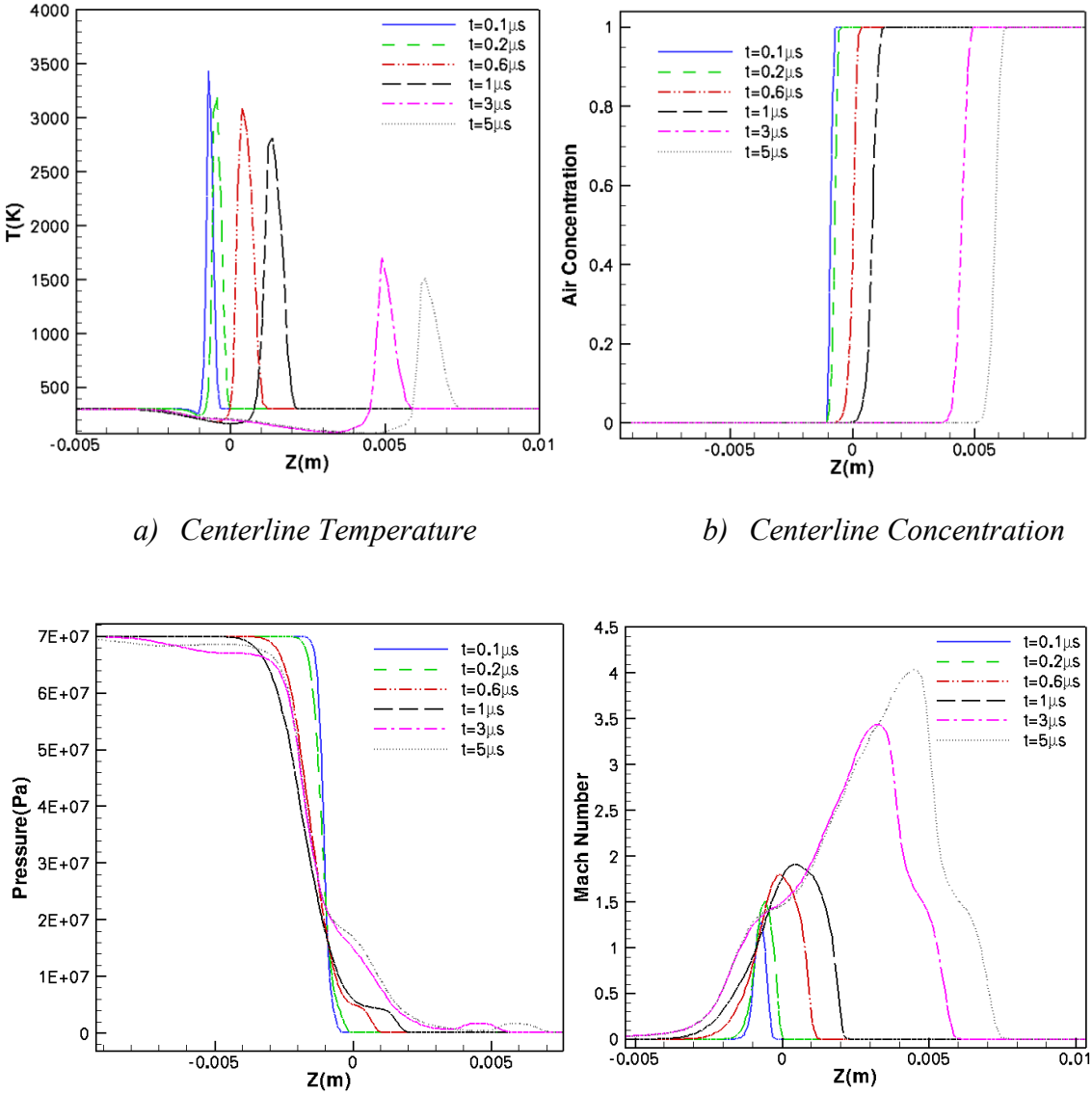

a) Centerline Temperature *b) Centerline Concentration*

c) Centerline Pressure *d) Centerline Mach Number*

Fig. 5.18: *Flow characteristics along the centerline at different times, the stretching hole, D=2mm, P=70MPa*

Chapter 6

CONCLUSIONS AND RECOMMENDATIONS

6.1 Conclusions

The initial stage of the incident releases of hydrogen from high-pressure reservoirs into the quiescent ambient air through various types of orifices have been numerically investigated using a 3D parallel in-house code. The work done in this thesis studied the effect of the exit hole geometry on the development and dispersion of highly underexpanded hydrogen jet issuing from different shapes of orifices. Varying feasible geometries and configurations of the exit hole including fixed orifices, expanding orifices and the combination of them were evaluated to predict the behavior of the hydrogen gas when escaping into the ambient air.

In the case of fixed opening, two types of orifices including circular and elliptical holes were examined. Three different areas based on 1 mm, 2 mm and 5 mm diameters of circular exits were modeled. For a given area, two varying dimensions of elliptic orifices with aspect ratios (major axis/minor axis) of AR=4 and AR=6 were considered and compared with their comparable circular counterparts (AR=1).

In case of moving orifices, three different approaches under varying conditions and configurations were considered such as the expanding of a small round hole which started moving before the release of hydrogen into air (t=0), the enlarging of a circular hole effective after the release of hydrogen (t> release time) and the deformation of a circular

aperture to an elliptical opening. In each case, two initial diameters of D_i=1 mm and D_i=2 mm were simulated and the results were compared with those from the fixed circular openings which had the same diameters. The growth rates of the initial round holes in all cases were similar and set to v=0.2 mm/μs. This value in the last scenario (the stretching exit hole) was restricted to the y coordinate axis. All cases were evaluated under two different storage pressures of 10 MPa and 70 MPa.

As convection dominates viscous effects in strongly under-expanded supersonic jets near the release exit, flow was modeled by the compressible Euler equations. Since the critical location of the auto-ignition is in the near field flow, in this study, only the near exit jet was simulated. The transport (advection) equation was applied to track the shape and the location of the hydrogen-air interface. The Abel Nobel real gas law was used since high-pressure hydrogen flow deviates from the ideal gas assumption.

The development of the hydrogen jet into the ambient air, the jet flow characteristics along the centerline and the expansion of the contact surface pressure along the centerline were studied and compared between all aforementioned cases.

The numerical analysis shows that the effects of the storage pressure and the size of the orifice on the dispersion and development of the hydrogen jet are more dominant than the effect of the orifice shape; however, the effect of the expanding orifice which is effective from the beginning of the simulation is considerable.

By maintaining the orifice area and comparing the hydrogen jets issuing from the fixed elliptical and fixed circular orifices, it is concluded that, as the aspect ratio of the orifice increases, the contact surface pressure decreases and expands more rapidly. Therefore,

the contact surface pressure of the elliptical jet decays more quickly than the comparable circular jet. Increasing the orifice area led to intensify the effect of the orifice geometry. Meanwhile, for a given orifice shape, the larger orifice area resulted in the more pronounced contact surface pressure expansion.

The same comparison between the hydrogen jets from varying configurations of expanding orifices and fixed round orifices was carried out. Results have predicted that the hydrogen jet escaping from the enlarging orifice effective from t=0 experiences a rapid interface pressure expansion with a steeper temporal pressure gradient compared to its equivalent from the fixed orifice. Nevertheless, this behavior was not recognized for the scenario that the orifice area started enlarging when the hydrogen-air interface reached the exit hole. In this case, the contact surface pressure decayed with virtually a similar pattern as its comparable fixed round orifice and had a slower expansion compared to the moving orifice effective at the beginning of the simulation. For the configuration at which a small circular hole stretched into an elliptical opening, the interface pressure on the centerline decreased faster compared to fixed case but slower in comparison with the uniform enlarging orifice.

Due to the change in the expansion of the contact surface pressure by using different shapes and configurations of the orifice, the temperature profiles were affected and the rates of hot air temperature drop were altered case to case. This behavior can affect the auto-ignition possibility of the hydrogen jet escaping from different shapes and sizes of exit holes.

6.2 Recommendations

The following areas are suggested for further explorations through numerical analyses:

- The adaptive mesh refinement technique can be added to our in-house code to change the accuracy of a solution in certain regions such as the interface of two species and regions with high pressure gradient. This method can reduce the amount of CPU time required for simulation.
- The spring analogy method which was implemented in our in-house code does not contain the remeshing method. So, for a large displacement of the boundary grids, the call quality can deteriorate which results in the negative cell volumes. Therefore, it is required to add remeshing or mesh refinement methods to update the highly skewed cells with the new cells.
- To evaluate the long term dispersion of hydrogen in air and also to predict its propensity to ignition far from the exit, the viscosity and the gravity effects must be considered. Therefore, an appropriate turbulence model needs to be applied. Although the last version of our in-house code contains this feature, it has not been used for modeling of two species flow.
- Large Eddy Simulation (LES) can be used as a turbulence model to study the dispersion and ignition of hydrogen in air.
- The current advection equation in our code is required to be modified in the conservative form of the transport equation and solved coupled with the Euler or the Navier Stokes equations to calculate the length of flammable envelop and safety distance which are important for the development of the safety codes and standards.

- The effect of the presence of obstacles close to the release exits on the spontaneous ignition and dispersion of hydrogen can be studied. Different shapes of orifices can be considered for this evaluation.

REFERENCES

[1] Earth System Research laboratory (2013), *monthly means CO_2 at the Mauna Loa observatory,* U.S. Department of Commerce, National Oceanic & Atmospheric Administration, accessed 5 June 2013, <http://www.esrl.noaa.gov/gmd/ccgg/trends/>.

[2] International Energy Agency, *IEA Energy Technology Perspectives 2012*, scenarios and strategies to 2050, 2012.

[3] Tajallipour, N., Kumar, V., Paraschivoiu, M., *Large-eddy simulation of a compressible free jet flow on unstructured elements*, International Journal of Numerical Methods for heat & Fluid, **23,** No. 2, 2013, pp. 336-354.

[4] Hatanaka, K., satio, T.*, Influence of nozzle geometry on underexpanded axisymmetric free jet characteristics*, Shock Waves, **22**, 2012, pp. 427-434.

[5] Menon, N., *Analysis of non-axisymmetric underexpanded jet flow fields*, Ph.D. Thesis, University of Witwatersrand, 2009.

[6] Menon, N., Skews, B. W., *3-D shock structure in underexpanded supersonic jets from elliptical and rectangular exits,* Shock Waves, 2005, pp. 529-534.

[7] Menon, N., Skews, B. W., *Shock wave configurations and flow structures in non-axisymmetric underexpanded sonic jets*, Shock Waves, **20**, 2010, pp. 175-190.

[8] New, T. H., Lim, T. T. and Luo, S. C., *Elliptic jets in cross flow*, Journal of Fluid Mechanics, **494**, 2003, pp. 119-140.

[9] Panda, J., Zaman, K. B. M. Q. and Seasholtz, R. G., *Measurement of Initial Conditions at Nozzle Exit of High Speed Jets*, NASA/TM, AIAA, 2004, pp. 2001-2143.

[10] Ishii, R., Fujimoto, H., Natta, N., Umeda, Y., *Experimental and numerical analysis of circular pulse jets,* Journal of Fluid Mechanics, **392**, 1999, pp. 129-153.

[11] Krothapalli, A., Baganoff, D. and Karamcheti, K., *on the mixing of a rectangular jet*, Journal of Fluid Mechanics, **107**, 1981, pp. 201-220.

[12] Makarov, D., Molkov, B., *Structure and Concentration Decay in Supercritical Plane Hydrogen jet*, Proceedings of the Eighth International Symposium on Hazards, Prevention and mitigation of Industrial explosions, 5-10 September 2010, Yokohama, Japan.

[13] Zheng, J.Y., Bie, H.Y., Xu, P., Liu, Y.L., Zhao, Y.Z., *Numerical simulation of hydrogen release from high-pressure storage vessel*, 3rd International Conference on Hydrogen Safety, Ajacco, France, Sep. 16-18, 2009.

[14] Xiao, J., Travis, J., Breitung, W., *Hydrogen release from a high-pressure GH2 reservoir in case of a small leak*, 3rd International Conference on Hydrogen Safety, Ajacco, France, Sep. 16-18, 2009.

[15] Han, S.H., Chang, D. and Kim, J.S., *Release characteristics of highly pressurized hydrogen through a small hole*, International Journal of Hydrogen Energy, **38**, No. 8, 2013, pp. 3503-3512.

[16] Peneau, F., Pedro, G., Oshkai, P., Benard, P. and Djilali, N., *Transient supersonic release of hydrogen from high pressure vessel: A computational analysis*, International Journal of Hydrogen Energy, **34**, No. 14, 2009, pp. 5817-5827.

[17] Mohamed, K. and Paraschivoiu, M., *Real gas simulation of hydrogen release from a high-pressure chamber*, International Journal of Hydrogen Energy, **30**, No. 8, 2005, pp. 903-912.

[18] Cheng, Z., Agranat, V., Tchouvelev, A. V., Houf, W., Zhubrin, S. V., *PRD hydrogen release and dispersion; a comparison of CFD results obtained from using ideal and real gas law properties*, First international conference on hydrogen safety, Pisa, Italy September 8–10, 2005.

[19] Khaksarfard, R. and Paraschivoiu, M., *Numerical simulation of high pressure hydrogen release through an expanding opening*, International Journal of Hydrogen Energy, **37**, No. 10, 2012, pp. 8734-8743

[20] Maxwell, B.M. and Radulescu, M.I., *Iignition limits of rapidly expanding diffusion layers: Application to unsteady hydrogen jets*, Combustion and Flame Journal, **158**, No. 10, 2011, pp. 1946-1959.

[21] Radulescu, M.I., Law, C.K., *The transient start of supersonic jets, Journal of Fluid Mechanics*, 2007, pp. 331-369.

[22] Golub, V. V., Baklanov, D. I., Golovastov, S. V., Ivanov, M. F., Laskin, I. N., Saveliev, A.S., Semin, N. V., Volodin, V. V., *Mechanisms of high-pressure hydrogen gas self-ignition in tubes*, Journal of Loss Prevention in the process industries, **21**, 2007, pp. 185-198.

[23] Mogi, T., Kim, D., Shiina, H., Horiguchi, S., *Self-ignition and explosion during discharge of high-pressure hydrogen*, Journal of Loss Prevention in the process industries, **21**, No. 2, 2008, pp. 199-204.

[24] Yamada, E., Watanaba, S., Hayashi, A. K., Tsuboi, N., *Numerical analysis on auto-ignition of a high pressure hydrogen jet spouting from a tube*, preceding of 32nd International Combustion Symposium, **32**, 2009, pp. 2363-2369.

[25] Golub, V. V., Baklanov, D. I., Bazhenova, T. V., Bragin, M. V., Golovastov, S. V., Ivanov, M. F., Volodin, V. V., *Shock-induced ignition of hydrogen gas during accidental or technical opening of high-pressure tanks*, Journal of Loss Prevention in the process industries, **20**, 2007, pp. 439-446.

[26] Yamada, E., Watanabe, S., Hayashi, A. K., Tsuboi, N., *Numerical analysis on auto-ignition of a high pressure hydrogen jet spouting from a tube*, Proceedings of the Combustion Institute, **32**,

[27] Xu, B.P., El Hima, L., Wen, J.X., Dembele, S., Tam, V.H.Y. and Donchev, T., *Numerical study on the spontaneous ignition of pressurized hydrogen release through a tube into air*, Journal of Loss Prevention in the process industries, **21**, No. 2, 2008, pp. 205-213.

[28] Wen, J.X., Xu, B.P. and Tam, V.H.Y., *Numerical study of spontaneous ignition of pressurized hydrogen release through a length of tube*, Combustion and Flame Journal, **156**, No. 11, 2009, pp. 2173-2189.

[29] Velikorodny, A. and Kudriakov S., *Numerical study of the near-field of highly underexpanded turbulent gas jet*, International Journal of Hydrogen Energy, **37**, No. 22, 2012, pp. 17390-17399.

[30] Kameshki, M. R., *Simulation of Hydrogen Jet Exiting a High Pressure Reservoir*, M. Sc. Thesis, Concordia University, 2007.

[31] Cadiou, A., *NadiaLES : Manuel Theorique*, Note Technique CODICIEL-LMFAN, 2003-01.

[32] Khaksarfard, R., *Numerical Investigation of Hydrogen Sonic jet With Real Gas Model*, Ph.D. Thesis, Concordia University, 2011.

[33] Mohamed, K., *Simulation of Hydrogen Release from a High-Pressure Chamber Considering Real Gas Effects*, M. Sc. Thesis, Concordia University, 2004.

[34] Burg, C. O. E.**,** *A Robust Unstructured Grid Movement Strategy using Three-Dimensional Torsional Springs*, 34th AIAA Fluid Dynamics Conference and Exhibit, 2004-2529, 2004.

[35] Khaksarfard, R., Kameshki, M. R. and Paraschivoiu, M., *Numerical simulation of high pressure release and dispersion of hydrogen into air with real gas model*, Shock Waves, 20, No. 3, 2010, pp. 205-216.

[36] Shishehgaran, N., Paraschivoiu, M., *CFD based simulation of hydrogen release through elliptical orifice shapes*, The 5th International Conference on Hydrogen Safety (ICHS), Brussels, Belgium, Sep. 2013.

[37] Shishehgaran, N., Paraschivoiu, M., *Hydrogen release from high pressure reservoirs through elliptical orifices*, The 21st Annual Conference of the CFD Society of Canada (CFD Canada), Sherbrooke, Quebec, Canada, May 2013.

[38] Afroosheh, M. A., Shishehgaran, N., Nakhle, W., Paraschivoiu, M., *Simulation of Compressed Hydrogen Flow and Auto-Ignition*, The 3rd Climate Change Technology Conf. (CCTC), Montreal, Quebec, Canada, May 2013.

[39] Montagne, J.L., Yee, H.C., and Vinokur M., *Comparative study of high-resolution shock-capturing schemes for a real gas*, AIAA Journal, 27, No. 10, 1989, pp. 1332–1346.